6-12-1987

Explosion Structures in Grande Ronde Basalt of the Columbia River Basalt Group, Near Troy, Oregon

Leonard Lee Orzol
Portland State University

AN ABSTRAST OF THE THESIS OF Leonard Lee Orzol for the Master

of Science in Geology presented June 12, 1987.

Title: Explosion Structures in Grande Ronde Basalt of the

   Columbia River Basalt Group, near Troy, Oregon.

APPROVED BY MEMBERS OF THE THESIS COMMITEE:

Michael L. Cummings, Chairman

Marvin H. Beeson

Ansel G. Johnson

    Explosion structures occur in flows of Grande Ronde Basalt in

the study area near Troy, Oregon. Data from nineteen stratigraphic

sites indicate that the maximum number of flows that contain

explosion structures at any one site is six. In the informally

named Troy flow, explosion structures are widespread.

    Each flow that contains explosion structures can be divided

into two cooling units. The first cooling units occupy troughs in

the pre-eruption topography and are up to 10 meters thick. The

second cooling units contain the explosion structures and are up to

100 meters thick. The thickness of flows that contain explosion

structures range from 10 meters to 150 meters. A plot of the thickness of an explosion structure against the total thickness of the flow is linear with slope of approximately 0.5. The breccias within explosion structures average 42% of the total thickness of a flow.

The overall shape of an explosion structures is similar to a three-dimensional nested arch with a central spine of breccia that cuts through the uppermost arches. Jointing patterns follow the shape of the arches. The linear trends of the central spines within explosion structures of the Troy flow parallel either the northeast-trending Grande Ronde (N 3° E) fault system or the northwest-trending dike system in the area (N 15° W).

Two processes operate during the formation of explosion structures 1) mixing and 2) fragmentation. These two processes produce unique intraflow zones within the second cooling unit. Petrographic textures of these intraflow zones range from vitrophyric to intersertal to intergranular. All three textures can be observed in thin bands or layers in samples from the upper intraflow zones of the second cooling units. Individual bands or layers are twisted, pinched, and swirled due to mixing. Fragmentation and mixing produce a vertically stratified central spine composed of three main types of clasts: vesicular to non-vesicular, scoriaceous, and pahoehoe types. Clast sizes range from lapilli in the outer matrix-supported margin to block in the inner clast-supported core.

Broad overall trends occur in geochemical data for the Troy

flow and a flow stratigraphically above the Troy flow. Concentrations of particular elements increase or decrease in samples towards the base of the flow relative to the uppermost sample. K, La, Eu, and Ta are enriched and Fe and Co depleted greater than 10% towards the base of a flow in areas away from explosion structures. Particular elements are enriched (Ce, Hf) or depleted (Th) less than 10% towards the base. Where explosions structures are present within the flow, these broad overall trends are less pronounced and few elements display these trends of enrichment or depletion.

EXPLOSION STRUCTURES IN GRANDE RONDE BASALT OF THE

COLUMBIA RIVER BASALT GROUP, NEAR TROY, OREGON.

by

LEONARD LEE ORZOL

A thesis submitted in partial fulfillment of the
requirements for the degree of

MASTER OF SCIENCE
in
GEOLOGY

Portland State University

1987

TO THE OFFICE OF GRADUATE STUDIES AND RESEARCH:

The members of the Committee approve the thesis of Leonard Lee Orzol presented June 12, 1987.

Michael L. Cummings, Chairman

Marvin H. Beeson

Ansel G. Johnson

APPROVED:

Ansel G. Johnson, Department of Geology

Bernard Ross, Vice Provost for Graduate Studies

ACKNOWLEDGEMENTS

TABLE OF CONTENTS

LIST OF TABLES

LIST OF FIGURES

FIGURE   PAGE

CHAPTER I

INTRODUCTION

Hydrovolcanic activity ranges from relatively minor phreatic events to catastrophic eruptions like the 1982 eruption of El Chichon (Sheridan and Wohletz, 1983). Hydrovolcanism refers to volcanic phenomena produced by interaction of magma or magmatic heat with an external source of water, such as a body of surface water or an aquifer (Macdonald, 1972; Sheridan and Wohletz, 1983). Variables controlling explosions related to hydrovolcanic processes are poorly understood, because not all water-lava interactions result in explosive activity. Sheridan and Wohletz (1983) argue the degree of explosivity is controlled primarily by the mass ratio of water to melt or lava. High mass ratios are related to low-energy or explosion-free interactions such as those that result in pillow formation in surface water. Low mass ratios are related to explosive activity such as in the formation of maars by interaction of magma with aquifers. Buchanan (1974), Witte and others (1970), and Board and others (1974; 1975) have modeled hydroexplosions by comparison to fuel-coolant interaction (FCI) to simulate natural explosive processes that occur in melts or magmas that range in composition from rhyolite to basalt.

Interaction between surface or subsurface water and basaltic

lavas of the Miocene Columbia River Basalt Group (CRB) have produced several hydrovolcanic features. These features include palagonite breccias, pillow-palagonite breccias, pillowed lavas, pipe vesicles, vesicle pipes, peperites, vesicle trains, and spiracles. Earlier investigators such as Fuller (1931) and Waters (1960) argue that these hydrovolcanic features were produced during minor explosive events. This study investigates features in basalt flows of the CRB that resulted from explosive water-lava interaction.

This water-lava interaction produced a structure of steeply dipping breccia by a violent upward release of subjacent steam through the still molten lava (hereafter called an explosion structure). Typically these structures are approximately 40 m across and occupy the upper 1/3 to 1/2 of a flow (Figure 1). The explosion structures were investigated within Grande Ronde Basalt of the Columbia River Basalt Group in northeastern Oregon and southeastern Washington in the steep canyons of the Wenaha and Grande Ronde Rivers near Troy, Oregon (Figure 2). The objectives of this study are 1) to describe and characterize these hydrovolcanic features, and 2) to examine the mechanisms of development of the explosion structures.

SCOPE AND PRODUCTS

The following five main tasks were completed.

1) Map the distribution and determine the characteristics of explosion structures within flow units and within the stratigraphic section of Grande Ronde Basalt in the Troy area, Oregon (Figure 2).

ZONES   DIVISIONS

RUBBLE TOP

CENTRAL SPINE

CONFINING WALLS

2nd COOLING UNIT

(UP TO 100 m THICK)

VESICULAR CLASTS/POCKETS

PLATY JOINTED ZONE

CHILLED PAHOEHOE BASE

SCORIA BRECCIA

VESICULAR ZONE

CHILLED PAHOEHOE BASE

1st COOLING UNIT

RED BAKED CLAY ZONE

(UP TO 10 m THICK)
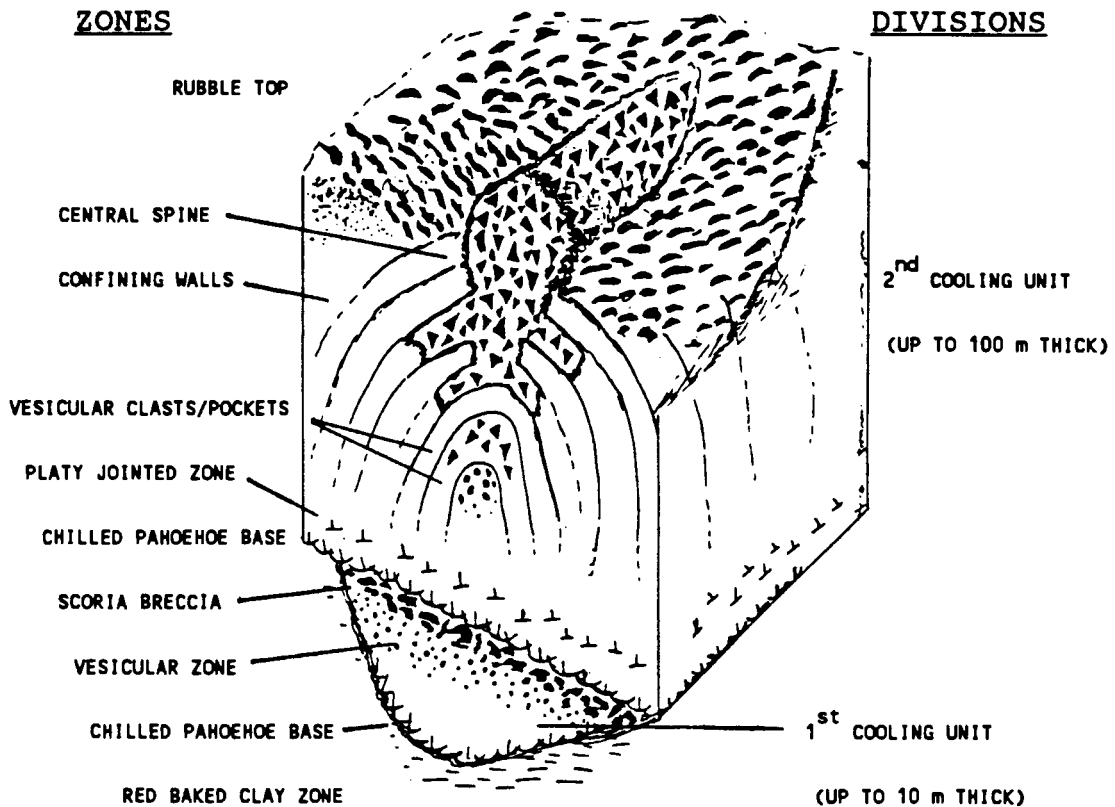
Figure 1.   Generalized schematic of a brecciated flow
showing a brecciated flow area and an explosion structure.

The study area covered portions of the Troy, Eden, and Flora 7 1/2

minute quadrangles of Oregon and the Saddle Mountain, Mountain View,

Diamond Peak, and Fields Spring 7 1/2 minute quadrangles of

Washington (1:24,00 scale).

2) Determine the textures and fabrics produced during the

formation of explosion structures.

3) Compare major and trace element geochemistry where

explosion structures are present within the Troy flow and locations

where the Troy flow is non-brecciated.

4) Determine iron oxidation states using Mossbauer
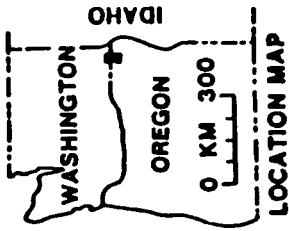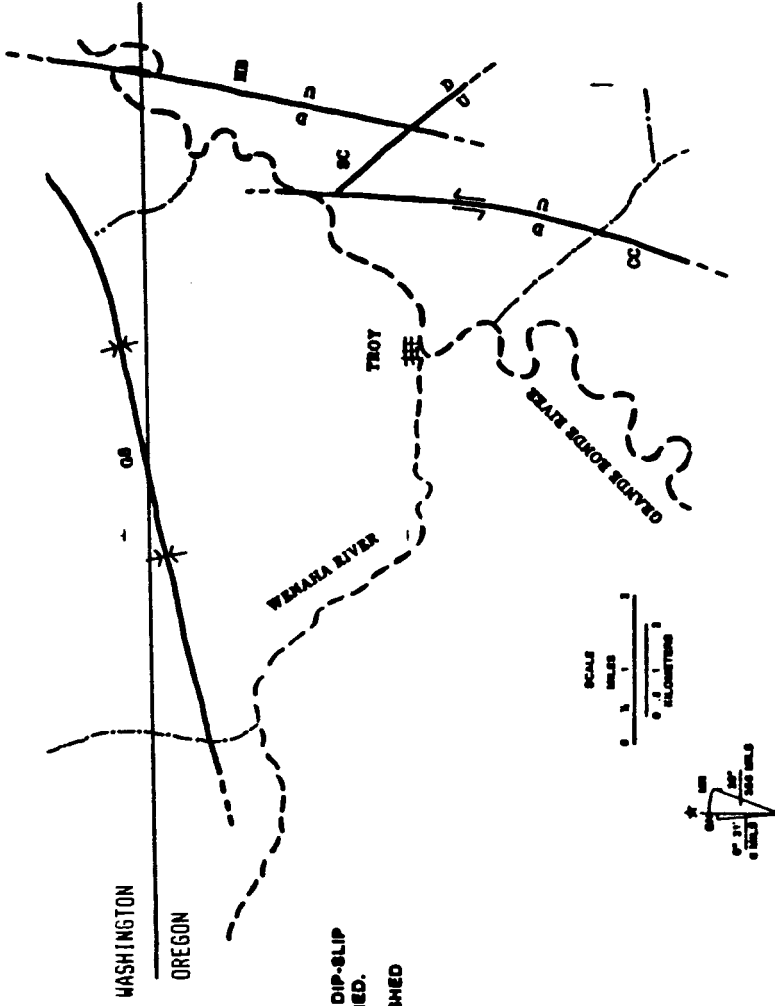
<u>Figure 2.</u> Location map for the study area showing its relation to the states of Oregon and Washington. Included on the larger-scale map are structural features mapped by Ross (1978). (after Ross, 1978)

spectroscopy on samples from various textural zones within the structures.

5) Develop a model for the formation of the structures.

Products from this investigation are a geologic map of the study area that shows the distribution of the breccia structures within Grande Ronde Basalt, a model developed for the explosion structure formation in basaltic lava and the variables that constrain the behavior of the system.

LOCATION AND SETTING

The Grande Ronde and Wenaha Rivers have incised deep canyons into flows of the Columbia River Basalt Group and interflow sediments within the Grande Ronde River-Blue Mountain region of Oregon and Washington (Figure 2). The basalt flows are those of the Grande Ronde, Wanapum, and Saddle Mountains Basalts and interflow sediments are those of the Grouse Creek and Squaw Creek members of the Ellensburg Formation (Ross, 1978, 1980; Stoffel 1981, 1984). The area of study centers on Troy, Oregon at the junction of the Wenaha and Grande Ronde Rivers (Figure 2). This study area encloses roughly six 7 1/2-minute quadrangles of northeast Oregon and southeast Washington and is approximately 200 square kilometers.

NOMENCLATURE

Several terms are used in this text and review of these terms will be helpful to the reader (see definitions in appendix E). The terms were developed to indicate a locality where explosion

structures may or may not be present or to describe a particular type of clast found within the breccia of an explosion structure.

Briefly, the Troy flow was singled out and named by Ross (1978) because of unusual lobes of dense basalt that penetrate into a thick flow-top breccia. These lobes form part of an explosion structure that occupies the upper 1/3 to 1/2 of a flow (Figure 1). A symmetrical collection of dense basalt lobes encloses a steeply dipping breccia in the center of an explosion structure and is called the confining walls. This steeply dipping breccia is called a central spine. An individual lobe is separated by a joint trace from the adjacent lobes and is called a basaltic arm. The confining walls form individual layers in the overall shape of an arch when viewed in cross-section perpendicular to the plane of the central spine (Figure 1).

A flow containing explosion structures is called a brecciated flow, whereas a flow lacking explosion structures is called a non-brecciated flow. An explosion structure is formed by the interaction of water and basalt. The portions of a basalt flow containing explosion structures and the rocks immediately adjacent to an explosion structure within the same flow are called a brecciated flow area. Areas of basalt within a flow that contains explosion structures, but that are not immediately effected by the formation of explosion structures will be called unbrecciated flow areas. Areas of basalt within a flow that contain explosion structures but are not situated near explosion structures are called non-brecciated flow areas (Figure 3).
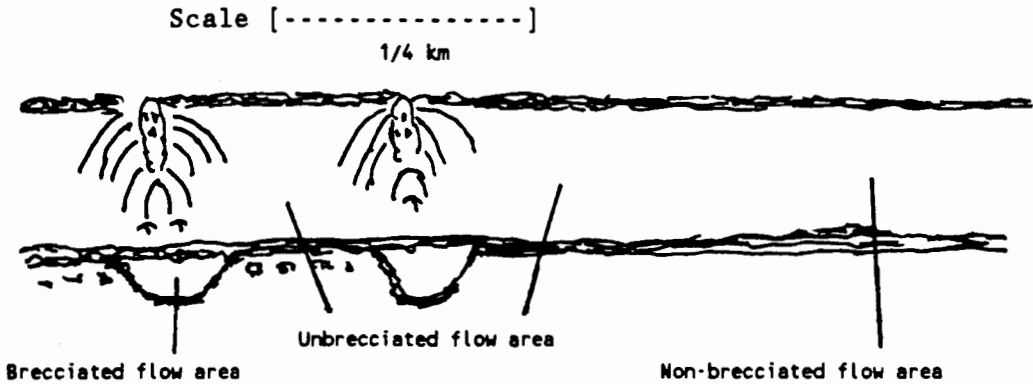
Figure 3.   Generalized schematic showing the relationships betwwen different flow areas within a single hyopethical flow. Brecciated flow areas are immediately affected by the process of formation, while unbrecciated to non-brecciated flow areas are not.   Vertical features have been exaggerated approximately five times.

<div align="center">METHODS</div>

Field Studies

All field work was conducted during a six-week period in the summer of 1985 and a one-week period during the fall of 1985. Traverses were accomplished on foot and reconnaissance observations were conducted either by foot or from a truck.   The following four tasks were accomplished:

1) Stratigraphic sections were measured at key localities along valley walls of the Wenaha and Grande Ronde Rivers near Troy, Oregon.   Elevations of each flow were from readings using an M-1 altimeter.   Stratigraphic sequence, thickness, and variations in textures within basalt flows that contained explosion structures were investigated.   Thickness of various textural zones within each flow were noted or determined.   The thickness of the portion containing steeply dipping breccias and the superjacent flow-top

breccia within flows containing explosion structures were measured.

2) Samples of fresh basalt were collected from flows containing explosion structures for geochemical analysis. Data from geochemical analyses were used to infer formational processes of these structures.

3) The distribution of clast types, clast sizes, and widths of steeply dipping breccia zones were measured for flows with explosion structures by using either a 100 foot tape and/or a 2 foot by 2 foot square grid.

4) Trends of the central spines were measured. A search for fractures within the flows which underlie brecciated flow areas was made to determine whether the orientations of the central spines are related to such fractures.

A more detailed description of field techniques and equipment is presented in Appendix F.

Laboratory Studies

1) Fresh samples of basalt were analyzed by x-ray fluorescence (XRF) at Washington State University, Washington, instrumental neutron activation analysis (INAA) at Oregon State and Portland State Universities, and Mossbauer spectroscopy at Portland State University.

a) XRF was used to determine major oxide concentrations within various textural zones.

b) INAA was used to determine distribution of major and trace elements within explosion structures.

c) Mossbauer spectroscopy determined differences in

oxidation states of iron within various textural zones produced during the formation of explosion structures and the iron-bearing oxide minerals present within these zones. Mossbauer spectroscopy and interpretation of the resulting spectrums were done by Donald L. Howard of Portland State University.

2) Petrogaphic analysis of various textural types within the flows determined the textural development of the samples and, in particular, features which indicate the dynamics of the processes by which explosion structures were developed.

A more detailed description of laboratory techniques and equipment is presented in Appendix F.

CHAPTER II

PREVIOUS INVESTIGATIONS

The study area was mapped on a reconnaissance basis as part of
a regional study by Russel (1897). Waters (1961) completed a
stratigraphic section at the northern end of Powatka Ridge, south of
the town of Troy, that was included in an early geochemical
investigation of the stratigraphy of the Columbia River Basalt
Group. Walker (1973, 1979) defined on a reconnaissance basis two
major chemical types in the study area, the Yakima and Late Yakima
chemical types. Swanson and others (1977) included portions of the
study area in a regional reconnaissance map of southeastern
Washington and adjacent Idaho.

Regional structural geology has been described by Ross (1975;
1978; 1980) (Figure 2) and Hooper and Camp (1981). An east-to-west
regional tilting from isostatic rise of older rocks along the
eastern margin of the Columbia Plateau, initiated before Miocene
time, caused offlap of progressively younger basalt units. Faulting
and folding through middle and late Miocene time occurred during a
compressional stress regime with the primary compressive stress
oriented in a northwest-southeast direction and reactivation of
structural grain in the pre-Miocene basement. Within the study
area, the Grande Ronde fault system, adjacent Grouse Flat syncline,

and other structural features were produced during the compressional regime and a subsequent extensional period (Ross, 1978). Ross (1978) inferred that an initial subsidence of the Grouse Flat syncline, an initial uplift of the Saddle Butte anticline, and the subsequent strike-slip movement on the Grande Ronde fault system occurred during the compression regime and started before the Troy flow was erupted. Dip-slip movement on the Grande Ronde fault system developed during the extensional period and after the eruption of the Wenaha flow of the Saddle Mountains Basalt.

Ross (1978) mapped most of the study area at a scale of 1:12000 and determined the stratigraphy of the basalts in this area (Figure 4 modified with revisions by Swanson and others 1979). The Troy flow of the Grande Ronde Basalt was informally named by Ross (1978). He described the Troy flow as a mappable unit that consistently was the thickest Grande Ronde Basalt flow exposed within the boundaries of his study area. At the best exposures of the Troy flow along the Wenaha River near the town of Troy, Ross (1978) measured a thickness of 84 meters and indicated thickening northward to 102 meters near Diamond Peak and thining southward from the Grande Ronde River.

Ross (1978) reported that at some localities, the Troy flow had an unusally thick flow-top breccia into which lobes of dense rock penetrate from below or occur as large isolated masses within the flow-top breccia. He sampled the Troy flow at localities where these unusual lobes or masses of dense rock were present and at other localities where these lobes were absent. The geochemical
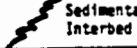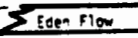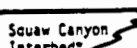
Wright and others, 1973			Central Portion of Study Area	Southern Portion Of Study Area
Columbia River Group	Yakima Basalt	Upper	Buford Flow	Buford Flow
			Sedimentary Interbed	Sedimentary Interbed
			Menaha Flow	Menaha Flow
			Grouse Creek Interbed* / Eden Flow	Eden Flow*
				Grouse Creek Interbed*
			Bear Creek Flow*	
			Umatilla Flow	Umatilla Flow
			Squaw Canyon Interbed*	
		Middle	Roza Flow / Powatka Flow*	Kuhn Ridge Flows*
			Dodge Flow(s)	Dodge Flow(s)
		Lower	Undifferentiated	Undifferentiated
			Troy Flow*	Troy Flow*
			Undifferentiated	Undifferentiated
				Mud Creek Flow*
				Undifferentiated
	Imnaha Basalt (not exposed in study area)			

Figure 4. The stratigraphy of the study area as determined by Ross (1978). Nomenclature has been revised by Swanson and others, (1979). The Troy flow occurs in the upper section of the Grande Ronde Basalt (Lower Yakima) followed by Wanapum Basalt (Middle Yakima) then Saddle Mountains Basalt (Upper Yakima). (after Ross, 1978)

data indicated that the Troy flow had the highest silica (SiO_2) concentration among the basalts within his study area with only 3 samples containing less than 54%. Several other distinct chemical characteristics included low MgO and CaO and high P_2O_5, K_2O, and TiO_2 when compared to other Grande Ronde Basalts.

Features generated from interaction of water and flows of the Columbia River Basalt have been reported by many authors: Fuller

(1931), Waters (1960), Schmincke (1967), Swanson (1967). These features include pillow bases of some flows (Fuller, 1931), pillow-palagonite breccia (Fuller, 1931), pipe vesicles (Waters, 1960), vesicle cylinders (Waters, 1960), and spiracles (Fuller, 1931; Waters, 1960; Swanson, 1967), and peperites (Fuller, 1931; Waters, 1955; Schmincke, 1967; Swanson, 1967). All features except peperites are formed where surface flows trap pockets of air, gas from burnt vegetation, and steam expelled from soils and water-soaked sediments, or produced by advance of the flow into either relatively shallow or deep bodies of water (Fuller, 1931; Waters, 1960). Peperites, basalt-sediment breccias on the Columbia River Plateau, result from intrusion of fluid basaltic dikes and sills or burrowing of surface flows into moist, soft sediments (Schmincke, 1967).

Within the study area, Ross (1978) reported hyaloclastite deposits superjacent to the Troy flow at one stratigraphic location (Driveway Ridge secton) and subjacent at two locations (Bald Butte and Crooked Neck Creek sections). Typically these deposits are yellow brown to light gray in color, fine to coarse-grained, contain angular fragments, and are, in some localities, well-bedded.

CHAPTER III

STRATIGRAPHY AND PETROGRAPHY

Stratigraphic sections in the study area were studied in order
to examine the relation of regional scale features to the spatial
distribution of explosion structures and the total number of flows
that contain explosion structures (brecciated flows). The basalt
flows in the study area are those of the Grande Ronde Basalt,
Wanapum Basalt, and Saddle Mountains Basalt. Nineteen stratigraphic
sections were measured at key locations (stratigraphic information
is compiled in Appendix A, the site locations are shown on Plate 1
and the locations are listed in Table I). Stratigraphic locations
were selected for exposure and location within the study area.
Three types of measured sections were conducted. 1) Vertical
sections were measured of all flows present at each stratigraphic
site. 2) Partial vertical sections were measured for selected
flows. 3) Lateral sections were measured to determine horizontal
variations within a flow.

Results show explosion structures are only found within Grande
Ronde Basalt and are not present in Wanapum and Saddle Mountains
Basalt within the boundaries of this study area. The measured-
section sites contain one or more brecciated flows and the Troy flow
is one of these brecciated flows (Table I). The maximum number of

TABLE I

SUMMARY OF LOCATIONS, MAP SYMBOL, FLOW TYPES FOR EACH STRATIGRAPHIC SECTION

Stratigraphic site label	*Map symbol	+Type section	$Total Flows	&Troy Brecciated	Starting Location 7 1/2 minute quadrangles
Eden Bench	EB	VC	6	Y	NE1/4,NW1/4,SE1/4 Sect 5 T5N R43E Troy
Wenaha Camp	WC	V	1	Y	SE1/4,NE1/4,NW1/4 Sect 5 T5N R43E Troy
Wenaha Camp Road	WCR	V	3	Y	SE1/4,NE1/4,NW1/4 Sect 5 T5N R43E Troy
Umatilla	U	VC	4	Y	SE1/4,NE1/4,NE1/4 Sect 1 T6N R42E Eden
Crooked Creek	CC	VC	2	Y	SW1/4,SW1/4,NE1/4 Sect 27 T6N R42E Eden
South Wenaha	SW	V	2	Y	SW1/4,NE1/4,NE1/4 Sect 5 T5N R43E Troy
Wenaha Ravine	WR	V	1	Y	SE1/4,NW1/4,NE1/4 Sect 5 T5N R43E Troy
Elloit Bend	EF	B	$\geq$3	Y	NW1/4,NW1/4,SE1/4 Sect 9 T5N R43E Troy
Grouse Creek	GC	VC	0	0	NE1/4,SW1/4,SW1/4 Sect 24 T5N R43E Troy
Hoodoo Trail	H	VC	3	Y	SE1/4,NE1/4,SW1/4 Sect 29 T6N R42E Eden
Maggie Canyon	MC	B	$\geq$2	Y	NW1/4,SE1/4,NW1/4 Sect 3 T5N R43E Troy
Lighte Flat	LF	B	$\geq$2	Y	NW1/4,SW1/4,NW1/4 Sect 3 T5N R43E Troy
Squaw Canyon #1	SC1	B	$\geq$4	Y	NW1/4,SE1/4,NW1/4 Sect 35 T6N R43E Troy
Squaw Canyon #2	SC2	B	$\geq$2	Y	NE1/4,SW1/4,NE1/4 Sect 35 T6N R43E Troy
Floral Grade	F	V	$\geq$2	C	SE1/4,SW1/4,NW1/4 Sect 1 T5N R43E Troy
South Grande Ronde	SG	B	3	Y	NW1/4,SW1/4,NW1/4 Sect 17 T5N R43E Troy
Saddle Mountain	SM	B	$\geq$2	Y	SE1/4,SW1/4,NE1/4 Sect 29 T7N R43E Saddle Butte
Wenaha River	W	V	$\geq$1	Y	SW1/4,SW1/4,NW1/4 Sect 5 T5N R43E Troy
Cougar Creek	C	V	$\geq$1	Y	NE1/4,NE1/4,NW1/4 Sect 32 T7N R44E Mountain View

* Map Symbols are used to indentify the stratigraphic sections on Plate 1 and used to indentify each section in Appendix A.
+ Type section indicates the method used to measure each stratigraphic section.
    VC - vertical complete section through all flows present at the site.
    V - partial vertical section through selected flows.
    B - lateral section to dtermine horizontal variations through one or more flows.
$ The total number of brecciated flows present.
& Troy Brecciated indicates if the Troy flow contained explosion structures (Y) or lacks explosion structures (0) or the Troy flow was covered (C).

brecciated flows in one section is six at the Eden Bench section (EB) near the town of Troy and west of the Grande Ronde fault system. The spatial distribution of the stratigraphic sites and the observed number of brecciated flows at each stratigraphic or reconnaissance site show brecciated flows occur on both sides of the Grande Ronde fault system (Figure 5).

At the Grouse Creek stratigraphic section (GC), brecciated flow areas are not present and do not occur within at least one km of this site (Figure 5). The Grouse Creek site (GC) is located northeast of the town of Troy, is near the junction of the northeast-trending Courtney Creek fault and the northwest-trending Squaw Canyon fault, and is west of the Horseshoe Bend fault (Figure 5; the Grouse Creek section is the only solid circle). These faults are part of the Grande Ronde fault system (Ross, 1978). Brecciated flows occur on either side of the axis of the Grouse Flat syncline and adjacent to the Saddle Butte anticline.

During the measurement of each stratigraphic section, intraflow characteristics were measured or noted (see appendix A for complete stratigraphic data). These intraflow characteristics include the total thickness of each flow determined by elevations of both upper and lower contacts, jointing patterns and the relative position of each pattern within the flow, morphological profile of each flow, occurrence of vesicular or scoriaceous zones, and subjacent clay zones. If an explosion structure was observed within a flow, two major vertical intervals within the flow and, if possible, the trend of the central spine (the bearing of the plane

18
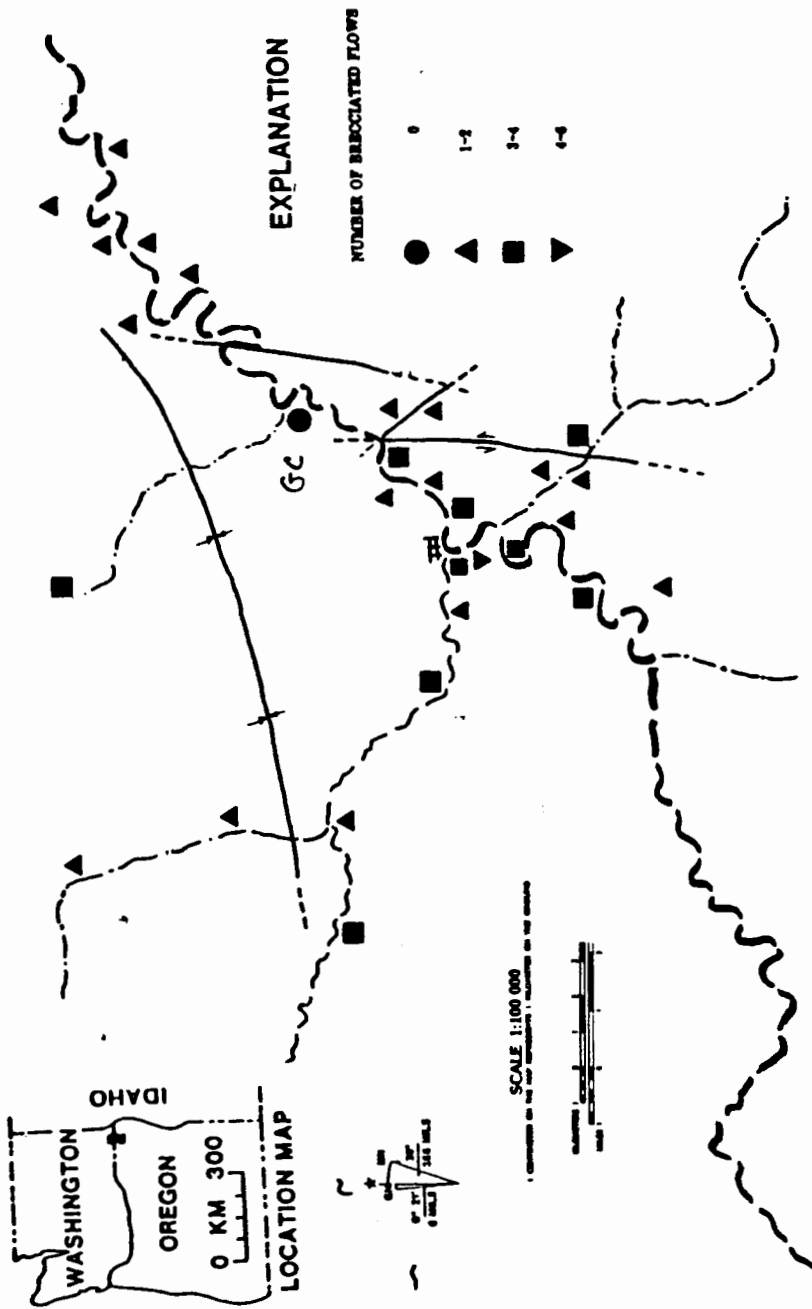
Figure 5. A map showing the maximum number of brecciated flows observed at locations within the study area. The distribution indicates brecciated flows are present on both sides of the Grande Ronde fault system. Grouse Creek (GC) section is the only site lacking brecciated flows (solid circle left of the word "explanation").

of the central spine) were measured. The two major vertical intervals are: 1) the breccia interval that consists of the vertical thickness between the first observation of breccia in an explosion structure to the upper contact with the overlying flow, and 2) the compact interval that consists of the remaining lower portion of the flow (Figure 6 and definitions section).

Data from the measurements from the two vertical intervals show that flows containing explosion structures range in thickness from thin flows (10 m) to thicker flows (125 m) (Table II). Although brecciated flows thinner than the Troy flow have similar explosion structures, these structures are less fully developed and are developed at a smaller scale than within the Troy flow. Figure 6 is a plot of the breccia interval against the total thickness of the brecciated flow. The graph indicates that thick brecciated flows greater than 30 m thick have a greater proportion of their thickness brecciated than thinner brecciated flows. For the thicker flows, 45% of the thickness is breccia whereas the average is less than 45% for thinner flows (Figure 6). The thinner brecciated flows are either younger or older than the Troy flow. The Troy flow data points plot towards the upper right hand of the graph, because they are generally thicker and have thicker breccia intervals than the thinner brecciated flows.

Trends of the central spine for the Troy flow are northeasterly at locations near the Grande Ronde fault system (Figure 7). To the west, away from the fault system, the preferred orientation is to the northwest. Northeast orientations within the
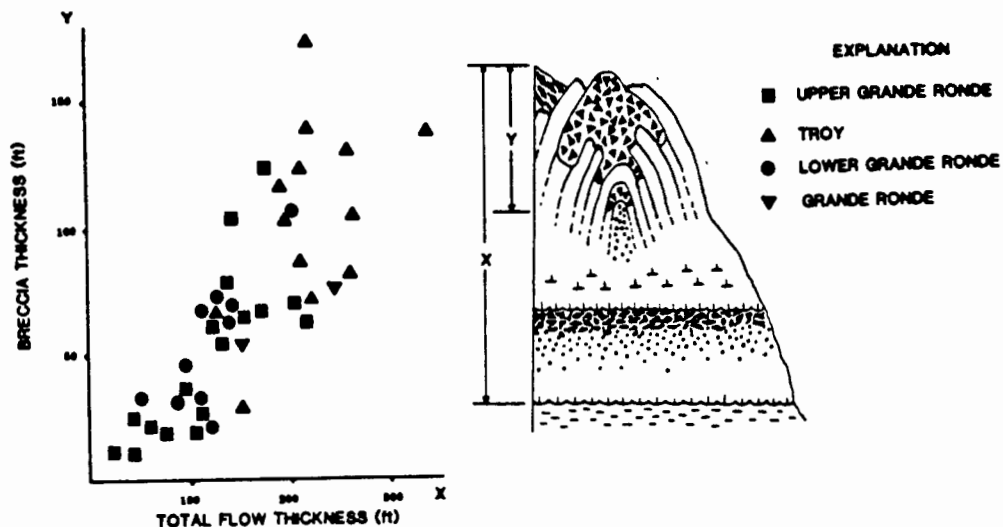
Figure 6. A graph showing the individual breccia intervals plotted against the total thickness of that flow. The collection of data points is grouped approximately along a line that has a slope of 0.5. Troy flow data are grouped towards the upper right portion of the graph.

Troy flow nearly coincide with the northeast-trending faults of the Grande Ronde fault system; northwest orientations nearly coincide with the northwest-trending faults of the fault system and northwest orientation of the regional dikes. For flows above and below the Troy flow, orientations are both northwest and northeast.

The Troy flow was the primary flow studied, because within this flow explosion structures are large and widely distributed. Explosion structures within the Troy flow have been generalized to show only one central spine, but more than one spine may be present in some localities. Explosion structures locally occur in clusters with as little as 30 meters separating the structures. These

TABLE II

THICKNESS OF BRECCIA TOP AND COMPACT INTERVALS FOR

BRECCIATED FLOWS AT VARIOUS LOCATIONS

| &Location symbol | ∂Flow type | Thickness (feet) | | *TOTAL | &Fraction of breccia interval |
		*Breccia interval	*Compact interval		
EB	UGR	60	69	129	.47
	UGR	13	7	20	.65
	UGR	125	48	173	.72
	TROY	124	85	209	.59
WC and WCR	TROY	72	148	220	.49
	TROY	157	181	338	.46
	UGR	23	82	105	.28
	UGR	28	80	108	.26
U	LGR	70	69	139	.50
	TROY	128	130	258	.50
	UGR	26	13	39	.67
CC	TROY	68	55	123	.55
WR	TROY	138	200	338	.41
	TROY	105	159	264	.40
EF	LGR	34	16	50	.68
	LGR	85	16	101	.84
	TROY	173	46	219	.79
	TROY	139	80	219	.63
H	UGR	22	35	57	.39
	UGR	66	136	148	.45
	TROY	39	123	152	.26
LF	LGR	107	89	196	.55
	LGR	63	72	135	.47
	LGR	46	49	95	.48
	TROY	45	130	175	.26
	TROY	93	164	257	.36
	TROY	35	140	175	.20
	TROY	90	154	244	.37
	UGR	65	58	123	.53

&Location symbol refers to the stratigraphic labels of Table I.
∂Flow type differentiates between the Troy flow (TROY), a Grande Ronde flow below the Troy flow (LGR), and a Grande Ronde above the Troy flow (UGR).
*Intervals used in Figure 6.
&The percentage of the flow that is brecciated.

TABLE II CONTINNUED

THICKNESS OF BRECCIA TOP AND COMPACT INTERVALS FOR

BRECCIATED FLOWS AT VARIOUS LOCATIONS

&Location symbol	@Flow type	Thickness (feet) *Breccia interval	*Compact interval	*TOTAL	&Fraction of breccia interval
MC	LGR	31	89	120	.26
	LGR	42	42	84	.50
	TROY	75	57	132	.57
	UGR	65	61	126	.52
SC1	UGR	83	52	135	.61
	UGR	104	36	148	.70
	UGR	134	44	178	.75
	UGR	113	44	157	.72
SC2	UGR	70	134	214	.34
	UGR	55	75	130	.42
	UGR	21	50	71	.30
	UGR	67	102	169	.40
	UGR	11	27	38	.29
F	UGR	162	44	206	.79
	UGR	86	282	368	.23
SW	TROY	138	200	338	.41
	TROY	112	240	352	.32
W	TROY	105	159	264	.40
GC	TROY	0	172	172	.00
SG	LGR	72	58	130	.55
	LGR	15	49	64	.23
	TROY	104	90	194	.54
SM	GR	77	170	247	.45
	GR	55	93	148	.37

&Location symbol refers to the stratigraphic labels of Table I.
@Flow type differentiates between the Troy flow (TROY), a Grande Ronde flow below the Troy flow
 (LGR), and a Grande Ronde above the Troy flow (UGR).
*Intervals used in Figure 6.
&The percentage of the flow that is brecciated.
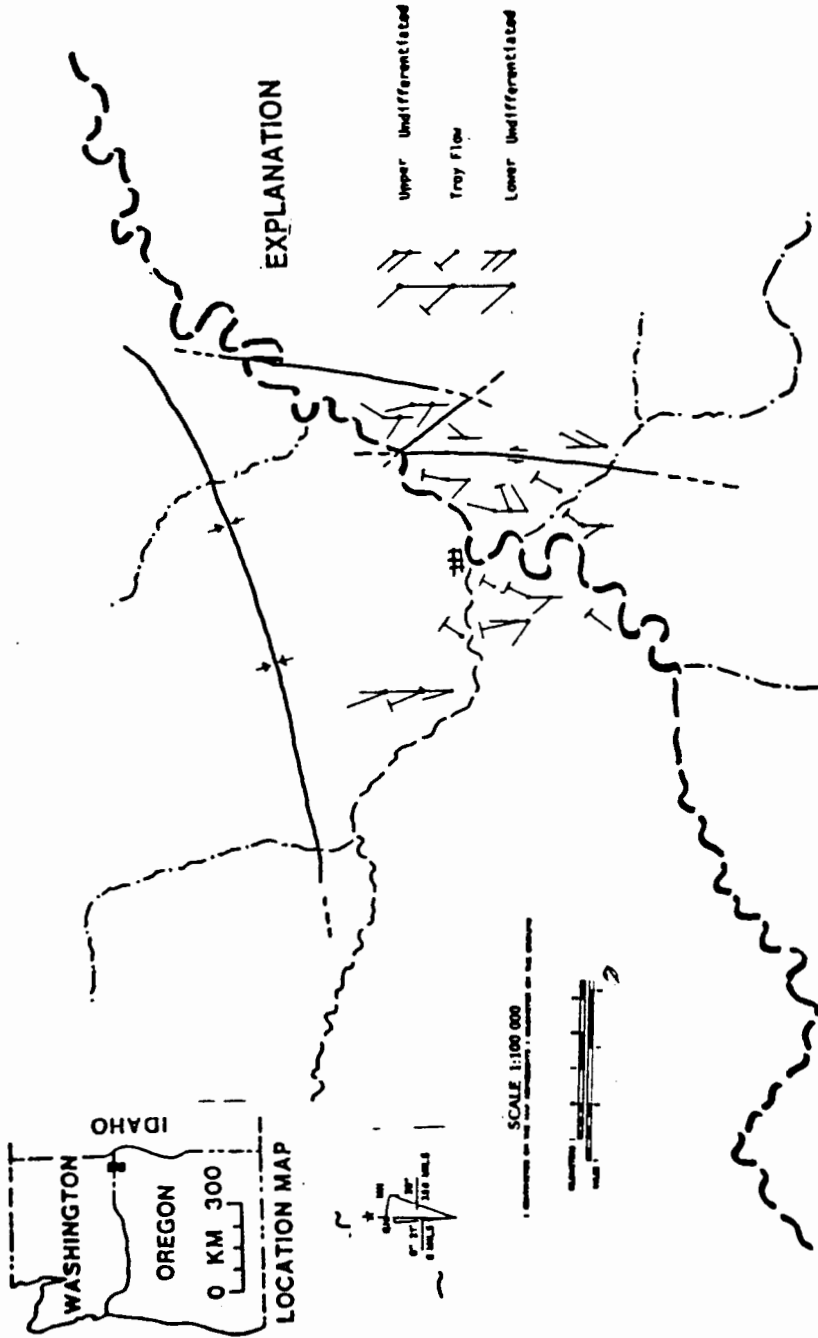
Figure 7. A map showing the trends of the central spine for brecciated flows. Trends for the Troy flow (depicted by the small bars on the end trend lines) have an eastward orientations that changes to a westward orientation nearer the axis of the Grouse Flat syncline. The orientation of upper (above Troy flow) and lower (below Troy flow) Grande Ronde flows are shown.

ZONES   DIVISIONS

RUBBLE TOP

CENTRAL SPINE   2nd COOLING UNIT

CONFINING WALLS   (UP TO 100 m THICK)

VESICULAR CLASTS POCKETS

PLATY JOINTED ZONE

CHILLED PAHOEHOE BASE

SCORIA BRECCIA

VESICULAR ZONE   1st COOLING UNIT

CHILLED PAHOEHOE BASE   (UP TO 10 m THICK)

RED BAKED CLAY ZONE
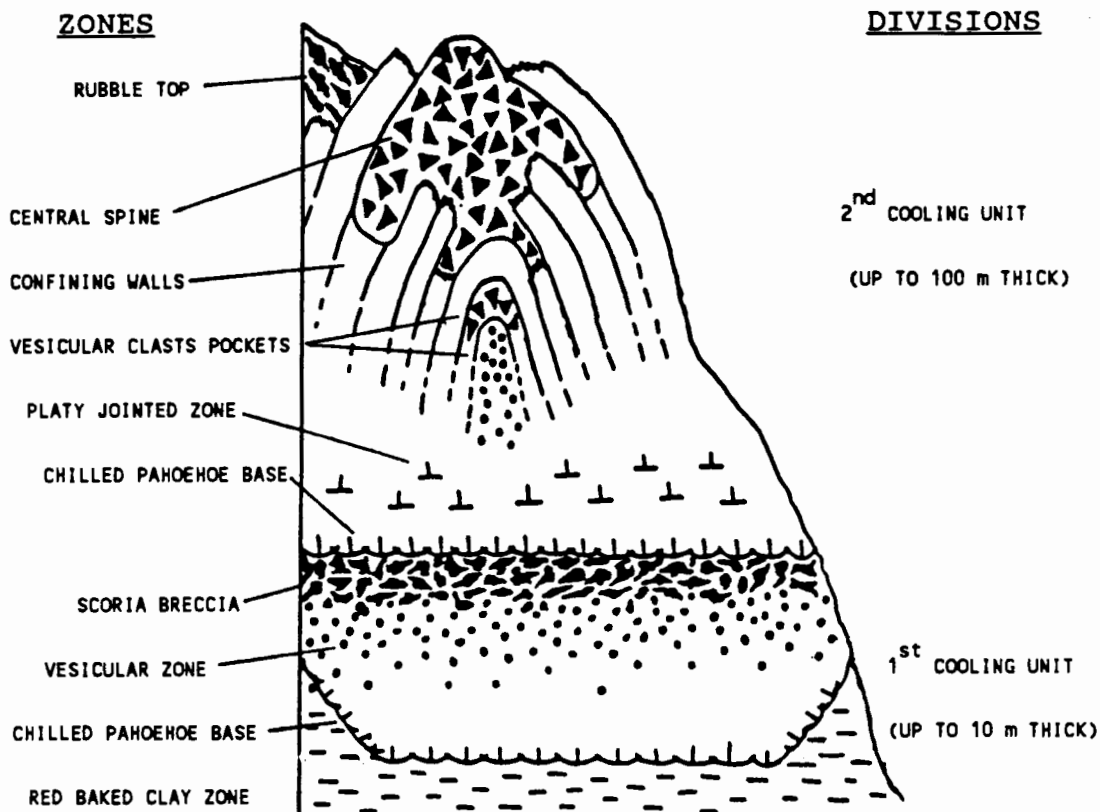
Figure 8.   Generalized schmetic of a brecciated flow area
showing two cooling units. The view is along the plane of the
central spine. Intraflow zones are depicted for both units.

clusters may occur in close proximity to each other or may be widely

spaced. The number of individual explosion structures in a cluster

varies. Two well-exposed explosion structures were selected for

vertical and horizontal traverse measurements.

The Troy flow at two stratigraphic locations, the Wenaha

Ravine (WR) and the Elliot Farm (EF) sections, consists of two

cooling units (Plate I). The term cooling unit is used as defined

by Smith (1960), where a thinner precusor lobe of a flow represents

the first cooling unit and is followed by a second lobe, the second

cooling unit (Figure 8). For the Troy flow the first cooling unit

is thin, up to 10 m in thickness whereas the second cooling unit is up to 100 m thick. A first cooling unit occupies a trough into the subjacent undulating pre-eruption topography. The amplitude of these undulation can be as great as 15 m. A red, baked-clay zone up to a maximum of 2 m in thickness is present within the trough. This clay zone grades into the underlying, weathered flow-top breccia or scoriaceous top of the underlying flow. A Grande Ronde flow above the Troy flow shows similar cooling units within brecciated flow areas at the Squaw Canyon #1 (SC1) and the Squaw Canyon #2 (SC2) sections. At locations where flows were unbrecciated or non-brecciated, only one cooling unit was found and a subjacent trough was absent.

The first and second cooling units in a brecciated flow area can be further subdivided into intraflow zones (Figure 8). Similar zones occur in the lower portions of the first and second cooling units. The zones are thinner in the second cooling unit than the first unit. These zones include a chilled pahoehoe base zone, inclined platy-jointed zone, sheared vesicular zone, banded vesicular zone, and, finally, a vesicular zone. The basal contact of both cooling units is marked by a chilled pahoehoe base (Figure 9). The chilled contacts have petrographic textures similar to textural zones found along the margin of a pillow of basalt (Bryan, 1972) (Table III). Samples from this chilled zone show quenched textures, including swallow-tailed microphenocrysts of plagioclase and clinopyroxene in a matrix of non-vesicular brown glass, that grades inward to vesicular intersertal textures with black glass.

Figure 9.   Samples from the chilled pahoehoe base of both the first and second cooling units of a brecciated flow area of the Troy flow. The three samples on the left side are from the base of the second unit, while the samples on the right are from the base of the first cooling unit. A pillow-like rind is visible on the upper right sample. Quench cracks are visible on the two lower left samples as dark lines on the surface of each sample. The ruler is approximately 15 cm long.

Rare cross-shaped microphenocrysts and microlites are found in thin

sections and are composed of just one type of mineral in a cross

shape. Cross-shape microphenocrysts and microlites can be found in

most intraflow zones within both cooling units.

        Another petrographic feature similar to a cross-shape grain is

a skewed cross consisting of plagioclase and clinopyroxene. An

TABLE III

SUMMARY OF FIELD AND PETROGRAPHIC CHARACTERISTICS FOR

THE ZONES OF A FIRST COOLING UNIT

Zone	Field characteristics followed by Petrographic characteristics

Chilled Pahoehoe base   Field: The rocks have an outer reddish-colored, coarse sandpaper textured rim, up to 15 mm thick. This outer surface is cut by quench fractures that are v-shaped, up to 15 mm deep, and are perpendicular to the surface of the sample. The undulating base consists of smooth lobate knobs of basalt that project into the underlying clay zone. These lobate knobs of basalt have wavelengths of 50 mm and ampitudes of 25 mm. Commonly scoriaceous clasts from the flow project into the Pahoehoe base and are surrounded by projections from the base.
Thickness: $\leq$6 cm
Jointing: none
Petrography: Textures: Vitrophyric textures grade inward from the contact surface. Quench cracks are observed to penetrate approximately 5 mm.
Microphenocrysts: Rare microphenocrysts of plagioclase have quenched, swallow-tailed terminal ends. Microphenocrysts and microlites, where present, parallel the contact surface with the subjacent clay zone and grade inward to a subparallel alignment. Modal percent of microphenocrysts is 3.9%; plagioclase (3.1%) and clinopyroxene (0.8%).
Vesicles: Vesicles occur towards the interior of the rock and away from the contact surface.

Inclined platy zone   Field: Wedge-shaped plates are up to 100 mm thick and up to 300 mm wide. Plates consist of black-colored basalt that has sparse circular vesicles commonly filled with milkly white crystalline material or vesicules are coated with greenish-brown material. Grades upward into the overlying zone.
Thickness: $\leq$2.0 m
Jointing: Joints of the individual plates are inclined upward 30 to 40 degrees and parallel to the subjacent contact base.
Petrography: Texture: Intersertal texture that generally lacks microphenocrysts of plagioclase or clinopyroxene.
Microphenocrysts: Modal percent of microphenocrysts is 0.1%.
Vesicles: Vesicles with a modal percent of 0.3% are randomly placed and filled.

Sheared vesicular zone Field: Zone composed of vesicular basalt in which the vesicles are shaped similar to flattened diamond forms. The surfaces of the vesicles are marked by sharp jagged projections of basalt. Grades upward into the overlying zone.
Thickness: $\leq$1.0 m
Jointing: None
Petrography: Textures: Intersertal texture and plagioclase and clinopyroxene have increased in number from subjacent inclined platy zone.
Microphenocrysts: Microphenocrysts are parallel to the plane of the flat crenulated vesicles. Modal percent of microphenocrysts is 11.2%; plagioclase (8.9%) and clinopyroxene (2.2%).
Vesicles: Vesicles are concentrated in zones when observed in thin section. Modal percent of vesicles increased to 7.8%.

Field characteristics were from vertical and horizontal traverses through an explosion structure described in appendix C and field notes at the outcrops. Petrographic characteristics are from appendix B.

TABLE III CONTINUED

SUMMARY OF FIELD AND PETROGRAPHIC CHARACTERISTICS FOR

THE ZONES OF A FIRST COOLING UNIT

Zone	Field characteristics followed by Petrographic characteristics
Vesicular bands	Field: Zone composed of basalt containing planar bands of vesicles, that compose up to 60 percent of the rock and the bands are parallel to the joints of the inclined platey jointed zone. These vesicular bands have various thicknesses, but commonly up to 1 cm thick. Vesicles within the bands range from large (up to 10 mm in diameter) to small (2 mm in diameter), but are nearly circular in form. Large vugs, up to 50 mm long, are highly irregular to ellipsoidal in shape and the longest axis is parallel to the tilt of the subjacent inclined platy jointed zone. Grades upward into overlying zone. Thickness: 1 m Jointing: None Petrography: Textures: Very poorly to poorly developed intergranular-textures in which vesicles are concentrated in bands. Microphenocrysts: Modal percent is 1.3% for plagioclase; clinopyroxene is observed in the thin section. Vesicles: The modal percent of vesicles increases to 23.0 % from the subjacent sheared vesicular zone.
Vesicular zone	Field: Zone consists of highly vesicular basalt and vesicles compose up to >60 % of the rock. Vesicles range from circular (up to 2 mm in diameter) to larger ragged vesicles (up to 7 mm in diameter). Small pockets of reddish-purple colored basalt are found as twisted/swirled forms towards the gradational contact with the superjacent zone. Thickness: 2 m Jointing: None Petrography: Not determined
Scoria breccia	Field: Scoriaceous breccia composed of a subjacent layer of matrix-supported, reddish purple-colored clasts in black-colored basaltic matrix that grades into a superjacent layer of clasts-supported reddish purple-colored clasts. Clast shapes range from rounded to sharp and generally are larger, up to 50 mm in diameter, in the matrix-supported layer and decrease in diameter to 30 mm in the superjacent, clast-supported layer. Thickness: 4 m Jointing: None Petrography: Not determined

Field characteristics were from vertical and horizontal traverses through an explosion structure described in appendix C and field notes at the outcrops. Petrographic characteristics are from appendix B.

example of a skewed-cross grain consists of a single lath of plagioclase. Two grains of clinopyroxene project away from either side of the plagioclase grain at acute angles near the middle of the plagioclase lath. The two projecting grains lie in the same plane and often have similar optical extinction patterns. The reverse case also can be viewed in thin section, where the central lath is a clinopyroxene grain. These skewed crosses and glomero-microphenocrysts of plagioclase and clinopyroxene have been observed in many of the intraflow zones in both cooling units (complete petrographical information in Appendix B).

Above the pahoehoe base, each successive zone grades upward into the overlying zone (Figure 10) (Table III). Intersertal textures are found in the inclined platy-jointed zone. Sparse vesicles occur within this zone, but the number of vesicles greatly increases in the overlying zones: sheared vesicular, banded vesicular, and vesicular zones. Vesicle shapes change from the inclined platy-jointed zone where sparse vesicles are small and spherical, to elongated vesicles in the three superjacent zones. The vesicles are not randomly distributed as in the inclined platy zone, but are grouped into layers or bands in sheared vesicular and vesicular bands zones. Vesicle shapes range from planar to crenulated in the sheared vesicular zone and range from spherical to irregular in the vesicular bands zone. Petrographic textures in the sheared vesicular and banded vesicular zones have that range from intersertal to very poorly to poorly developed intergranular. Microphenocrysts and microlites are arranged parallel to the

ZONES

SCORIA BRECCIA

VESICULAR ZONE

VESICULAR BANDS

SHEARED VESICULAR ZONE

INCLINED PLATY ZONE

CHILLED PAHOEHOE BASE

RED BAKED CLAY ZONE

UP TO 10 m
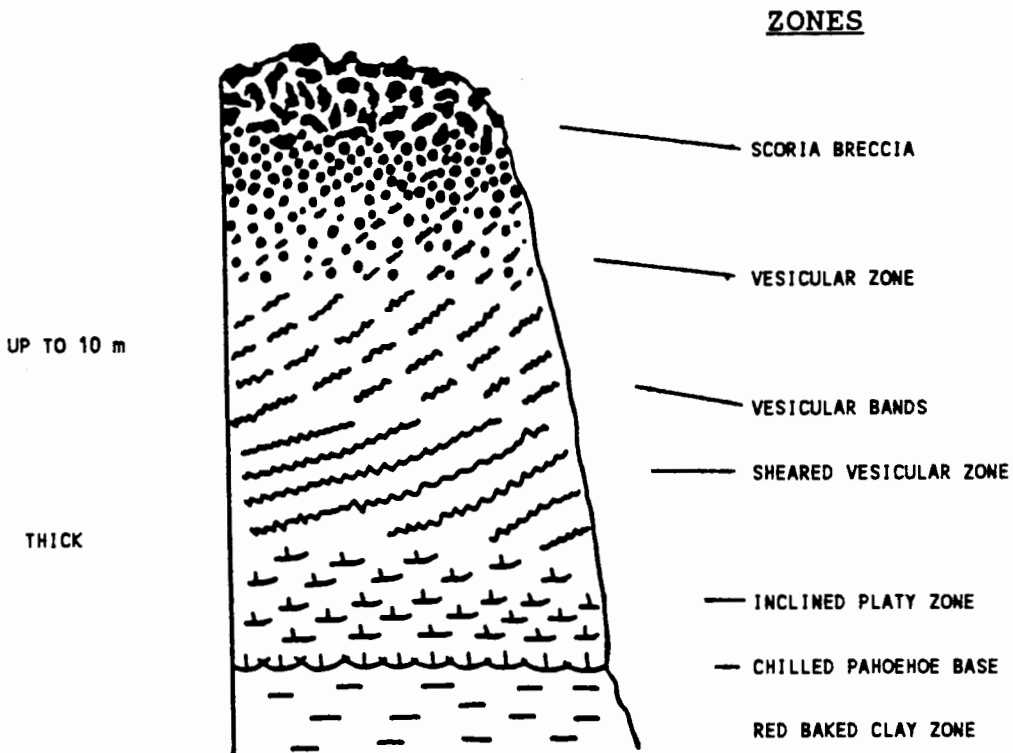
THICK

Figure 10. Generalized schematic of the first cooling
unit parallel to the plane of the central spine.
Intraflow zones are shown in detail as each zones grades
upward into the superjacent zones. The vertical thickness
of each intraflow zone is generalized. The actual
thicknesses are recorded in Table III.

alignment of the vesicles within the sheared vesicular zone.

In summary, a transition occurs at the base of the cooling

units from the vitrophyric textures to poorly developed

intergranular textures in the banded vesicular zone. The modal

percentages of microphenocrysts of plagioclase and clinopyroxene

decrease from the pahoehoe base, where microphenocrysts are the most

abundant. The modal percentage of vesicles increases from sparse in

the inclined platy-jointed zone to 23% in the vesicular bands zone.

Distribution of vesicles is random only in the inclined platy zone,

whereas in the other four zones, vesicles occur in distinct

patterns.

A scoriaceous breccia caps the first cooling unit. The

scoriaceous breccia grades from a lower matrix-supported breccia to

an upper clast-supported breccia. Clast sizes decrease from the

lower matrix-supported breccia to the upper clast-supported portion.

This scoriaceous breccia zone is the thickest zone of the first

cooling unit and is approximately twice the thickness of any of the

subjacent zones.

The second cooling unit is also subdivided into zones; however

markedly different zones occur in the upper portion of the unit

(Figure 11 and Table IV). The lower zones of the second cooling
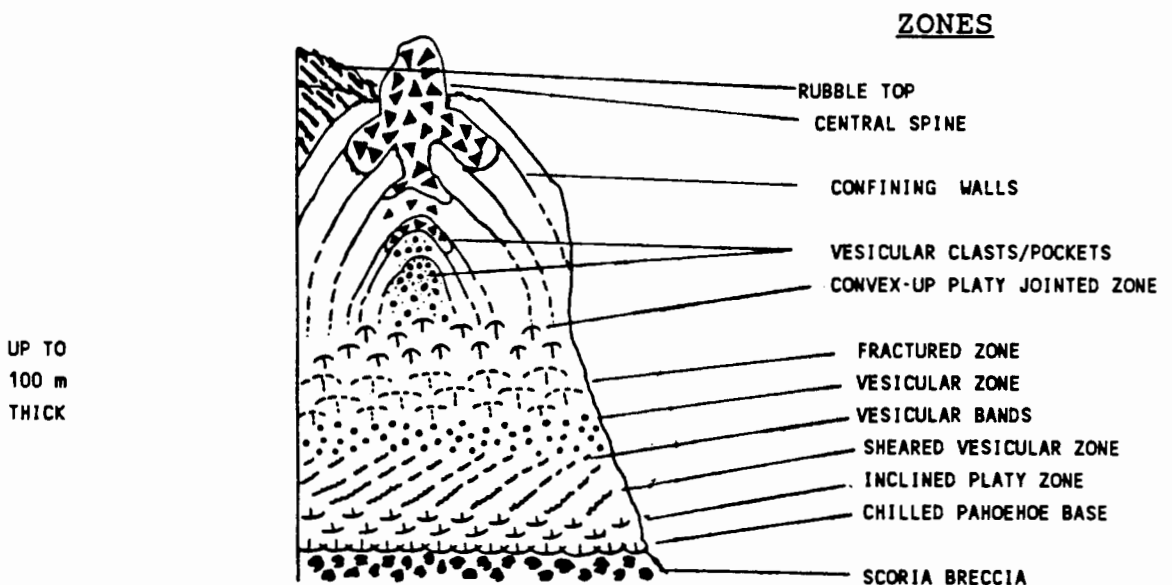
Figure 11. Generalized schematic of the second cooling unit
viewed perpendicular to the plane of the central spine.
Intraflow zones are shown in detail including similar basal
zones to first cooling unit. The vertical thickness of each
intraflow zone is generalized. The actual thicknesses are
recorded in Table III.

TABLE IV

SUMMARY OF FIELD AND PETROGRAPHIC CHARACTERISTICS FOR

THE INTRAFLOW ZONES OF A SECOND COOLING UNIT

Zone	Field characteristics followed by Petrographic characteristics
Chilled Pahoehoe base	Field: Similar field characteristics to first cooling unit. Thickness: 6 cm Jointing: None Petrography: Textures: Similar to first cooling unit. Micropenocrysts: Modal percent is 0.5% Vesicles: Modal percentage is 1.6%.
Inclined platy zone	Field: Similar field characteristics to first cooling unit. Thickness: .2 m Jointing: None Petrography: Not determined
Sheared vesicular zone	Field: Similar field characteristics to first cooling unit. Thickness: .1 m Jointing: None Petrography: Not determined
Vesicular bands	Field: Similar field characteristics to first cooling unit. Thickness: .1 m Jointing: None Petrography: Not determined
Vesicular zone	Field: The vesicular zone consists of basalt containing vesicles which account for 40 to 60 percent of the rock. Vesicles are randomly distributed within this zone and are circular to slightly elongate with diameters from 2 mm, generally circular, to 10 mm, generally elongate. Thickness: $\leq$.3 m Jointing: None Petrography: Not determined
Fracture zone	Field: Zone is composed of highly fractured undulating platy jointed basalt. Individual plates are up to 150 mm in thickness and cut by irregular vertical fractures. This zone grades upward into the superjacent zone. Thickness: $\leq$ 20 m Jointing: Joints are parallel to the unduating base of the second cooling unit. Petrography: Not determined

Field characteristics were from vertical and horizontal traverses through an explosion structure described in appendix C and field notes at the outcrops. Petrographic characteristics are from appendix B.

TABLE IV CONTINUED

SUMMARY OF FIELD AND PETROGRAPHIC CHARACTERISTICS FOR

THE INTRAFLOW ZONES OF A SECOND COOLING UNIT

Zone	Field characteristics followed by Petrographic characteristics
Convex-up platey zone	Field: Zone grades from the underlying zone and individual plates are not cut by the irregular vertical fractures as in the underlying fractured zone. Individual plates have similar sizes as in the underlying zone, but are shaped with convex plane pointed upward. Away from an explosion structure, this zone grades and merges into a platy jointed zone in the unbrecciated flow areas. Thickness: 7 m Jointing: Joints are convex-up. Petrography: Textures: Black-colored bands or layers of different textured basalt that range from vitrophyric to very poorly developed intergranular textures. Bands or layers can twist, swirl, pinch, and swell. Microphenocrysts: Modal percentages of microphenocrysts for plagioclase are 1.5% and 0.3% for clinopyroxene. Vesicles: None
Vesicular clasts/pockets and confining walls	Field: Dense glassy basalt forms arch-shaped limbs that enclose either pockets of vesicles or clasts containing vesicles. Vesicles are contained in either reddish purple-colored and or black colored basalt. Individual vesicular clasts or pockets can be up to 100 mm zone in diameter and have circular to elongated vesicles with diameters up to 5 mm. Vesicles can be partially filled with yellowish-green material. The number of vesicular clasts or pockets increases upward towards the central spine. Initially, lower in this zone, few vesicular pockets cut across the confining walls, but are enclosed and concentrated in small bodies at the top the arch. Upward through this zone, vesicular clasts cut the confining walls in greater numbers at the area near the top of the arch, finally grading into enclosed bodies of breccia. The vesicular clasts or pockets zone grades upward into the central spine zone. Thickness: Vesicular clasts/pockets zone can be up to 30 m thick, while the confining walls can continue upward to the overlying contact. Jointing: Jointing patterns are vertical in the areas away from the center of the explosion structure, but each joint trace tilts to horizontal in the center of the explosion structure. At the center of the arch in the lower portion of this zone, the joints pinch and swell around a choatic arrangement of plates compose of welded fragments. Surface features resembling ripple-like marks are observed on the individual plates. Petrography: Texture: In the black-colored confining walls, similar bands, layers, and spheres of different textured basalt as in the convex-up platy zone are repeated. Confining walls adjacent to the trapped body of vesicular clasts or breccia again have different textured basalt, bands or layers or spheres, but the individual textures can be colored either red or black. Red-colored textures are generally intergranular, while black-colored textures are typically vitrophyric to intersertal. In the trapped bodies of vesicular clasts and breccia, similar differing textures are found, but distinct clasts occur interwoven in the different textures and the different textures can be either red or black in color. The intensity of the deformation of the individual textures is more pronounced.

Field characteristics were from vertical and horizontal traverses through an explosion structure described in appendix C and field notes at the outcrops. Petrographic characteristics are from appendix B.

TABLE IV CONTINUED

SUMMARY OF FIELD AND PETROGRAPHIC CHARACTERISTICS FOR

THE INTRAFLOW ZONES OF A SECOND COOLING UNIT

Zone	Field characteristics followed by Petrographic characteristics
	Microphenocrysts: Modal pecentage of microphenocrysts is highest in the confining walls typically above 1.5%, while in the enclosed bodies modal percentage is below 1.5%. Vesicles: Vesicle abundance is largest in the enclosed bodies of vesicular clasts/pockets or breccia (15.1%). Vesicle shapes in the enclosed bodies form irregular tears, while in the confining walls adjacent to these trapped bodies, vesicles shapes are planar and crenulated. Intraclast vesicles of the enclosed bodies are spherical to enlongate and sharply contrast with the vesicles tears surrounding the clasts.
Central spine	Field: Central spine is composed of an inner core of clast-supported breccia, which grades outward into a matrix-supported breccia. Clast sizes range from blocks up to 1.5 m across in clast-supported core to lapilli sizes in the outer matrix-supported breccia. Clast types range from predominantly brecciated types to vesicular or scoriaceous and rare Pahoehoe types. Jointing is predominantly horizontal or convex-up. A central spine can continue to the superjacent contact and project above the surrounding flow-top breccia at some localities (stratigraphic section Elloit farm (EF)). Thickness: Vertical thickness varies from 1/2 to 1/3 of the second cooling unit thickness. Jointing: Convex-up to horizontal in the lower third of the central spine and massive in the upper portion of the central spine. Petrography: Not determined
Rubble top	Field: A zone containing flow-top breccia clasts and clasts from the explosion structure. Flow-top breccia clasts are scoriaceous, reddish-colored basalt and generally less than block sized. Clasts from the explosion structure are similar to types found in a central spine or are broken and weatered fragments of the confining walls. Thickness: This zone is typically thicker adjacent the explosion structure (15 m) grading laterally into the flow-top breccia. Jointing: None Petrography: Not determined

Field characteristics were from vertical and horizontal traverses through an explosion structure described in appendix C and field notes at the outcrops. Petrographic characteristics are from appendix B.

unit grade laterally away from the explosion structure into a

vesicular base that underlies a non-vesicular, platy-jointed zone.

The textures at the lower contacts of unbrecciated and non-

brecciated flow areas are markedly different from the chilled

pahoehoe base within brecciated flow areas. The surface textures are rough and vesicular rather than smooth and non-vesicular (Figure 12).

Intersertal textures are found in the basal contact zone of

Figure 12. A vesicular sample of the base from a non-brecciated flow area that shows a rough surface texture. This sample is quite different from the chilled Pahoehoe base in brecciated flow areas that are nonvesicular and have smooth surface textures. The ruler is approximately 15 cm long.

unbrecciated to non-brecciated flow areas and grade upward into the intergranular-textured interior of the flow. The intergranular texture is better developed within unbrecciated and non-brecciated flow areas than within the confining walls of an explosion structure where poorly intergranular-textured bands are present. The most

well-developed intergranular texture occurs in the non-brecciated
flow areas. The abundance of microphenocrysts in unbrecciated flow
areas is initially high within the basal contact zone (17.0%), but
decreases and remains fairly constant through the interior of the
flow (averaging nearly 3.9%). The abundance of microphenocrysts
within non-brecciated flow areas is fairly constant at 3.5% while in
brecciated flow areas the abundance of microphenocrysts, vesicles,
and groundmass varies.

The zones that overlie the basal portion of the second cooling
unit are varied and contain the most prominent breccia features in
the flow. A highly fractured zone overlies the vesicular zone; this
zone is platy jointed. Individual plates are cut by vertical
fractures and the vertical fractures pinch and swell in irregular
patterns. This fracture zone grades upward into another platy-
jointed zone, the convex-up platy zone, where individual plates have
convex-upward shapes. The convex-up platy zone is laterally
discontinuous, but grades laterally away from an explosion structure
into a thick platy jointed zone.

The jointing pattern changes in the vesicular clasts/pockets
and the confining walls zones from platy-jointing within the
underlying convex-up platy zone to a joint pattern in the shape of
an arch (Figure 11 and Table IV). The orientation of the joints is
determined from the relative position within these two zones.
Typically, joints are horizontal near the center of an explosion
structure and vertical along the periphery. Surface features that
resemble ripple marks are seen on the joint surfaces in each of

these locations (Figure 13). The basaltic arms at the center of the arch and in the lower portion of these two zones are composed of

Figure 13. Samples from the confining walls zone showing the ripple-like marks along the joint traces. The two samples were collected from different locations with the Troy flow, but display similar patterns. The upper left sample has two parallel surfaces. A view parallel to the surface is seen in the center sample (a piece of the larger sample). The ruler is approximately 15 cm long.

plates consisting of welded fragments. These fragments are coated with clear-colorless, mammillary material and the individual surfaces of each plate have ripple-like textures (Table IV and Figure 14). These ripple-like marks are similar to ripple-like textures observed along the joint traces.

Vesicular pockets concentrate in bodies enclosed between

Figure 14. A single plate composed of welded fragments
(the dark colored basalt). The plate was collected from
the apex portion of the arch that is formed by the
confining walls. Sample location is below the first
appearances of vesicular clasts and pockets. Suface
textures resembling ripple marks can be seen along the top
surface as small ridges. The ruler is approximately 15 cm
long.

black-colored basaltic arms near the center of an explosion

structure (Figure 11). Vesicular pockets increase in number and

size upward in an explosion structure and grade into vesicular

clasts. Vesicular clasts are observed as a train of clasts cutting

through the superjacent basaltic arms at the center of an arch and

gathering in enclosed bodies of reddish-purple-colored breccia

(Figure 15 and Figure 11). Reddish-colored basaltic arms enclose

these bodies of breccia and grade into adjacent black-colored arms.

Figure 15. A scoriaceous clast observed within confining walls near the apex that includes several less distinct vesicular clasts. Collectively these vesicular clasts form a train between superjacent and subjacent enclosed bodies of vesicular clasts. Tape measure is approximately 11 cm long.

These differently colored basaltic arms are locally fragmented and become incorporated into the reddish-purple-colored breccia.

Petrographic evidence indicates a boundary occurs between a clast or a pocket and the surrounding basalt, but becomes evident in hand samples only in the upper portion of these zones as a dark reddish-colored rind. The black-colored basaltic arms enclosing vesicular pockets consist of vitrophyric to very poorly developed intergranular-textured basalt. The textures occur as thin intercalated bands or layers of poorly developed intergranular-textured basalt and vitrophyric-textured basalt. These bands or

layers can have twisted, swirled, pinched and swelled patterns
(Figure 16). The basaltic arms adjacent to the enclosed bodies of
breccia consist of similar intercalated bands; however both types of
bands are visibly reddish-purple.
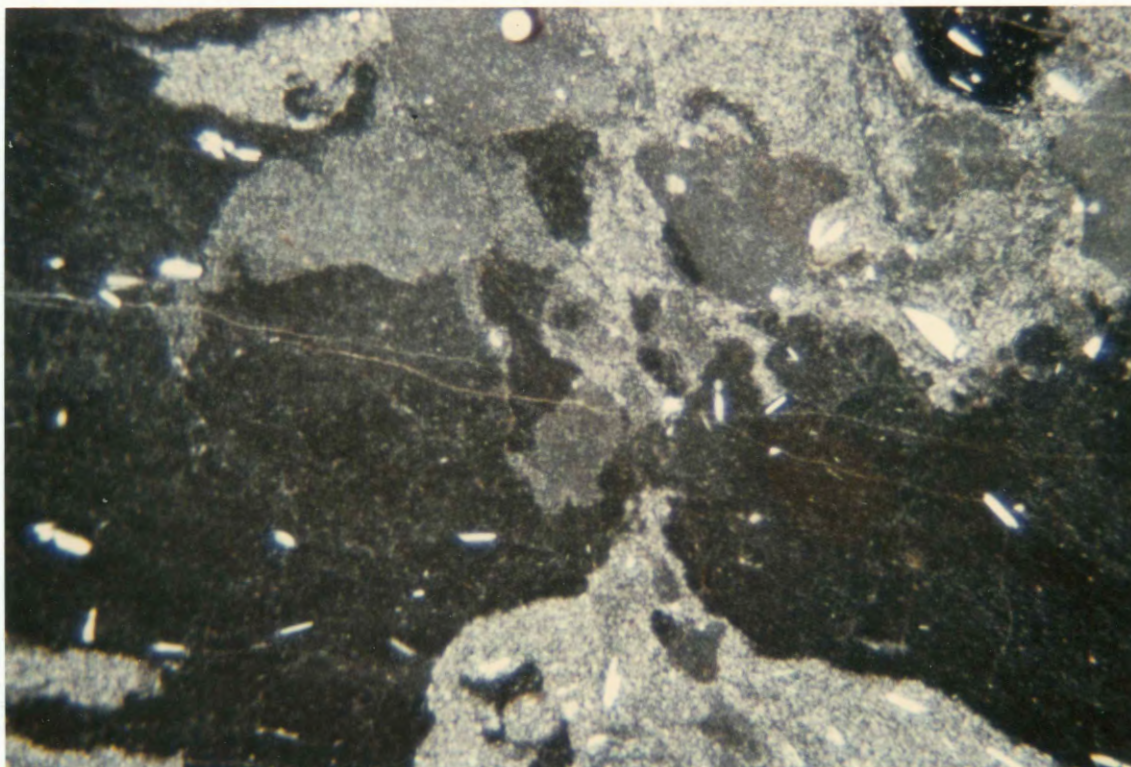
Figure 16. Petrographic textures in a sample from a
basaltic arm that shows the twisting, pinching, swelling,
and swirling of the individual bands or layers. Textures
range from intergranular (lighter colored) to vitrophyric
(dark colored). The view is approximately 1 cm across.

The transition from black-colored arms to reddish-colored arms
is marked by planar bands of poorly developed intergranular-textured
basalt, visible as reddish-colored bands, intercalated with black-
colored bands of vitrophyric-textured basalt (Figure 17). These
bands can be less than 2 mm in thickness. Microphenocrysts of

plagioclase are more abundant in reddish, intergranular-textured

bands and are aligned parallel to the planar boundaries of the

individual bands.
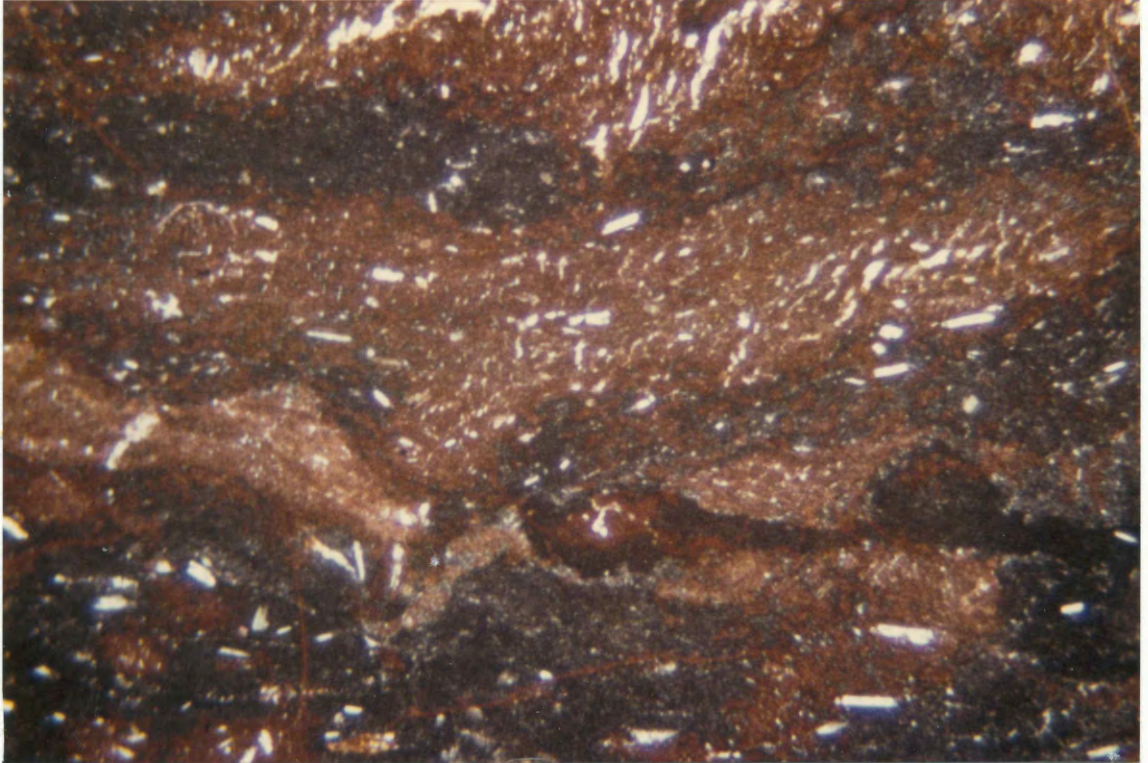
Figure 17. Petrographic textures showing the reddish-
colored intergranular bands and the black-colored
vitrophyric to intersertal bands. Vesicle tears (light
colored) are evident in the intergranular bands as
irregular wavy shapes especially in the center and upper
reddish colored bands. The view is approximately 1 cm
across.

The bodies of breccia in these settings are composed of

matrix-supported clasts of reddish-purple-colored or black-colored,

non-vesicular to vesicular to scoriaceous basalt in reddish-purple-

colored basalt matrix (Figure 18). The size of the clasts varies

from 30 mm in diameter to 2 mm. The petrographic textures of the

clasts within the breccia bodies range from textures similar to the black-colored basaltic arms to the reddish-colored arms. The abundance of vesicles within individual clasts varies. Vesicle shapes are spherical to elongated in the clasts; however vesicles within the matrix occur as irregular tears (similar to vesicle tears in Figure 18). The reddish-colored supporting matrix consists of bands or layers with vitrophyric to intergranular textures, but the chaotic patterns of these bands or layers is more pronounced than in the basaltic arms.

Figure 18. Two samples from a trapped body of breccia. The weathered surface of the right sample shows the outline of the individual clasts. The clasts in the center of this sample are non-vesicular, but a clast to the left of this one is vesicular. The matrix is better seen in the sample to the left and is reddish in color. The ruler is approximately 15 cm long.

Farther upward, these enclosed bodies of breccia grade into a central spine zone of an explosion structure (Figure 11). The central spine in the lower portion of this zone may have confining walls or single basaltic arms that penetrate into the spine (Table IV). These projections terminate into fragments and are incorporated into the breccia along the peripheral margin of a central spine. The confining walls or arms typically contain vesicular clasts adjacent to the spine and then grade laterally into black dense basalt that lacks vesicular clasts or pockets.

Confining walls may extend upward to the contact with the overlyed basalt flow. The confined walls in this upper portion of an explosion structure become fragmented into small spheroids with diameters up to 10 mm. The fragments are surrounded by a distinctly black-colored matrix and weathering accentuates the color differences in the field (Table IV and Figure 19).

Petrographic differences show a textural change from the spheroids to the darker matrix. Textures range from vitrophyric to intersertal in the black-colored matrix and very poorly developed intergranular in the spheroids. The color change observed in the field is related to these different textures. The vitrophyric to intersertal textures occur in alternating crenulated bands or layers that terminate in a swirled pattern. The intergranular textures occur as distinct spheroids within the other two textures. The abundance of microphenocrysts of plagioclase changes between the dark colored matrix and the spheroids, increasing abruptly in the intergranular textures. This rock is easily weathered into

Figure 19. Two samples from the confining walls of an explosion structure showing differnt colored layer of basalt. These samples were collected near the contact with the overlying flow. The darker colored layers or streaks have greater proportions of glass, while the lighter basalt is more crystalline. The ruler is approximately 15 cm long.

fragments and these fragments occur within the sloped rubble top of an explosion structure.

A central spine is matrix-supported along the peripheral margins and within the lower portion of a spine. Individual clasts are elongate parallel to the sharp contact trace between the central spine and the adjacent confining walls. The resistant matrix-supported margin grades into a less resistant inner core of clast-supported breccia (Figure 20). Typically the inner core of breccia

has been removed by erosion leaving a "v-shaped" notch in a central

spine. Generally, field textures of the clasts are non-vesicular,

aphyric basalt that may be red to black in color in the outer

matrix-supported margin. In the inner clast-supported core,

vesicular to scoriaceous-textured clasts increase in abundance.

Clasts range from rare vesicular to scoriaceous blocks, up to .63 m

across, in the clast-supported breccia core to lapilli-sized clasts

in the outer matrix-supported breccia.

Figure 20. A transition to larger diameter clasts occurs
from the outer matrix-supported breccia (left side) to the
inner clast-supported breccia (right side). The largest
clasts (bottom left) are composite type clasts. The
wooden frame is 2x2 feet square.

Clast types were separated into two size categories, less than

64 mm and greater than 64 mm. Lapilli-sized clasts were more

difficult to count, because of the lichen cover on the outcrop

surface. Three major types of clasts were used in the three counted traverses through both matrix and clast-supported breccias in a central spine (Figure 21). 1) A composite-type clast of welded fragments of non-vesicular to vesicular basalt in a reddish-purple-colored basalt matrix occurring as a single clast (BVA) (Table V).

Figure 21. An assortment of three major clast types: pahoehoe clast (6), scoriaceous clasts (2,3), vesicular BVA (1), and nonvesicular BVA (4,5). Clast (4) shows intraclast cracks and fractures and clasts (5) has a rind of finely brecciated fragments. The ruler is approximately 15 cm long.

The reddish matrix can be twisted, swirled, or stretched around the black to reddish-colored fragments. Intraclast cracks and fractures are often filled with fused finely brecciated fragments of basalt.

A rind of finely brecciated fragments of black aphyric basalt and reddish-purple-colored matrix can be found on some of the block-sized clasts. 2) Scoriaceous-type clasts composed of black or reddish-colored scoriaceous basalt. 3) Pahoehoe-type clasts with ropey surfaces similar to Hawaiian pahoehoe flow-tops (Wentworth and others, 1953).

TABLE V

SUMMARY OF PERCENTAGES FOR CLAST TYPES ENCOUNTED DURING COUNTING TRANSVERSES

Type of Support!	Type of clast										!
	BVA		!	S		!	PAH		!	SP	!
	<64mm	>64mm	!	<64mm	>64mm	!	<64mm	>64mm	!	<64mm	>64mm	!
Matrix	86	4		6	4		0	1		- -	- -	
*Matrix	89	11										
Clast	62	9		19	5		0	2		1	1	

CLAST DESCRIPTIONS :

BVA - Clast is a composite of clasts or fragments of black vesicular or non-vesicular, vitrophyric to intergranular-textured basalt with a reddish purple colored basaltic matrix. The matrix can be twisted, swirled, or stretched into layers that can be cracked or fractured. The cracks can contain very small fragments of rock, $\leq$ 1 mm in size. Some block-sized clasts are coated with a fused layer, up to 1 mm thick, of finely brecciated black-colored basalt and reddish-purple-colored matrix. Shapes of clasts range from sharp angular to planar to agglutinated froms. Rare empty interclast voids.
S   - Clast composed of black or reddish colored scoriaceous basalt. Scoriaceous clasts show two types of either randomly placed vesicles through the clast or vesicles are concentrated in inflated vesicular margins. Shapes of clasts range from subrounded forms for the random vesicle type to plate-shaped forms for the inflated type of clast.
PAH - Clast composed of vesicular basalt with vesicles that are elongated and twisted parallel to the surface shape of the clast. Vesicles are up to 50 mm long, 2 to 3 mm thick, and up to 20 mm wide with vesicles often filled along the peripheral surface by dark green material. Clasts are colored blue gray internally and grade outward from yellow green to an orange-brown rim. Clasts have ropy surface texture. Clast shapes have generally plate-like forms.
SP - Measurement of void space difficult to measure with 100 foot line method.

*Clasts were differentiated by size and not type.

The percentage of clasts from highest to lowest within a central spine are the composite-type (BVA), scoriaceous clasts, and pahoehoe clasts. Commonly, the size of the clasts is in the lapilli range ($\leq$64 mm). The size of intraclast voids were measured,

however, since voids in the breccia are three-dimensional features and irregular in shape, the void space was difficult to measure. A change in the distribution of clast-types occurs from the outer matrix-supported breccia to the inner clast-supported core. Composite-type clasts are predominant in both breccias, but the abundances of scoriaceous and pahoehoe-type clasts increase in the inner clast-supported core (Table V).

A central spine widens upward, the walls become less defined, and the breccia merges into a rubbly flow-top (Figure 11). Within the rubbly flow-top, clasts of composite (BVA), vesicular and non-vesicular clasts, scoriaceous clasts, and basaltic bombs are present. Clasts of the composite type (BVA) greatly increase in number within the upper portion of a central spine. Away from an explosion structure, a thick flow-top breccia is present and grades downward into the main body of the flow through scoriaceous and vesicular zones. The base of the flow-top breccia undulates and is at its lowest level within the flow adjacent to an explosion structure.

GEOCHEMISTRY

Samples were collected in conjunction with stratigrahic measurements or were collected from different textural zones during horizontal and vertical traverses (Appendix A for stratigraphic samples and Appendix D for traverse samples). Various samples were analyzed by three methods: INAA, Mossbauer spectroscopy, and XRF (Table VI and Appendix E for preparation). All analyzed samples

were analyzed by INAA; XRF was used on selected sets of brecciated, unbrecciated, and non-brecciated flow areas from the total sample set. Mossbauer spectroscopy was applied to a sample set at the interface of a trapped body of reddish-colored breccia and the adjacent confining walls.

Thirty-two samples were collected in five sample sets. Each sample set represents a complete or partial traverse within the three types of flow areas, brecciated, unbrecciated, or non-brecciated. Twenty-two samples were collected through portions of either brecciated, unbrecciated, or non-brecciated flow areas, in the Troy flow. A special six sample set from these twenty-two samples was collected across an interface between a central spine and the adjacent confining walls of the Troy flow. A set of six samples, Squaw Canyon (SC1), was collected from a brecciated flow area of a Grande Ronde flow above the Troy flow. The position of each sample was recorded by the sample elevation within the flow and the textural features at that point. Since the Troy flow in the study area varies in thickness, each sample was given a relative position within a generalized model of the Troy flow; thus, comparisons were made between these corresponding sets of samples (Table VII). Each sample from the Squaw Canyon sample set was assigned a relative position based on similar textural characteristics with the brecciated flow area.

TABLE VI

SUMMARY OF SAMPLE LOCATION AND SAMPLE LABORATORY ANALYTICAL METHODS

Stratigraphic section label	Location 7 1/2 minute quadrangle	Sample label	Labatory analytical method			
			Thin section	INAA	XRF	Mossbauer
SC1	NW1/4SE1/4NW1/4	8-22-SC#1	Y	Y		
	Sect 35 T6N R43E	8-22-SC#2	Y	Y		
	Troy	*8-22-SC#2B		Y		
		8-22-SC#3	Y	Y		
		8-22-SC#4		Y		
Wenaha.C	SE1/4SE1/4SE1/4	8-20#1		Y		
	Sect 31 T6N R43E	8-20#2	Y	Y		
	Troy	8-20#3	Y	Y		
		8-20#4	Y	Y		
		8-20#5	Y	Y		
Wenaha.B	NE1/4SE1/4SE1/4	8-22-T1A1	Y	Y		Y
	Sect 31 T6N R43E	*8-22-T1AR		Y		
	Troy	8-22-T1A2	Y			
		8-22-T1A3	Y	Y		Y
		8-22-T1B	Y	Y		
		8-22-T1C	Y	Y		Y
WR	SE1/4NW1/4NE1/4	$M	Y	Y	Y	
	Sect 5 T5N R43E	M1	Y	Y		
	Troy	M2	Y	Y		
		M3	Y	Y		
		M4		Y		
		$N	Y	Y	Y	
		8-22#1C		Y		
		8-22#3C		Y	Y	
		8-22#4C	Y	Y	Y	
MC	NW1/4SE1/4NW1/4	&MC4D	Y	Y		
	Sect 3 T5N R43E					
	Troy					
GC	NE1/4SW1/4SW1/4	8-21#1CC		Y		
	Sect 24 T5N R43E	8-21#2C		Y		
	Troy	8-21#3C	Y	Y		
		8-21#4C		Y		
		8-21#5C	Y	Y		
EF	NW1/4NW1/4SE1/4	$8-21#2A	Y	Y	Y	
	Sect 9 T5N R43E	8-21#3A	Y	Y	Y	
	Troy	8-21#5A	Y	Y	Y	
		8-21#6A		Y	Y	
		8-21#7A	Y	Y	Y	
EF	NW1/4NW1/4SE1/4	8-21#3B		Y		
	Sect 9 T5N R43E	8-21#4B		Y		
	Troy					

Symbol * -- Selected red colored chips within breccia sample
Symbol $ -- Selected fresh chips
Symbol & -- Included in WR sample set

TABLE VII

EQUIVALENT SAMPLES COMPARING RELATIVE POSITIONS WITHIN A FLOW

Location label Sample labels	Flow type	Location label Sample labels	Flow type	Location label Sample labels	Flow type	Location label Sample labels	Flow type	Location label Sample labels	Flow type	Intra-flow Zones
Wenaha Ravine(WR)		Elloit Farm(EF)		Grouse Creek(GC)		Wenaha.C		Squaw Canyon(SC#1)		
MC4D	B					8-20#1	B	8-22-SC#4	B	CW
						8-20#2	B			CW
						8-20#5	B			CW
						8-20#4	B	8-22-SC#3	B	EB
								8-22-SC#2B	B	CW
8-22#4C	B					8-20#3	B	8-22-SC#2	B	CW
								8-22-SC#1	B	CW
8-22#3C	B	8-21#7A	U	8-21#5C	N					CP
N	B	8-21#6A	U	8-21#4C	N					BB
M4	B	8-21#5A	U	8-21#3C	N					VZ
M3	B									VB
M2	B	8-21#3A	U	8-21#2C	N					SV
M1	B									IP
M	B	8-21#2A	U	8-21#1CC	N					BB
8-22#1C	B									BB

Positions were established by the sample's relative position to either the corresponding cooling (first or second) and the field textural zone within that particular cooling unit. Sample elevations are shown in the stratigraphic measured section figures.

Symbols used in the above table

* -- samples are from a Grande Ronde flow, above the Troy flow.
B -- a brecciated flow area sample
U -- a unbrecciated flow area sample
N -- a non-brecciated flow area sample

Symbols used in intraflow zones

CW -- confining walls
EB -- enclosed breccia
CP -- convex-up platey jointed
VZ -- vesicular
VB -- vesicular bands
SV -- sheared vesicular
IP -- inclined platy jointed
BB -- basal chilled pahoehoe

INAA

Broad overall trends in INAA data were indentified between brecciated flow areas and unbrecciated to non-brecciated flow areas. If the concentration of an element within a sample set for any of the seventeen elements analyzed increases towards the base of the flow, the element was considered to be enriched. The element was considered to be depleted if the concentration decreases in the sample set towards the base of the flow. Certain elements were either enriched or depleted from the top of the Troy flow through the base of the flow. Generally, the unbrecciated and non-brecciated flow areas have similar enrichment or depletion trends towards the base of the Troy flow (Figure 22). In brecciated flow areas, the trends of enrichment or depletion are less pronounced than the trends in unbrecciated or non-brecciated flow areas (Figure 23). A statistical comparison bewteen a brecciated flow area (WR) and a non-brecciated flow area (GC) revealed seven elements have F values equal or greater than the critical value. Ten elements in unbrecciated and non-brecciated flow areas have higher variances than elements in brecciated flow areas (Appendix G).

Non-brecciated and unbrecciated flow areas (GC and EF) have similar transitions towards the base of the Troy flow for particular elements. K, La, Eu, and Ta are enriched and Fe and Co are depleted greater than 10% within the Troy flow. Sm is enriched less than 10% (Table VIII). The elements Hf and Ce are enriched and Th is depleted towards the base the Troy flow, but the overall differences between the concentrations from upper and lower samples within the

53
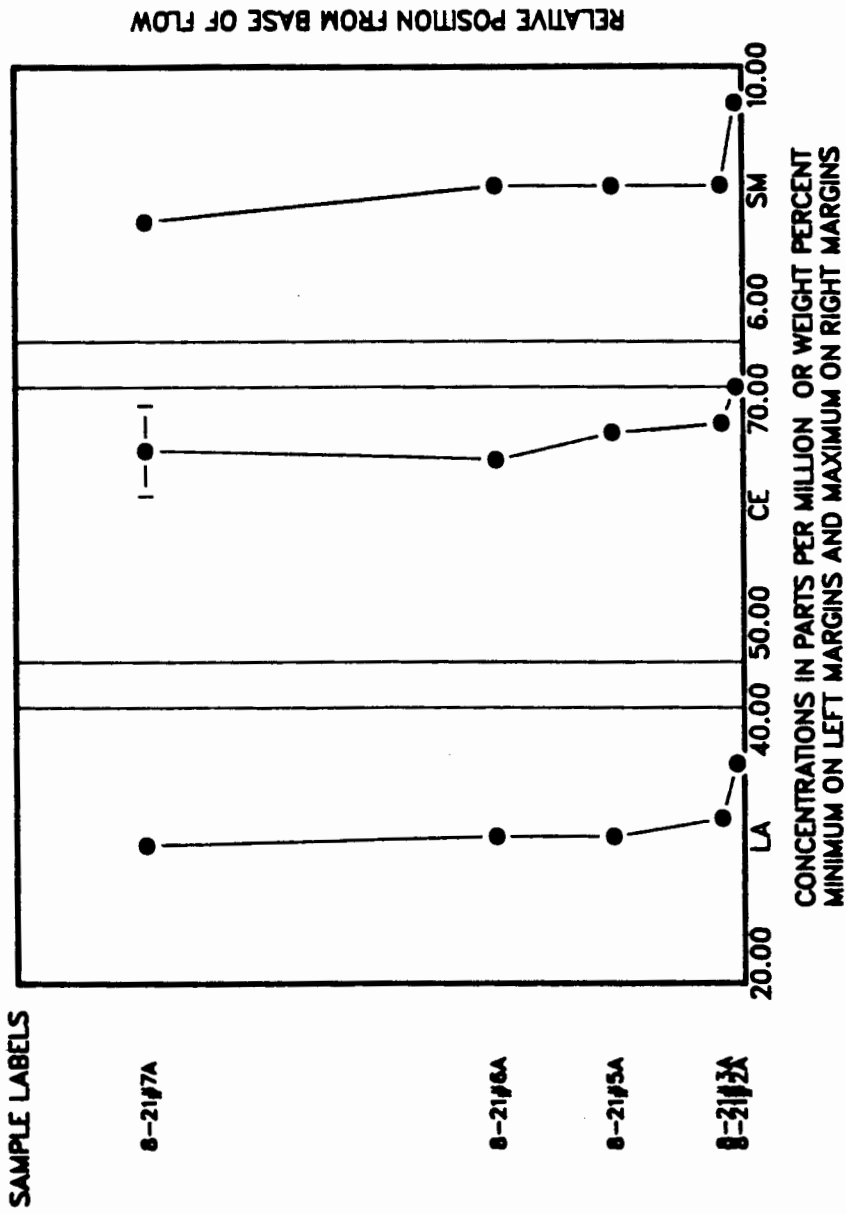
Figure 23. Concentration trends in brecciated flow areas for La, Ce, and Sm for a sample set from Wenaha Ravine showing less pronounced enrichment towards the base of the Troy flow. Error bars are included for each element, but are within the diameter of the solid circles for La and Sm.
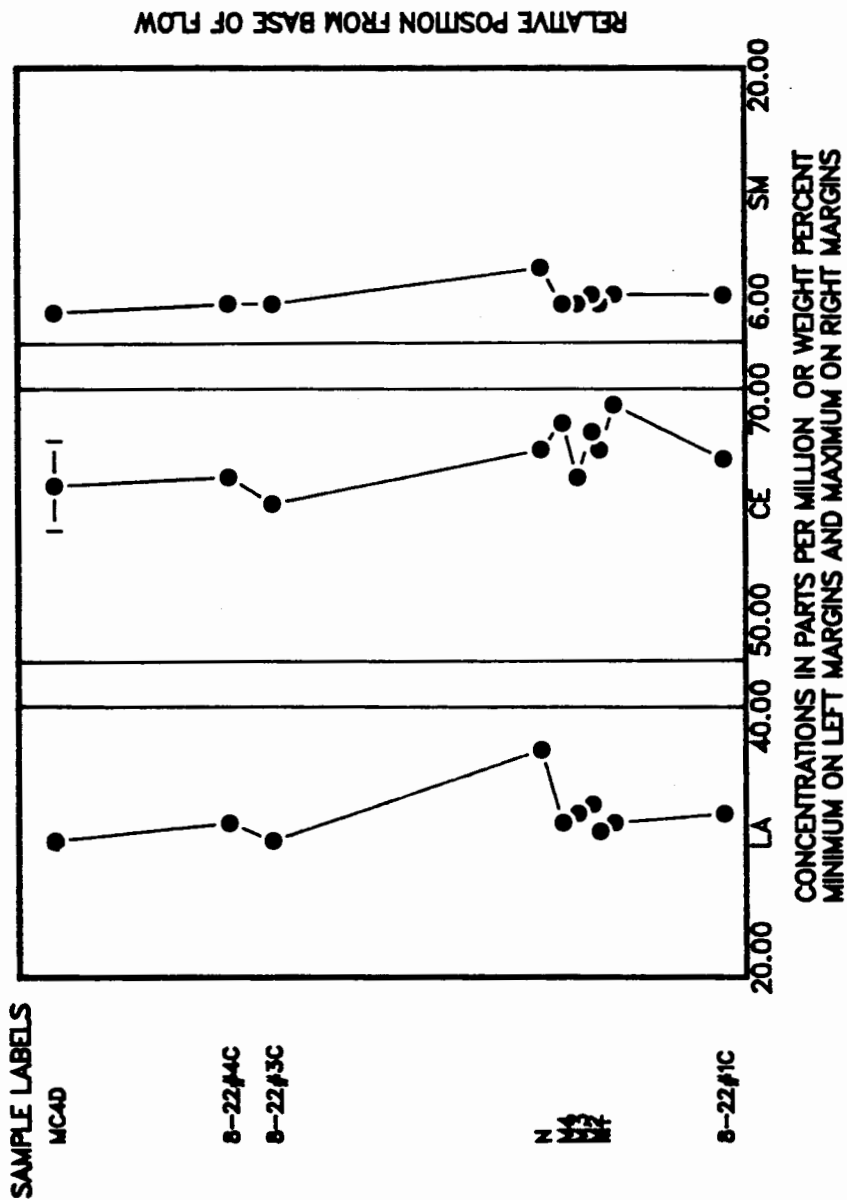
Figure 22. Concentration trends in unbrecciated flow areas for La, Ce, and Sm for sample location site Elloit Farm showing enrichment towards the base of the Troy flow. Error bars are included for each element, but are within the diameter of the solid circles for La and Sm.

TABLE VIII

SUMMARY OF ENRICHED OR DEPLETED ELEMENTS FOR SAMPLE SETS

Elements	Sample set label				
	GC	EF	WR	Wenaha.C	SC#1
K	E	E	D	E	
La	E	E		d	
Eu	E	E	e		
Ta	E	E		D^B	
Rb	E		D		
Sm	e	E			e
Ba		E	D		
Na	d	e	d	e	E
Tb			E		E
Ce	e	e^B	e	d	
Hf	e^B	e			
Sc		e	e		
Fe	D	D	d		e
Lu	D				
Co	D	D	D	D	
Th	d	d^B			

* Enrichment and depletion were calculated by substracting the concentration of an element of the lower sample from the concentration of the upper sample then dividing by the larger of the two sample concentrations. If the lower sample concentration was larger then the trend is considered enrichment and if the upper sample concentration was larger then the trend is considered a depletion.

B The element has a quotient equal to the maximum error of the entire sample set from the INAA analysis.

Symbols:
    Enrichment   > 10 % -- **E** $\leq$ 10 % -- e

    Depletion   > 10 % -- **D** $\leq$ 10 % -- d

flow are equal to the maximum error of the entire sample set. In equivalent brecciated flow areas (WR) within the Troy flow, Tb is enriched and Co, Ba, Rb, and K are depleted more than 10%. Ce, Sc, and Eu are enriched and Na and Fe are depleted less than 10%. Fe, Co, Ce, and Eu have similar transitions in all three types of flow areas towards the base of the Troy flow. The remaining six elements have contrasting transitions of enrichment or depletion towards the base between brecciated and unbrecciated to non-brecciated flow areas (Table VIII).

The sample set Squaw Canyon (SC#1) from a Grande Ronde flow stratigraphically above the Troy flow was collected within the upper portion of a breciated flow area. The set occurs at an interface between an enclosed body of breccia and the surrounding confining walls. An equivalent set of samples was collected in the upper portion of a brecciated Troy flow, Wenaha.B sample set. Comparisons between these data sets are not as conclusive as in the above three sample sets, because the geochemistry of the Troy flow differs from that of the upper Grande Ronde flow (Figure 24). Generally, few elements show enrichment or depletion greater than 10% towards the base of the flow, which matches the above trend of a brecciated flow area in the Troy flow.

A special sample, 8-22-SC#2B, was separated from the chips of sample 8-22-SC#2 that was collected at the interface of the enclosed bodies of breccia within a younger Grande Ronde flow above the troy flow (Squaw Canyon SC#1 sample set). Reddish-purple-colored chips were selected and analyzed. Concentrations in this special sample
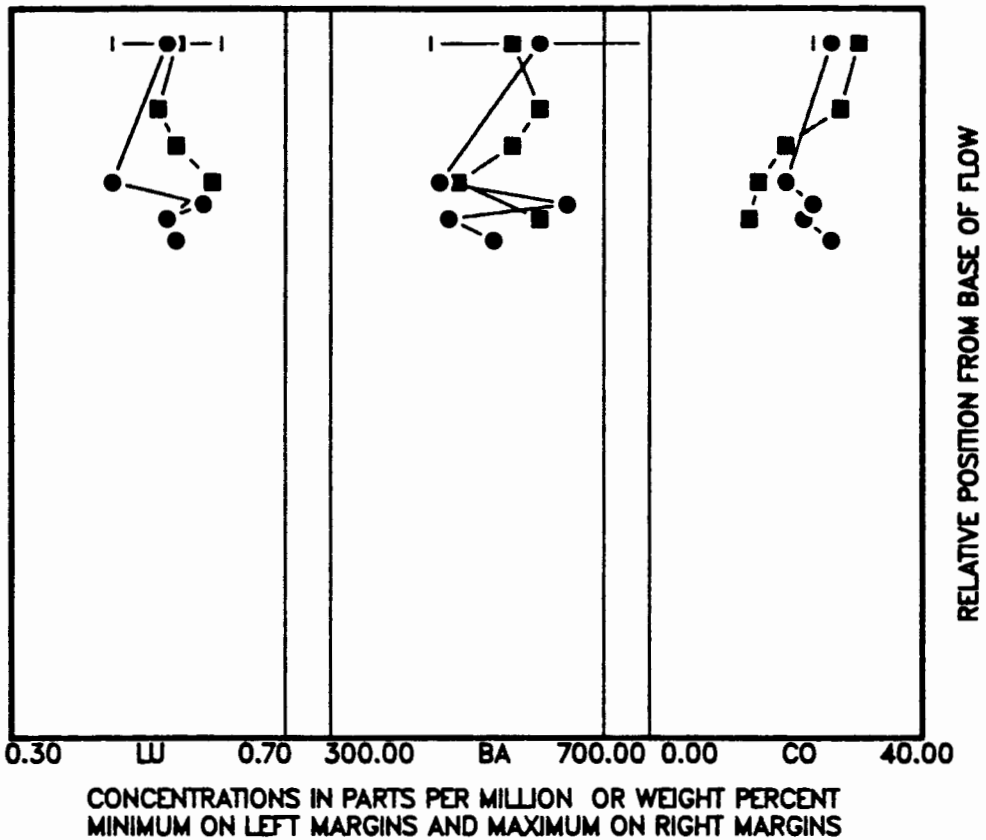
Figure 24. Concentration trends in brecciated flow areas for the Troy flow (■) and a younger Grande Ronde basalt flow (●) shows similar patterns towards the base of each flow. Error bars are included for each element.

do not conform to the trends established by the surrounding samples (Figure 25). Comparisons within this sample set SC#1 show the special sample has abrupt changes in concentration greater than the maximum error within the sample set (Table IX). In seven out of the seventeen elements, the special sample has either the highest or lowest concentration for that element within the entire sample set. Furthermore, one sample, 8-22-SC#3, was collected from the enclosed body of breccia immediately above this special sample (Figure 26).

Figure 25. Concentration trends in the sample set from Squaw Canyon (SC#1) showing the discrepancy caused by the special sample 8-22-SC#2B. Notice samples 8-22-SC#3 behavior compared to samples 8-22-SC#1 and 8-22-SC#4. Error bars are included for each element. This sample set was collected from a younger Grande Ronde flow than the Troy flow.

TABLE IX

INAA CONCENTRATIONS, EQUIVALENT DEPTHS, DEPTH IN FLOW, ELEVATION OF

SAMPLES FROM SAMPLE SET SQUAW CANYON #1 (SC#1)

SAMPLE LABELS	*DEPTH IN FLOW	$ELEVATION IN FLOW	LA	CE	SM
8-22-SC#1	&(33)82.00	2087	26.90	58.00	7.18
8-22-SC#2	(30)72.00	2097	26.60	56.00	6.83
8-22-SC#2B	(28)71.50	2097.5	25.80	52.00	7.08
8-22-SC#3	(25)71.00	2098	24.00	50.00	6.38
8-20-SC#4	(6)0.00	2169	26.40	56.00	7.10

LABELS			EU	TB	YB
8-22-SC#1			2.32	1.50	5.00
8-22-SC#2			2.24	1.40	6.10
8-22-SC#2B			2.30	1.20	4.70
8-22-SC#3			2.01	1.20	4.20
8-20-SC#4			2.38	1.30	4.90

LABELS			LU	BA	CO
8-22-SC#1			0.54	550.00	28.00
8-22-SC#2			0.53	480.00	24.00
8-22-SC#2B			0.59	660.00	25.00
8-22-SC#3			0.45	470.00	20.00
8-20-SC#4			0.53	610.00	27.00

LABELS			+FEO	+K_2O	HF
8-22-SC#1			12.45	1.80	5.20
8-22-SC#2			12.12	1.80	5.20
8-22-SC#2B			12.73	1.70	5.20
8-22-SC#3			10.89	1.80	5.10
8-20-SC#4			11.77	2.00	5.40

LABELS			+NA_2O	RB	SC
8-22-SC#1			3.44	47.00	36.32
8-22-SC#2			4.21	47.00	33.19
8-22-SC#2B			3.07	32.00	34.98
8-22-SC#3			3.09	42.00	31.76
8-20-SC#4			2.98	60.00	34.71

LABELS			TA	TH	
8-22-SC#1			0.49	5.70	
8-22-SC#2			0.44	5.20	
8-22-SC#2B			0.51	5.30	
8-22-SC#3			0.29	5.40	
8-20-SC#4			0.51	5.60	

&(xx) enclose equivalent depths used to compare concentrations against another sample set in a hypothetical flow of 100 feet thick.

* Depth in flow is calculated from field elevations during measurement of stratigraphic section

$ Elevation of the sample within the flow was measured during stratigraphic section or traverse measurements

+ Oxides concentrations in weight percent (iron is in total FeO) and remaining concentrations in part per million

8-22-SC#4

8-22-SC#3

8-22-SC#2B

8-22-SC#2

8-22-SC#1

<u>Figure 26</u>. A schematic showing the sample locations for sample set Squaw Canyon (SC#1) in a younger Grande Ronde basalt flow. Notice the position of samples 8-22-SC#1 and 8-22-SC#4 relative to sample 8-22-SC#3 in the breccia.

Sample 8-22-SC#3 has the lowest concentration within the entire set for thirteen of the seventeen elements (Table IX). A sample, 8-22-SC#1, was collected in the confining walls immediately below the special sample 8-22-SC#2B. Sixteen of the seventeen elements, except Fe, have higher concentrations within the confining walls than in the sample collected from the trapped body of breccia. Sample 8-22-SC#4 was collected from the confining walls near the superjacent contact with the overlying flow and above the special sample 8-22-SC#2B. Sixteen of the seventeen elements except Na, again have higher concentrations than the concentrations of the

sample 8-22-SC#3 (Table IX).

Another sample set, Wenaha.B, was similarily collected across
an interface between an enclosed body of breccia and the confining
walls in an explosion structure of the Troy flow (Figure 27). The
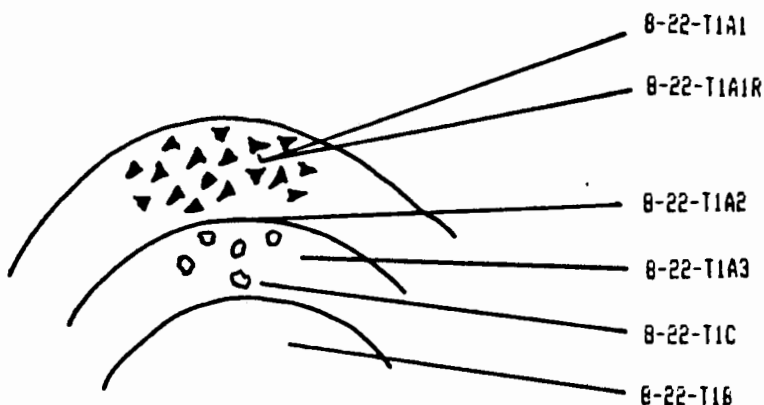
Figure 27. A schematic showing the sample locations for
sample set Wenaha.B in the Troy flow collected at the interface
between the confining walls and a trapped body of breccia.
Notice the positions of each sample relative the breccia sample
8-22-T1A1.

collection site is at the center of an arch formed by the confining
walls. At this site, the confining walls contain vesicular clasts.
Another special split sample was made from reddish-purple-colored
chips of the breccia sample, 8-22-T1A1. This sample, 8-22-T1A1R,
has either the highest or lowest concentrations for seven of the
seventeen elements: La, Sm, Tb, Yb, Hf, Na, and Th (Table X).
Comparisons within this entire sample set show an abrupt change in
the trends of elements, caused by this special sample (Figure 28).
This abrupt change is similar to the those noted in sample set SC#1.

TABLE X

INAA CONCENTRATIONS, EQUIVALENT DEPTHS, DEPTH IN FLOW, ELEVATION OF

SAMPLES FROM SAMPLE SET WENAHA.B

SAMPLES LABEL	*DEPTH IN FLOW	$ELEVATION IN FLOW	La	Ce	Sm
8-22-T1A1	1.00	2200	30.40	62.00	7.71
8-22-T1A1R	2.00	2199	31.40	63.00	7.80
8-22-T1A2	3.00	2198	30.90	65.00	7.97
8-22-T1A3	4.00	2197	31.40	61.00	8.04
8-22-T1B	5.00	2196	30.20	65.00	7.87
8-22-T1C	6.00	2195	30.50	62.00	7.77

LABELS			Eu	Tb	Yb
8-22-T1A1			2.31	1.60	4.50
8-22-T1A1R			2.33	1.40	4.50
8-22-T1A2			2.45	1.80	5.20
8-22-T1A3			2.39	1.60	5.20
8-22-T1B			2.45	1.40	5.10
8-22-T1C			2.44	1.60	4.90

LABELS			Lu	Ba	Co
8-22-T1A1			0.56	500.00	19.00
8-22-T1A1R			0.63	640.00	20.00
8-22-T1A2			0.54	630.00	23.00
8-22-T1A3			0.60	720.00	30.00
8-22-T1B			0.68	660.00	17.00
8-22-T1C			0.56	550.00	24.00

LABELS			+FeO	+K_2O	Hf
8-22-T1A1			11.52	2.60	5.80
8-22-T1A1R			11.39	2.40	5.70
8-22-T1A2			11.78	2.20	6.40
8-22-T1A3			11.01	2.60	5.80
8-22-T1B			11.27	2.00	6.00
8-22-T1C			10.56	2.10	5.70

&(xx) enclose equivalent depths used to compare concentrations against another sample set
    in a hypothetical flow of 100 feet thick.
* Depth in flow is calculated from field elevations during measurement of stratigraphic
    section
$ Elevation of the sample within the flow was measured during stratigraphic section or
    traverse measurements
+ Oxides concentrations in weight percent (iron is in total FeO) and remaining
    concentrations in part per million

TABLE X CONTINUED

INAA CONCENTRATIONS, EQUIVALENT DEPTHS, DEPTH IN FLOW, ELEVATION OF

SAMPLES FROM SAMPLE SET WENAHA.B

LABELS	+Na$_2$O	Rb	Sc
8-22-T1A1	3.48	59.00	30.07
8-22-T1A1R	3.75	54.00	30.20
8-22-T1A2	3.45	66.00	31.80
8-22-T1A3	3.47	56.00	25.05
8-22-T1B	3.47	66.00	31.18
8-22-T1C	3.32	39.00	30.19

LABELS	Ta	Th	
8-22-T1A1	0.46	6.60	
8-22-T1A1R	0.52	6.20	
8-22-T1A2	0.51	7.10	
8-22-T1A3	0.37	6.40	
8-22-T1B	0.48	6.80	
8-22-T1C	0.47	6.50	

&(xx) enclose equivalent depths used to compare concentrations against another sample set
    in a hypothetical flow of 100 feet thick.
* Depth in flow is calculated from field elevations during measurement of stratigraphic
    section
$ Elevation of the sample within the flow was measured during stratigraphic section or
    traverse measurements
+ Oxides concentrations in weight percent (iron is in total FeO) and remaining
  concentrations in part per million

Sample 8-22-T1A2 collected in the confining walls immediately at the

interface has the highest concentrations for ten of the seventeen

elements. When compared to sample 8-22-T1A1, sample 8-22-T1A2 had

higher concentrations for fourteen of the elements, except Na, K,

and Lu.

Within the Squaw Canyon (SC#1) sample set, samples collected

from the confining walls generally increase in concentration for

most elements when compared to samples collected from the enclosed

body of breccia or the interface between the breccia and the

confining walls. Within the Wenaha.B set, similar results were

repeated, but for fewer elements. Vesicular pockets or clasts are
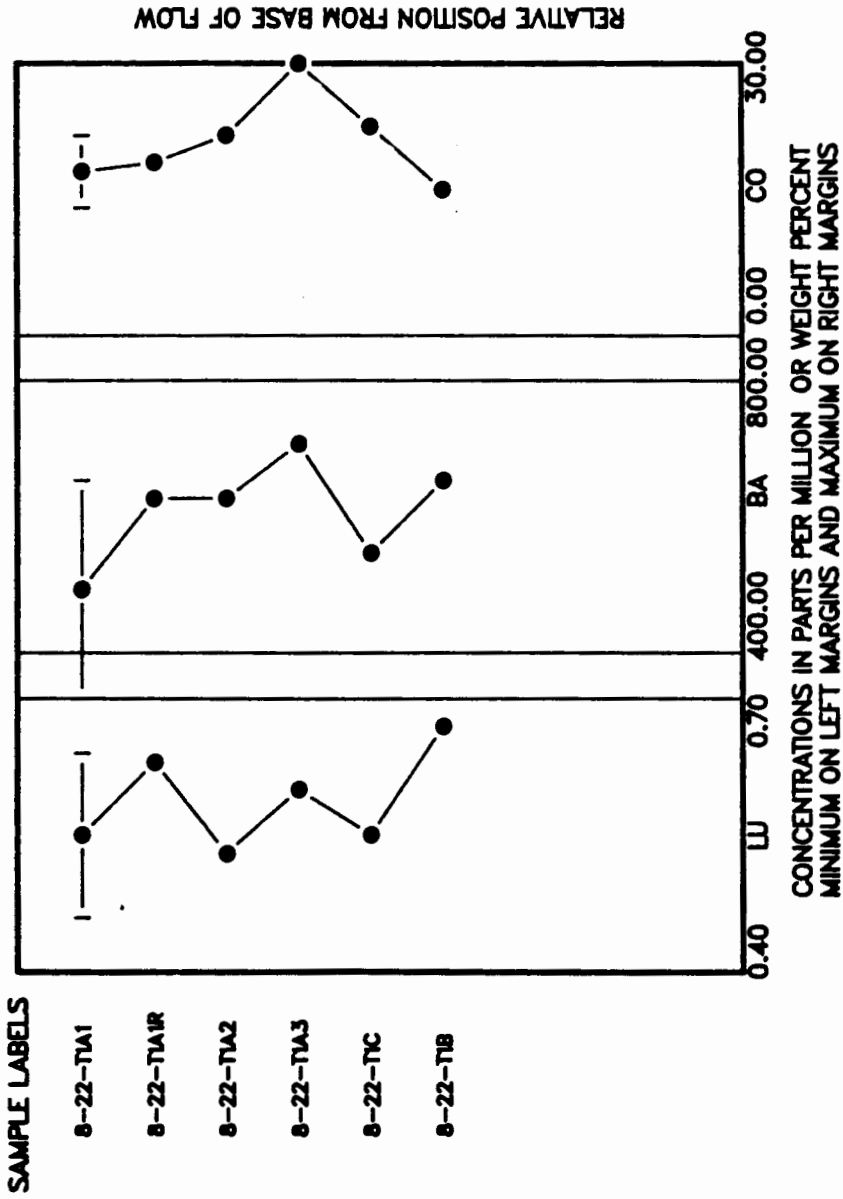
Figure 28. Concentration trends for the sample set Wenaha.B that show the discrepancy caused by the special sample 8-22-T1A1R. Error bars are included for each element.

absent from samples collected within the confining walls for the Squaw Canyon (SC#1) sample set. Vesicular pockets or clasts occur within the samples collected within the confining walls for the Wenaha.B set. The overall geochemistry is slightly different between these two sample sets. The Wenaha.B sample set was collected in the Troy flow, while Squaw Canyon SC#1 sample set is from an overlying Grande Ronde flow. However, elements La, Ce, Sm, Tb, Fe, Na, and Sc show abrupt changes for both sample sets across or at the interface between the confining walls and the enclosed body of breccia (Table XI).

TABLE XI

SUMMARY OF THE ELEMENTS WHICH CHANGED ACROSS THE INTERFACE FROM

THE SPECIAL SPLIT SAMPLE TO THE IMMEDIATE SUBJACENT SAMPLES

Sample set label	Elements
Wenaha.B	La Sm Tb Fe Na Sc Hf Eu
SC#1	La Sm Tb Fe Na Sc Ce Ba

Mossbauer

A sample set from the Wenaha.B site was analyzed by Mossbauer spectroscopy. Mossbauer spectroscopy allowed determination of the oxidation state of iron, Fe^{+3} or Fe^{+2}, and the mineralogy of the iron-bearing phases in three samples from sample set Wenaha.B. The iron-bearing phases in the Troy flow are pyroxenes (hypersthene, pigeonite, subcalcic, and augite) and opaques (titanomagnetite and

ilemnite) (Ross, 1978). Sample 8-22-TlAl was collected from an enclosed body of breccia, while samples 8-22-TlA3 and 8-22-TlC were collected in the immediate subjacent confining walls of the explosion structure (Figure 27). Sample 8-22-TlA3 was collected from confining walls that contain vesicular clasts. Results of the Mossbauer spectrum of sample 8-22-TlAl indicate that 70% of the iron present within sample occurs as Fe^{+3} and Fe^{+3} is present in hematite (Howard, D.F., personal communication, 1987). Magnetite was indentified in the two samples, 8-22-TlA3 and 8-22-TlC, from the confining walls. Thus the oxidation state of iron changed from Fe^{+2} in the black confining walls to Fe^{+3} in the reddish-purple-colored breccia.

XRF

Selected samples from brecciated, unbrecciated, and non-brecciated flow areas within the Troy flow were analyzed by XRF. Samples M, M4, and N (WR sample set) were collected within a brecciated flow area. Samples labelled 8-21#?A (EF sample set) were collected within an unbrecciated flow area and samples labelled 8-22#?C (GC sample set) were collected within a non-brecciated flow area. Results indicate samples within the Troy flow have SiO_2 concentrations greater than 55% (Table XII). Plots of oxide concentrations versus SiO_2 for samples from brecciated, unbrecciated, and non-brecciated flow areas indicate that three samples plot differently from the other samples (Figure 29). Two samples were collected from the basal contacts of first and second cooling units of the Troy flow, M and N respectively, and one

TABLE XII

XRF DATA FOR CERTAIN ELEMENTS

SAMPLE	SiO_2	Al_2O_3	TiO_2	Fe_2O_3	FeO	MnO	CaO
N	56.90	15.90	2.69	2.00	10.39	0.14	5.25
M4	56.22	15.29	2.55	2.00	10.98	0.18	5.37
M	57.02	15.76	2.63	2.00	9.49	0.19	5.55
8-21#7A	55.63	15.08	2.46	2.00	10.26	0.17	6.14
8-21#6A	55.67	15.25	2.57	2.00	9.84	0.18	6.40
8-21#5A	56.25	15.30	2.61	2.00	10.06	0.18	5.75
8-21#3A	55.78	15.08	2.52	2.00	10.25	0.21	6.10
8-21#2A	58.55	16.55	2.87	2.00	7.94	0.31	4.56
8-22#4C	56.34	15.15	2.48	2.00	9.96	0.23	6.01
8-22#3C	55.84	15.16	2.49	2.00	9.94	0.24	6.39

SAMPLE	MgO	K_2O	Na_2O	P_2O_5
N	1.93	2.07	2.22	0.51
M4	2.56	2.04	2.39	0.43
M	2.35	2.04	2.48	0.49
8-21#7A	3.48	1.79	2.54	0.44
8-21#6A	3.08	1.94	2.59	0.48
8-21#5A	2.84	2.10	2.41	0.48
8-21#3A	3.36	1.80	2.45	0.47
8-21#2A	1.29	2.90	2.49	0.57
8-22#4C	2.64	2.20	2.51	0.48
8-22#3C	3.19	1.85	2.48	0.42

Analyzed at Washington State University by P. R. Hooper, 1986.

sample, 8-21-2A, was collected from the basal contact of an unbrecciated flow area within the Troy flow. These three samples are separate from the remaining sample concentrations in six of ten oxides (Table XII).

Enrichment or depletion trends observed in INAA concentrations from the top of the Troy flow to the base can be applied to the concentrations determined by XRF. Similar behavior is noticed for sample sets EF and WR for both INAA and XRF concentrations. Within
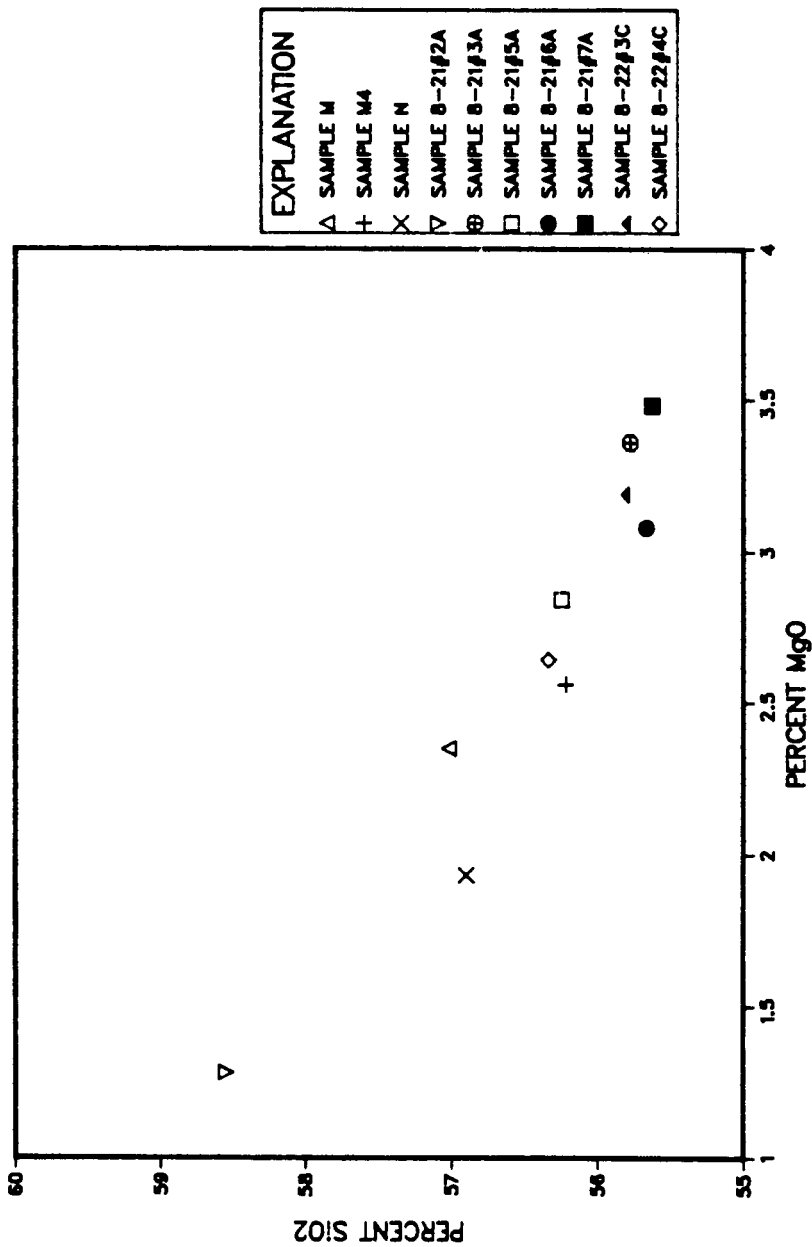
Figure 29. MgO data from XRF analysis plotted against percent SiO_2 for selected samples from brecciated to non-brecciated flow areas. Two samples from the base of brecciated flow areas (M and N) and one sample from the base of unbrecciated flow area typically are separate from the remaining samples.

sample set EF, oxides SiO_2, Al_2O_3, TiO_2, MnO, K_2O, and P_2O_5 show enrichment towards the base for an unbrecciated flow area in the Troy flow. Oxides CaO, MgO, Na_2O, and FeO show a depletion trend towards the base. Within sample set (WR), the trends of the XRF data are similar to the trends of the INAA data in brecciated flow areas. However, XRF concentrations for sample set WR are less conclusive since only three samples were analyzed.

CHAPTER IV

DISCUSSION

The objectives of this study were to describe and characterize the explosion structures and determine the mechanisms of development of these features. Explosion structures within brecciated flow areas of the Troy flow are characterized by differences in 1) intraflow petrographic textures, 2) jointing patterns, 3) geochemical trends, and 4) stratigraphic relationships from unbrecciated to non-brecciated flow areas. The mechanism of development of explosion structures are related to these four differences. This discussion will first deal with the development of the petrographic textures within the intraflow zones between brecciated to non-brecciated flow areas. The timing and development of the jointing patterns within an explosion structure will be discussed next followed by the geochemical trends. Stratigraphic relations and mechanisms of development of explosion structures will be discussed together, because of their interdependence.

The textures within brecciated flow areas are complicated by the intraflow zones developed in the two cooling units. Intraflow petrographic textures vary considerably between unbrecciated to non-brecciated flow areas to brecciated flow areas. Generally, unbrecciated and non-brecciated flow areas have predominantly

intergranular textures in flow interior zones, whereas brecciated flow areas have textures ranging from vitrophyric to intersertal to poorly developed intergranular. The textures of the groundmass in unbrecciated or non-brecciated flow areas indicate that during crystallization microlites of plagioclase and clinopyroxene and intersertal opaques were formed. In brecciated flow areas, crystal growth was inhibited and the proportion of glass is high.

Development of textures containing glass have been described as an effect of rapid cooling or supercooling (Cox and others, 1984; Williams and others, 1982). Two sets of physical controls operate during the crystallization process: 1) externally imposed variables governing the cooling process are time and temperature, and 2) thermodynamic properties of participating phases. Thermodynamic properties include characteristics involving the composition of the melt, degree of consolidation (viscosity), and chemical kinetic processes such as chemical reactions, crystal growth, and nucleation.

Gibb (1974) investigated factors controlling the crystallization of plagioclase from a sample of Picture Gorge Basalt. He reported the ability of the melt to crystalize plagioclase depended upon the degree of supercooling and the duration of the experiment. Supercooling is dependent largely on the composition and the nature of the liquidus phases. Lofgren (1983) argued that textures comparable to those produced by varying cooling rates can be produced by varying the kind and density of nuclei in a melt. These nuclei are trapped in cavities of

refractory impurities. He concluded that plagioclase crystallization was preceded by heterogeneous nucleation. Rock textures are defined by the plagioclase growth habits and are, in turn, controlled by heterogeneous nucleation. The abundance of plagioclase crystals in the experiments was controlled by 1) the composition and density of the nuclei, and 2) the cooling rate.

Kirkpatrick (1977) investigated nucleation and growth of plagioclase during crystallization in two Hawaiian lava lakes. He determined nucleation occurred heterogeneously on previously existing crystals and was primarly controlled by the rate of cooling. Rapid cooling rates produced glomero-microphenocrysts to microlites and interpenetrating crystals. Glomero-microphenocrysts and interpenetrating crystals (cross-shaped and skewed crosses of plagioclase and clinopyroxene) occur within the intraflow zones of brecciated to non-brecciated flow areas in the Troy flow. The Grande Ronde flow above the Troy flow contains similar crystals. This Grande Ronde flow was sampled (SC#1 sample set) and was approximately 50 m thick. Thus the rate of cooling was rapid within the Troy flow and the Grande Ronde flow above the Troy flow.

The rate of cooling controls the composition and the size of groundmass plagioclase and the amount of associated glass (Hoffer, 1966; 1970). The An contents of the microlitic plagioclase within brecciated to non-brecciated flow areas of the Troy flow do not significantly differ from each other. The amount of glass and the size of microlites change between the intraflow zones within brecciated flow areas and between brecciated to non-brecciated flow

areas. The abundance of glass is high within the basal chilled
pahoehoe zone of both cooling units and upward from the convex-up
platy jointed zone within the second cooling unit of the Troy flow.
Overall, the amount of glass increases and the size of microlitic
plagioclase decreases from non-brecciated to brecciated flow areas.

Crystal size is determined by both growth rate and nucleation
density (Dowty and others, 1974). If the growth rate is constant
and nucleation rate is rapid, crystals are smaller; if the
nucleation occurs continuously at a constant rate and the growth
rate is rapid, crystals are smaller. The rates of nucleation and
growth must be greater in brecciated flow areas than in unbrecciated
to non-brecciated flow areas, since the size of microlitic
plagioclase decreases in brecciated flow areas. Therefore, various
stages of crystallization can be related by the size and the
composition of the groundmass plagioclase and the amount of
associated glass.

Walker and others (1976) investigated the crystallization
history of a sample of lunar picritic basalt. They reported the
phases crystallized in the order olivine, chromium spinel, pyroxene,
plagioclase, and ilmenite during equilibrium crystallization.
Ilmenite and plagioclase reversed their order of appearances and
silica crystallizes in the groundmass during controlled cooling
experiments. Cooling rates greater than 10^4 C/hour produce
vitrophyric textures in experimental samples.

The proportion of glass in unbrecciated and non-brecciated
flow areas is lower than in brecciated flow areas within the Troy

flow. The lower amount of glass suggests the Troy flow in unbrecciated and non-brecciated flow areas crystallized under quasi-equilibrium conditions, while crystallization in brecciated flow areas crystallized under non-equilibriun (supercooled) conditions.

Ross (1978) plotted the abundance of plagioclase against opaques plus glass and the abundance of clinopyroxene against opaques plus glass for the Troy flow. Plagioclase and clinopryoxene curves when projected to 0.0% intersect the glass plus opaques axis at 100% and 96% respectively. He concluded that both plagioclase and clinopyroxene began crystallizing early and plagioclase began slightly earilier. Similar plots have been prepared by Swanson (1967) for Grande Ronde Basalt and he reported near simultaneous crystallization of clinopyroxene and plagioclase in these flows.

Ross (1978) argued that the oscillatory zoning of the microphenocrysts and phenocrysts of plagioclase was produced during crystallization just prior or during eruption of the Troy flow. Vance (1962) concluded oscillatory zoning within plagioclase crystals occurs when plagioclase crystallizes before or after the release of volatiles from a flow. Microphenocrysts are more abundant near the basal contacts of brecciated, unbrecciated, and non-brecciated flow areas than within the overlying intraflow zones. This greater abundance supports early crystallization of plagioclase and subsequent clinopryoxene. Ross (1978) concluded the formation of the groundmass occurred following the extrusion of the Troy flow.

Crystallization within basalt is affected by stirring within the basalt during flow and by the cooling rate (Kouchi and others,

1986). Stirring greatly increases the nucleation rate and changes the morphology of crystals when the undercooling is greater than 45° C. Under these conditions, crystals of plagioclase and clinopyroxene are small and adopt acicular morphologies in hyalopilitic textures. The intergranular textures in unbrecciated and non-brecciated flow areas would not result from the influence of stirring from flow or mixing and a high cooling rate. However, the textures in the intraflow zones of an explosion structure within the Troy flow may have resulted from mixing during the upward release of water/steam and/or volatiles and possibly a higher cooling rate.

In this study, primarily the Troy flow of the Grande Ronde Basalt was investigated. The physical properties within the flow should be fairly similar from one location within the study area to another location. Lateral chemical variations within flows of Grande Ronde Basalt are slight (Meyers and Price, 1979). The initial emplacement temperature of the Troy flow should be similar for all locations. Lava temperatures varied little for 10 km downstream from the vent during the 1984 eruption of Mauna Loa (Lipman and Banks, 1987). The cooling rates and overall composition of the Troy flow should be the same unless the system is perturbed such as in brecciated flow areas. Therefore, cooling rates and/or composition properties must have differed to produce the textures observed in brecciated, unbrecciated, and non-brecciated flow areas.

Vitrophyric and intersertal textures occur in the basal intraflow zones of the Troy flow, in brecciated to non-brecciated flow areas. These textures are probably due to the rapid cooling

rate adjacent to the relatively cold subjacent topography. A lack of nuclei in the base of the flow did not influence the nucleation process that resulted in these textures. The abundance of nuclei is related to the composition. Geochemical differences do exist through the vertical profile of the Troy flow within unbrecciated to non-brecciated flow areas. These differences should be present at all locations. The number and denisty of nuclei should be similar at each of the three kinds of flow areas. The composition of the Troy flow would have to rapidly change at each location for the number and denisty of nuclei to play a deciding role influencing where explosion structures are located. Rapid composition changes are unlikely from one location to another location within the Troy flow.

The modal abundance of microphenocrysts of clinopyroxene and particularly plagioclase differ sharply from brecciated to non-brecciated flow areas. Modal abundances of microphenocrysts have been linked to pre-eruption water content of the magma (Anderson, 1973). Desai and Anderson (1974) have suggested that the size, shape, number, and volume of plagioclase microphenocrysts in the crust of a basaltic lava change very little, while the flow is near the source. However, the distribution of microphenocrysts in brecciated flow areas fluctuates strongly among the intraflow zones. While in unbrecciated to non-brecciated flow areas, the abundances of microphenocrysts remains fairly constant. The discrepancy of modal abundances of microphenocrysts in brecciated flow areas may be related to the formation of an explosion structure and the intraflow

textures.

Textures within the intraflow zones of an explosion structure
can be grouped into three major catagories: vitrophyric,
intersertal, and banded. Vitrophyric textures are observed in the
basal chilled pahoehoe base, of both the first and second cooling
units. Intersertal textures occur in the other zones of the first
cooling unit and in similar zones of the second cooling unit.
Banded textures are observed in the convex-up platy zone, in the
basaltic arms of the confining walls, and in the enclosed bodies of
vesicular clasts and pockets and in the eclosed bodies of breccia of
an explosion structure. Banded textures can consist of alternating
bands to swirled layers of differently textured basalt. Individual
bands or layers are composed of textures that range from vitrophyric
through intergranular.

These contrasting but intimately interlayered textures within
the bands or layers indicate an abrupt difference in the crystal
growth behavior from a vitrophyric-type band or layer to an
intergranular-type layer. These contrasting types of textured-
basalt could have 1) resulted from stirring during the formation of
an explosion structure, 2) resulted from a rapid change in cooling
rates, 3) rapid degassing of the volatiles within the flow or 4)
been brought together and mixed from separate source areas within
the flow during formation.

Stirring of basalt and high cooling rates cause small crystals
of plagioclase and clinoproxene to form in a hyalopilitic texture
(Kouchi and others, 1986). The vitrophyric to intersertal bands or

layers in an explosion structure could have resulted from these
conditions. However, the intergranular bands or layers would need
slightly different conditions to produce the more crystalline
groundmass. These bands or layers of different textured basalt are
extremely thin. The stirring process and cooling rates would have
to operate on an extremely small scale to produce these different
textured bands or layers immediately adjacent to each other.

Microphenocrysts and microlites within the different textures
are aligned parallel to the boundaries between each band or layer.
This alignment suggests these crystals were formed earlier than the
movement and then aligned by shear movement. Vesicle tears within
the intergranular textures are aligned nearly perpendicular to the
boundaries. These vesicle tears probably resulted from movement
between the different bands or layers and a higher viscosity within
the intergranular-textured band or layer, since vesicle tears are
not present in other textured bands or layers. Viscosity is a
function of temperature, composition, and crystal content (Shaw and
others, 1968; Shaw, 1969; 1972). A higher viscosity within the
intergranular bands or layers may have been affected by the greater
crystalline content of the intergranular bands or layers. Thus the
stirring process is not a reasonable explanation for the
crystallization of these interlayered bands.

However, the crystallization process operated differently
within each contrasting type of band or layer. The transition from
a vitrophyric-type of basalt to a intergranular-type, for example,
would have to have occurred often in less than a millimeter. The

transition would have involved an abrupt change of cooling rates or a sudden increase or decrease in the number of nuclei present in the flow. The probability of sudden transition in cooling rates does not seem very likely, since unbrecciated and non-brecciated flow areas show a gradational transition of textures from the base to top of the Troy flow.

Furthermore, the swirled, twisted, pinched and swelled nature of some contrasting bands or layers implies a transition in cooling rates from vitrophyric-type to intergranular-type. The transition in cooling rates would have to be parallel to the pattern of the bands or layers. Bands can occur in patterns where the individual bands are bent back on each other which would imply the transition in cooling rates does the same.

Rapid degassing of the volatiles within the Troy flow could have caused an upward movement of basalt if the upper crust of the flow were to break (Figure 30). The release of pressure, from fracturing of the crust may initiate degassing and an upward movement of volatiles towards this fracture. With depressurization of the flow at the vicinity of the fracture, the separation of gas undercooled the lava without actually lowering the lava temperatures, but initiated crystallization. Similar depressurization from the small volatile loss and subsequent rapid crystallization have been argued to cause vitrophyric textures within Hawaiian lavas (Lipman and Banks, 1987).

The abundance of vesicles on the first cooling unit of the Troy flow may have been caused by the presence of volatiles within
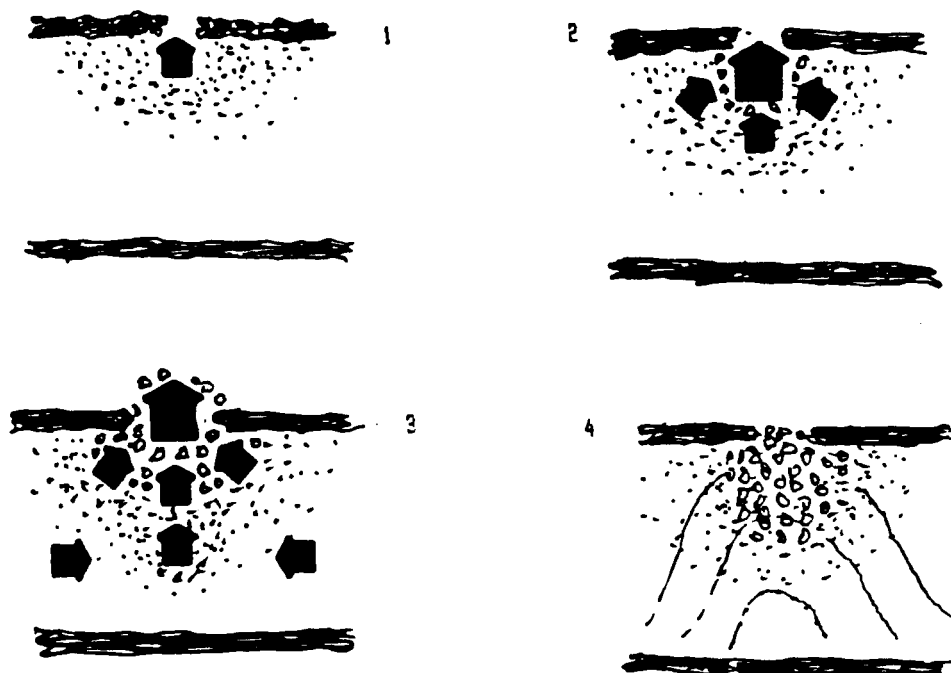
Figure 30. The crust fractures and the release of
pressure initiates degassing (1). Degassing
increases and movement of volatiles towards the
fracture from adjacent areas (2). Crystallization is
initiated from the loss of volatiles and
fragmentation results from the rapid degassing of
volatiles (3). An explosion structure is formed
surrounded by a halo of vesicles (4).

the flow. If these volatiles occurred in the second cooling unit as

well and fractures occur in the upper crust, the upward release of

volatiles may be sufficient to cause rapid crystallization resulting

in vitrophyric textures. However, the entire area adjacent to the

fracture would be affected similarly by the release of volatiles.

The subsequent rapid crystallization from volatile loss should

result in vitrophyric textures near the fracture and these textures

should grade into more crystalline textures away from the fracture.

The banded vitrophyric and intergranular textures that occur within

the confining walls of the Troy have typically sharp abrupt

boundaries. Vesiculation should gradually increase towards the

fracture, because the volatiles would move towards the fracture

(Figure 30). Vesicles tears occur within the intergranular bands or

layers of the confining walls of the Troy flow and are probably the

result of movement rather than release of volatiles.

The most reasonable explanation of the bands or layers of

vitrophyric and intergranular-textured basalt infers a mixing

process that involves a transfer upward of viscous vitrophyric to

intersertal-textured basalt during the formation of an explosion

structure. Possible source areas for vitrophyric and intersertal-

textured basalt during the formation are the subjacent and lateral

basal zones of the second cooling unit. Additional transfer

involves movement inward of more crystalline material from the

adjacent basalt during formation of explosion structures. Textures

of several samples from the confining walls or basaltic arms

indicate movement of material, because microphenocrysts and

microlites of plagioclase and clinopyroxene are arranged parallel to

the boundaries between the contrasting textured-types of basalt.

Pilotaxitic textures are indicative of movement parallel to the

alignment of the crystals (Williams and others, 1982).

Formation of an explosion structure would occur after the

initial crystallization of the basalt, but before the basalt was

solidified completely. Vesicles were trapped in place in the

growing crust of Makaopuhi Lava Lake, Hawaii at temperatures of less

than $1,070^{\circ}$ C (Wright and Okamura, 1977). Similarly vesicular

clasts and pockets in an explosion structure could have stopped
rising upward at approximately this same temperature, 1,070° C.
Initial crystallization of basalt already had begun, because of the
bands or layers of intersertal to poorly developed intergranular
textures observed in thin sections.

Sample 8-22-SC#1 contains the vitrophyric to intergranular
textures, but was collected from a steeply dipping enclosing
basaltic arm. Microphenocrysts and microlites are arranged parallel
to the boundaries of the bands or layers. The path of movement
within the flow inferred from the textures of this sample observed
in thin section would be very steeply dipping to vertical. Thus the
textures were not formed by the normal movement parallel to the base
of a flow, but by upward movement within the flow. Sample MC-4D was
collected even farther upward in a brecciated flow area near the
superjacent contact with the overlying flow. Textures from this
sample indicate, by the swirling nature of the contrasting
vitrophyric to intergranular textured-layers of basalt, that mixing
occurred in the upper portion of the Troy flow.

Sample 8-20#4 has textures that dramatically emphasize the
mixing and fragmentation process during formation of explosion
structures. Sample 8-20#4 was collected from an enclosed body of
breccia in the vesicular clasts/pockets zone. Petrographic textures
range from vitrophyric to intergranular. Vesiculation within each
texture type is different and the vesiculation is also different
between areas of similar texture types as well. Within the
individual bands or layers, vesicle tears are observed adjacent to

the boundaries between different textural types. Orientation of the vesicle tears suggest the band in which the vesicles are found was slightly more viscous than the adjacent band during development of the bands. Some bands of intergranular texture grade inward to a fine brecciated core that includes millimeter sized fragments.

In conclusion, the contrasting bands or layers can not be reasonably explained by a change in cooling rates or stirring (in-situ) on a millimeter scale. A difference in the composition and density of nuclei that influenced crystallization seems more likely. Movement of material can be inferred from the parallel alignment of the microphenocrysts and microlites found within samples of an explosion structure. A mixing process brought the contrasting types of textures together. Fragmentation processes can be observed in samples from the vesicular clasts/pockets zone in the second cooling unit of the Troy flow.

Overall jointing patterns of an explosion structure has been compared to an arch consisting of concentric layers surrounding a central spine (Orzol and Cummings, 1986a; 1986b). A single joint trace can be followed from the peripheral margin of an explosion structure to the center of an arch. The joint trace is nearly vertical at this point and tilts to horizontal at the center of the arch. Petrographic textures within the confining walls indicate the direction of movement was parallel to these joint traces. The alignment of the boundaries of contrasting textures, where present, and the alignment of the microphenocrysts and microlites within the textures are also parallel to these joint traces.

In the lower portion of an explosion structure, surface textures resembling small ripples were observed on joint traces. The locations of these ripple-like textured rocks occur within the confining walls where the rock consists of multiple layers. These surfaces may have formed from differential movement between individual layers in the lava as each was sliding past the other during the formation process of an explosion structure. The surfaces of each layer would have been viscous in order for the deformation to occur along the surface. Inclination of these layers is parallel to the joint system within an explosion structure.

Joints in the vesicular clasts/pockets zone and at the center of the arch, pinch and swell around a chaotic arrangement of plates. Plates are not arranged in a uniform pattern, but vary in size and ordering. Each plate is composed of welded fragments. If the basalt was still viscous during the formation, this fragmention could have occurred from differential movement with later welding of fragments into plates. The pinching and swelling of the joints may be another indication of continued movement during the formation process after the fragments were welded into plates. Each plate has surface textures resembling small ripple-like marks. The surface ripples may have resulted from differential movement between adjacent plates. These surface features suggest that movement continued after the fragments were welded into plates during the formation of an explosion structure.

The basal zones of the second cooling unit are platy jointed, but jointing grades upward to form convex-upward plates. The

convex-upward jointing is situated directly below the central spine
of an explosion structure. Away from the central spine area, joints
are no longer convex-up. Myers and Price (1979) argued that the
origin of platy joints is related to emplacement and primary cooling
and perhaps enhanced by later deformation. Clearly, if deformation
enhances platy jointing, a reasonable mechanism for the development
of convex-up plates occurred during the formation of an explosion
structure. Platy jointing has been proposed to occur after the
major vertical cooling joints have formed (Holmgren, 1968). The
major vertical joints in brecciated flow areas are in the form of an
arch. The arch shape of this joint pattern clearly contrast to the
form of an entablature or colonnade (Myers and Price, 1979).

Since the cooling fronts influence the joint location, the
orientation of a single joint trace would imply the direction
towards the cooling fronts for a hypothetical flow (Degraff and
Audin, 1987). Cooling fronts are generally parallel to the upper
and lower surfaces of a flow when entablature and colonnade jointing
are formed. If the cooling fronts moving through an explosion
structure parallel the joint traces, then the cooling fronts would
have the arch shape of the confining walls. A reasonable
alternative would be the joints formed as the basalt was still
slightly moving upward. This upward movement of the basaltic
material, greatest at the center of the arch could explain the arch
shape of the joint traces. Deformation that caused the ripplemarks
on the surfaces of the joint traces occurred during the latest
upward movement of basalt.

Clearly, the jointing pattern of an explosion structure suggests movement of basalt upward during formation. Possible shearing and fragmentation occurred at the center of the concentric layers of the confining walls, because plates consist of welded fragments. Movement between still viscous plates and layers caused deformation that resulted in ripple marks on surfaces of the plates and joint traces. Joints formed before final movement in the formation process and resulted in the arch shape of an explosion structure.

Movement and mixing during the formation of explosion structures may explain the vertical profile of the concentration of major and trace elements within the Troy flow. The vertical profile of geochemical concentrations within brecciated flow areas differ from those that occur within unbrecciated and non-brecciated flow areas (Cummings and others, 1987). Unbrecciated and non-brecciated flow areas have similar profiles towards the base of the Troy flow. Concentration of certain elements increase (enrichment) or decrease (depletion) towards the base of the Troy flow. The trends of enrichment or depletion towards the base of the Troy flow within brecciated flow areas are less pronounced than within the other flow areas.

The factor influencing trends may be the mixing of basalt of different textures. As the explosion structure is formed, basalt is drawn inward and moved upward then mixed within the different intraflow zones of the explosion structure (Figure 31). This mixing process could lead to weakening of the vertical patterns of
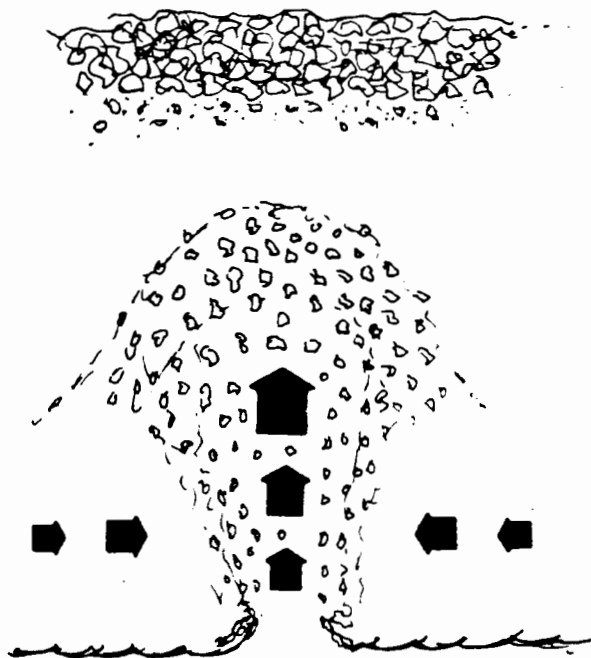
<u>Figure 31</u>. During the formation process, material is moved upward by the release of steam/water. Material is drawn in from the adjacent areas and moved upward. Thus depleted and enriched material can be mixed.

concentrations found in the geochemical data in brecciated flow areas. Most of the elements which significantly displayed the patterns of enrichment or depletion can be found in the plagioclase, clinopyroxene, and opaque minerals (Vlasov, 1966).

Similarly the distribution of the remaining elements could be explained by the same mixing manner. Overall, the petrographic textures, jointing patterns and geochemical trends reflect a mixing process during the formation of an explosion structure. The mechanisms that drive the process of formation must involve movement of basalt by vertical movement from immediate subjacent intraflow zones of an explosion structure and by material drawn in from the

areas surrounding an explosion structure.

Additionally, the process of formation causes fragmentation. Basaltic arms within the lower portion of the confining walls zone of an explosion structure have ripple-like surfaces along joint traces and are jointed into plates. The plates consist of welded fragments. The ripple-like marks and the fragments imply shearing and fragmentation of the lava. After formation of the fragments, sufficient heat was still available to weld the fragments into plates. Similar fragmentation is observed where basaltic arms penetrate into the edges of the central spine. The basaltic arms are fragmented into black-colored pieces and these pieces are, in turn, incorporated into the matrix-supported breccia of the spine. Sufficient heat still remained so that the breccia was welded together. These black-colored fragments are one source of the composite-type clasts in the spine.

Distribution of the clast types reflect the process of formation of an explosion structure. The black-colored basalt, vesicular to non-vesicular composite-type clast (BVA) have greater abundance than the other types of clasts. This type of clast could have been generated from shearing and fragmentation of the confining walls or basaltic arms. The more vigorous the process of formation or the longer the explosion process lasted, the more clasts would be produced. The distribution of clast sizes indicates lapilli-sized clasts are produced in greater abundance during the formation process than block-sized clasts.

However, the size distribution is misleading, because the

lapilli-sized clasts are generally found in greater abundance in the outer matrix-supported breccia of the central spine. Block-sized clasts increase in abundance in the inner clast-supported breccia core. This difference in size distribution would be reasonably explained by two different formation processes: 1) episodic explosions and 2) single event explosion. An episodic process consists of multiple pulses of intense activity followed by waning pulses. Different pulses produce clast types and sizes in different proportions. A single event process would distribute the strength of the explosion in time and across an explosion structure. This distribution influences size and abundance of the clast types.

The distribution of types of clasts changes slightly from the outer matrix-supported breccia to inner core of clast-supported breccia within the central spine. The abundance of scoriaceous or vesicular type of clasts increases in the core. This trend may indicate that during the formation process, the composite black-colored clasts (BVA) are fragmented from the peripheral, but are not incorporated as easily into the clast-supported core. Clasts of the inner core of the spine may be generated along the center of the arch of the confining walls, where the vesicular clasts and pockets are observed. The vesicular clasts and pockets that are now observed represent the dying stage of the formation process. During the height of the explosion process, the center of the arch served as a point of generation for the clasts of the inner core of a central spine. The boundaries of vesicular clasts and pockets are not visible in the field in the lower portion of an explosion

structure, but become apparent farther upward towards the central spine. If indeed this is true, then these vesicular clasts and pockets represent incipient clasts that during the height of the brecciation process form the majority of the type of clasts found in the inner core of the spine.

Clast sizes and types have been analyzed for natural systems and modeled in experimental systems for hydromagmatic or hydrovolcanic explosions (Wohletz and Sheridan, 1983, Wohletz and McQueen, 1984; Wohletz, 1983, 1986; Sheridan and Wohletz, 1983). Clast sizes are dependent on the strength of the explosion. The strength of explosion is determined by the ratio of the mass of water to the mass of lava. Smaller clast sizes are indicative of stronger more violent reactions and low mass ratios. Larger-sized clasts indicate weaker intereactions and high mass ratios. An explosion structure in the Troy flow has both lapilli and block sizes. Thus the process producing an explosion structure 1) involves separate explosions of different intensities or 2) the force of the explosions are distributed through a volume of lava.

One possible explanation for the size discrepancy could be that the process of formation is episodic. The lapilli size fragments are produced during each period of intense activity; block sizes are produced during periods of lower activity and high ratios of water to lava. An alternative process, a single event, distributes the energy across the explosion structure and through time. The distribution of energy release controls sizes and types of clasts as indicated in the traverse measurements of a central

spine that show an inner clast-supported breccia surrounded by matrix-supported breccia.

If the process of formation were episodic, then this process would produce a horizontally stratified breccia rather than the observed vertically stratified central spine. The lapilli size fragments would be produced during the intense explosions and these fragments are forced upward (Figure 32). A less intense explosion could follow and produce block size fragments. These fragments are forced upward and add another layer to the bottom of the central spine. If more explosions follow, the central spine may appear horizontally layered.
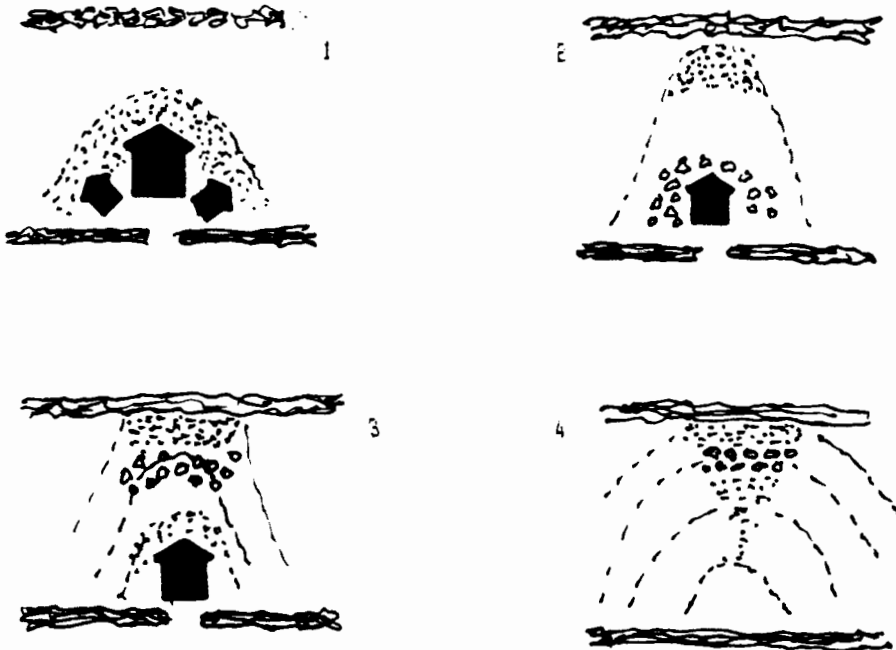
Figure 32. An episodic event process starts with an intense explosion that produces lapilli size fragments. A less violent explosion follows that produces block size fragments and these fragments add another layer to the breccia of the central spine. The cycle is repeated. These explosions wane and result in a horizontally stratified central spine.

The single event process may be more reasonable. During the
initial moments, low mass ratios cause extremely intense explosions
that produced lapilli-sized clasts (Figure 33). Fragmentation
processes were dominant over vesiculation. Lapilli-sized clasts
were forced upward and formed the outer matrix-supported breccia.
Energy waned when more steam/water interacted with the molten
basalt. Vesiculation became dominant. Block-sized clasts were
generated and carried upward by a greater proportion of steam/water
then produced the clast-supported core.
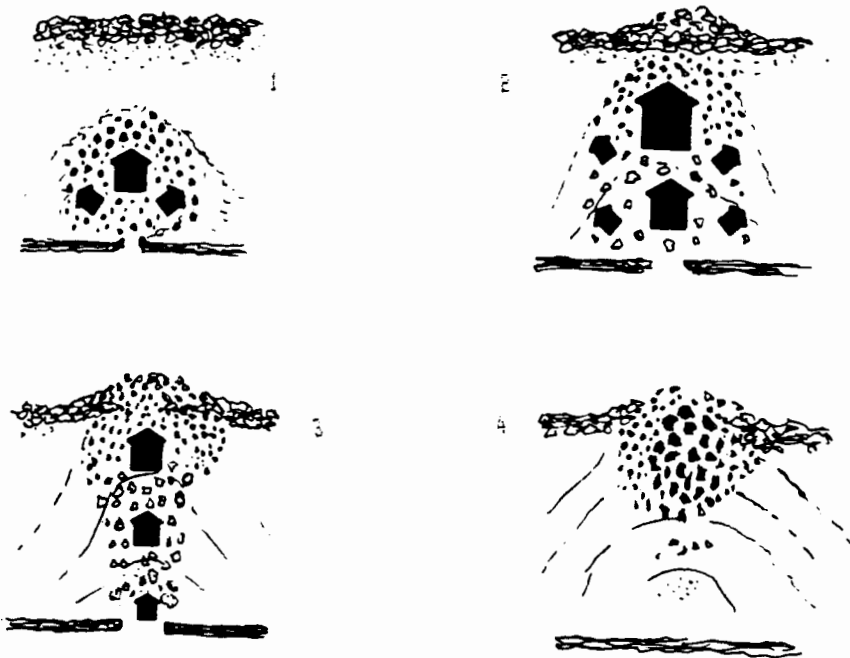
Figure 33. A single event process increases in
intensity as during the initial moments (1 to 2).
During these two steps, the finer breccia clasts are
formed, because the mass ratio of water to melt is low.
As more water is incorporated in the process, the mass
ratio increases and the strength of the release of
steam/water wanes. Larger clasts are formed during this
step (3). The final stage shows the stratification within
the central spine and the jointing formed.

The formation of an explosion involves mixing of basalt from either the subjacent intraflow zones of the second cooling unit or basalt drawn from the basal portion of the flow. The mixing process occurred after initial crystallization of the Troy flow as indicated by the formation of contrasting bands or layers of different textures of basalt (vitrphyric to intergranular) within the confining walls. The aligned microphenocrysts and microlites within these bands or layers of basalt indicate movement. That movement was upward through the Troy flow is indicated by the banded nature of different textural features, the alignment of microphenocrysts and microlites found within these features, and deformation along joint traces that resulted in ripple-like surfaces. The location of the explosion within the flow could be 1) within the body of the flow above the lower zones of the second cooling unit or 2) at the base of the second cooling unit.

A model for the formation of explosion structures depends on 1) water being present and available to interact with the basalt, 2) physical variables such as the transfer of heat from the flow to the trapped water, and 3) a mechanism to trigger and fragment the basalt so an explosion can take place. The presence of water at the time of the eruption of the Troy flow is indicated by the red clay zone below the first cooling unit and possible influence of water in the crystallization sequences within the intraflow zones of the second cooling unit.

The timing of the emplacement of the second cooling unit in relation to the first cooling unit is unclear from field

observations. The first cooling unit contains a greater portion of vesicles within the basal intraflow zones than the second cooling unit. The vesicles within the first unit are probably due to a high abundance of volatiles. High volatile contents within Hawaiian lavas reduce viscosity and increase fluidity within the flows (Lipman and Banks, 1987). The initial volume erupting at the vents produced the thinner first cooling unit and a greater subsequent volume produced the thicker second cooling unit. The lava of the first cooling unit was highly fluid and flowed rapidly from the vents following topographical lows. The thicker second unit followed and covered the topography that included the first unit. The second unit could influence the crystallization sequence within the first cooling unit, if crystallization within the first unit was not complete within this unit. The heat from the second unit may have slowed the cooling of the first unit.

The crystallization of the first unit, if influenced by sufficient heat transferred from the second unit, should have resulted in well-developed intergranular textures. Vesicles within the still molten first cooling unit should have risen upward and concentrated within the upper portion of the first unit, thereby producing a vesicle-free interior. Vesicles, if present within the interior of the first unit, should occur randomly and be spherical in shape. However, vesicles occur within the interior of the first unit and concentrate within bands or layers parallel to the base of the first unit. Vesicles are elongated parallel to the boundaries of the bands or layers. The elongated shape of the vesicles

indicates that movement parallel to the base of the first unit occurred as the lava crystallized. Thus, the crystallization of the first cooling unit was not influenced by the heat from the second cooling unit, because sufficient time (couple of days) may have passed before the second unit arrived.

An explosion structure is typically symmetrical, as illustrated by the symmetry of the jointing pattern forming an arch of concentric layers. Along the axis of symmetry of an explosion structure is the first cooling unit that occupies a trough in the subjacent topography (Orzol and Cummings, 1987). A red baked clay is present in the trough and the superjacent chilled pahoehoe base has quenched vitrophyric textures. Microphenocrysts of plagioclase and clinopyroxene show swallow-tailed crystal morphology similar to quenched textures found in pillow rinds of basalt described by Bryan (1972). This quenched texture implies that the red clay zone was saturated and/or surface water was present.

Since the second cooling unit also has a similar chilled pahoehoe base, water must have interacted to quench the base of this unit. A reasonable explanation could involve the first cooling unit flowing along a stream channel forcing channel water to ramp up and override the first unit. The second cooling unit followed, trapping the water between the separating cooling units. The much thicker second cooling unit would not allow ramping of water as did the much thinner first unit. The water could have been forced into the voids of the clast-supported scoriaceous top of the first cooling unit.

The presence of water is suggested at the time of the eruption

the Troy. Ross (1978) found hyaloclastite beds above and below the Troy flow that suggest water interacted with flows of Grande Ronde Basalt. He suggested that the Grouse Flat syncline was active at the time of eruption of the Troy flow. The Grouse Flat syncline could have served as a basin for a body of water, or, together with the Saddle Butte anticline, acted to develop relief upon which stream drainages developed. Furthermore, colonnade jointing occurs within the Troy flow and within other flows above and before the Troy flow locally. Long (1987) has reported the development of entablatures and colonnades in Columbia River Basalt depends upon quenching of partially crystallized basalt from lakes and streams inundating the Columbia Plateau. Thus water in streams or lakes was present at the time of the eruption the Troy flow.

Water is soluble in basaltic melts and solublity increases steadly with increasing pressures over 1,000 bars (Burnham, 1975; Hamilton and others, 1964; Khitarov and Kadik, 1973; Silver and Stolper, 1985). The mixing of water into a basaltic melt causes dramatic effects on crystallization and on such physical properties of the lava such as viscosity (Burnham, 1975; Loomis, 1979; Drake, 1976). The introduced water reacts with the silica tetrahedra resulting in an exchange of a proton from water with a cation within the tetrahedra thereby breaking the tetrahedra. Crystallization sequences and textures would change (Hamilton and others, 1964). The intraflow textures in brecciated flow areas indicate a different crystallization sequence than unbrecciated to non-brecciated flow areas. If water was forced into the base of the second cooling unit

of the Troy flow during the explosion process, silica tetrahedra within the basalt would break apart from interaction with water molecules. Thus this interaction would hinder the formation of plagioclase and pyroxene microlites and result in a greater portion of glass forming. This basal portion could be a source for the bands or layers of vitrophyric textures within the confining walls that were transported upward and mixed during the formation process of an explosion structure.

Oxygen fugacity in a melt can be influenced by the introduction of water (Hamilton and others, 1964; Osborn, 1959). Water would increase fo_2 in the melt and determine the course of the crystallization sequence. Hamilton and others (1964) reported that melts at high fo_2 and temperatures, when quenched, result in high proportion of glass. At lower fo_2, the quenched charges include clinopyroxene and plagioclase crystals. Thus high oxygen fugacity decreases the temperatures at which clinopyroxene and plagioclase begin to crystallize. These conditions may explain the black colored vitrophyric textures in the confining walls.

The enclosed bodies of breccia adjacent to the confining walls within an explosion structure have reddish-color. Results from Mossbauer analysis show hematite is present within these breccias, while results show magnetite is present within the adjacent black-colored confining walls. The steam/water may have reacted during the formation process 1) to alter magnetite grains to hematite or 2) to cause hematite to crystallize directly. Thus water was available to interact during the formation of an explosion structure within

the Troy flow.

Transfer of heat can be accomplished from the molten Troy flow to the water trapped between the first and second cooling units. Features in the bases of basaltic flows in Columbia River basalt resulting from interaction with water or gas have been reported by many authors: Fuller (1931), Waters (1960), Schminke (1967), and Swanson (1967). Features ranging from pillowed bases to peperites are generated from the contact of molten lava and water or water-saturated sediments or burnt vegetation. Phreatic-explosion pits near Mount St. Helens, Washington were generated when hot pyroclastic flows and debris flows covered water in streams, ponds, and springs (Rowley and others, 1981). The water flashed to steam and formed explosion pits. Minor steam explosions occurred where the 1801 Huehue lava flow, Hawaii, overran water-soaked ground (Moore, 1970). Similar explosion spatter rings and craters are observed in Iceland after water either entered or was trapped below a lava flow and exploded (Walker, 1971).

Lava flows entering the sea off the Hawaiian Islands can transfer sufficient energy to elevate seawater temperatures or have caused explosions that form littoral cones (Wentworth and others, 1953; MacDonald, 1949; Moore and others, 1973; Fisher and Schminke, 1984). The type of lava flow, aa or pahoehoe, influence the dynamics, because pahoehoe flows often form pillowed lavas and aa flows form littoral cones. A pahoehoe flow forms an insulating crust inhibiting the transfer of heat from the interior to the surroundings, while an aa flow has open fractures conducive to

transfer of heat by air or water.

Pahoehoe flows in Hawaiian Islands can form pillows, but not all flows do so (Moore and others, 1973). Some flows maintain coherence and extend along the sea bottom as lava tongues. If slopes are gentle, flows into the sea will not produce pillows; where slopes are steep, pillows to breccias will form (Moore and others, 1971). Slopes in the study area at the time of the eruption of the Troy flow were gentle. This is suggested by the maximum dips of the Grouse Flat syncline of only a maximum 3° (Ross, 1978). Neither the first nor the second cooling units of the Troy flow formed pillows.

The temperature of the Troy flow was probably maintained by rapid flowage and by processes similar to those acting during the flow of a Hawaiian lava. The temperatures of Hawaiian lavas are sustained by the heat of crystallization (Lipman and Banks, 1987) and by the heat derived from frictional deformation of the melt (Shaw, 1969). Shaw and Swanson (1970) calculated heat loss during flow was mainly by radiation and a typical flow cooled an average of 50° C over a distance of 200 km in approximately 10 hours. Cooling rates for a lava lake in Hawaii with a maximum depth of less than 30 meters took nearly four years from the initial temperature of 1190° C to reach temperatures below 1000° C at the base of the lava lake (Wright and Okamura, 1977). An estimate for the Troy flow, which is more than three times thicker, would be about 12 to 15 years. Estimates for the temperatures of erupting Hawaiian basalt range from 1225° C to 1050° C (Peck and others, 1964; 1966; Shaw and

others, 1968; Wright and others, 1977; MacDonald, 1963; and Shaw and others, 1977). Thermoconductivities are initially high for the cooling of a Columbia River Basalt sample at 1200° C, then are slightly influenced by the presence of crytals (Murase and McBirney, 1973). Thermoconductivities begin to climb again after cooling to approximately 1000° C.

Transfer of the heat occurs downward across the basal contact of the second cooling unit and possibly sufficient heat will turn the water trapped between the cooling units to steam. The pressure from the weight of the second cooling unit would act on the water trapped in the voids of the clast-supported breccia of the first cooling unit. Once the steam pressure reached a critical value, the basal contact would crack; the pressure release would cause remaining water to turn to steam and explode upward through the crack.

An alternate mechanism for fracturing the basal crust could be the result of tectonic activity. Trends of the central spines of explosion structures have either an orientation similar to the northeasterly trending Grande Ronde fault system or the northwesterly trending dike system in the study area. A northwest-trending fault, the Squaw Canyon fault, is also part of the fault system. Movement along these faults after the eruption of the Troy flow could fracture the base of the second cooling unit at various locations. These favorable locations could coincide with presence of the first cooling unit and subjacent troughs occupied by the first unit. Another explanation for the orientations of the central

spines is that the faulting of the Grande Ronde and folding of both

Grouse Flat syncline and Saddle Butte anticline could have

controlled the topography in the study area. Drainages developed on

the topography could have developed orientations in northeast and

northwest directions.

Another alternative to heating the water to produce sufficient

pressure to crack the basal crust involved fuel-coolant reactions.

Fuel-coolant reactions have been studied as analogs to natural

systems producing hydroexplosions. A chain of processes has been

advanced as a pathway model for a thermal explosion resulting from

contact of molten material and coolant (Figure 34) (Buchanan, 1974;

Board and others, 1974). The chain of processes has a feedback

```
              1. Thermal energy
                     ↓
          Initiating mechanisms
                     ↓
              2. Mechanical energy ←─────────────────┐
                     ↓                                │
              Mixing process                          │
                     ↓                                │
          3. Interfacial area enhancement             │
                                                      │
                                            Feedback  │
                     │                      process   │
                     ↓                                │
              4. Rapid heat transfer                  │
                     ↓                                │
              5. Pressure production                  │
                     ↓                                │
                  6. Expansion ─────────────────────┘
                     ↓
              7. Mechanical damage
```
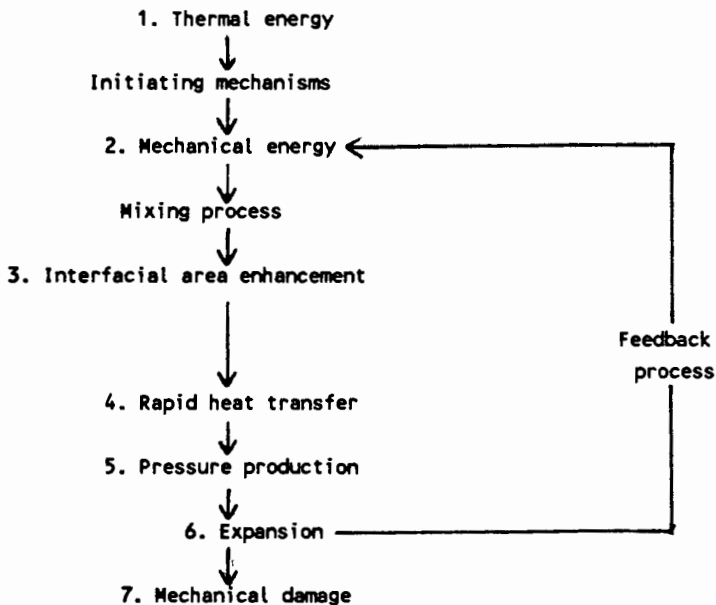
Figure 34. A schematic summarizing the logical sequence
of explosion processes involved in fuel-coolant reactions.
(after Board and others, 1974).

mechanism. The initiating mechanisms are not well understood, but a variety of proposed mechanisms exist. Witte and others (1970) proposed four triggering mechanisms: entrapment, violent boiling, shell theory, and Weber number effect. All four mechanisms produce fragmentation and thereby transfer the heat needed for an explosion, but do not fully explain recent experimental or field findings (Board and others, 1971; Wohletz, 1983; Wohletz and Sheridan, 1983; Wohletz and McQueen, 1984; Sheridan and Wohletz, 1983).

Kokelaar (1986) proposed four mechanisms: 1) magmatic explosivity caused by the explosive release of magmatic volatiles, 2) contact-surface steam explosivity from the explosive expansion and collapse of steam formed at magma-water contact surfaces, 3) bulk interaction steam explosivity produced by explosive expansion following enclosure of water in magma, or entrapment of water close to magma, and 4) cooling-contraction granulation from cooling and contraction of molten material. In the case of the Troy flow, the latter three mechanisms appear applicable.

Wohletz (1986) describes two models requiring film boiling prior to explosion (mechanism 2 from Kokelaar): the superheating model and the thermal detonation model. Film boiling permit the two processes to operate simultaneously: partial thermal insulation of the molten material from the water and gradual fragmention and mixing of the molten material by the instabilities from film boiling. The transfer of heat is accomplished by the increased area from mixing, thereby causing rapid vaporization followed by an explosion. This scenario will only happen if the water is

superheated to temperatures at or above the spontaneous vapor nucleation temperature of water and secondly if a pressure wave (thermal detonation) causes finer fragmentation and subsequent collapse of an insulating film surrounding the fragments. This cycle is repeated until an explosion is generated.

Superheating of a liquid involves raising the temperature of this liquid above the normal boiling point for any given pressure while still remaining a liquid. Wohletz (1986) reported the requirement of superheating is not easily met by the initial conditions of basalt-water contact. Several types of instabilities may cause oscillation of the layer of film boiling. These instabilities cause the surface of the magma or lava to distort into waves. The chilled pahoehoe base has unusual surface digitations which may be a result of oscillations that failed during the waning stages of formation. A thermal detonation causes differential acceleration of the melt particles relative to the water. Thermal detonation may not be likely, but volcanic systems satisfy detonation requirements (Wohletz, 1986).

Several triggering mechanisms of formation have been advanced that would result in formation of an explosion structure. Triggering mechanisms are 1) tectonic in origin from faulting or folding, 2) sufficient pressure to fracture the base, and 3) fuel-coolant type interactions. Triggering mechanisms must fracture and fragment the base and basal portion of the second cooling unit and transfer sufficient heat for steam/water to explode upward into the flow. After the explosion is triggered, the process may develop

episodically or as a single event. As steam/water exploded upward through the flow, superheating of the steam/water could operate during the transition towards the top.

Reid (1976) successfully demonstrated a model using a column of heated liquid. The column of liquid was heated greater at the top than the bottom; thus, convection did not operate within the column. Next, he injected a drop of lower density liquid from the bottom of the column. The drop formed a rising bubble that superheated and exploded. The situation involving the Troy flow is similar in that the steam/water will move upward through the flow towards the hotter molten interior. This superheating could cause further expansion of steam/water and possibly additional fragmentation. This additional fragmentation may have resulted in finer clast sizes such as the extremely small sizes observed in thin section of the textural bands in samples from trapped bodies of breccia. The finely brecciated rind on some breccia clasts from the central spine may have been produced by the additional fragmentation from superheating.

Upward movement of steam/water caused 1) fragments to be incorporated into a breccia of the central spine, 2) development of the intraflow zones and their petrographic textures from mixing of the basalt, and 3) the overall shape of an explosion feature in an arch delinearated by the joint pattern.

CHAPTER V

CONCLUSION

1) Explosion structures in the study area are restricted to
Grande Ronde Basalt and are absent in Wanapum and Saddle Mountains
Basalts. The distribution within Grande Ronde Basalts is not
controlled by the Grande Ronde fault system, because brecciated
flows are observed on both sides of the faults of the system. The
regional structural features, the Grande Ronde fault system, Grouse
Flat syncline, and the Saddle Butte anticline, probably controlled
the pre-eruption topography and thereby influenced the orientations
of the central spines within brecciated flows. Brecciated flows are
composed of two cooling units. The first unit occupying troughs in
the pre-eruption topography and the second unit containing the
explosion structure. The maximum number of brecciated flows at any
one stratigraphic site is six flows. Only one stratigraphic site,
Grouse Creek, lacked brecciated flows, the remaining sites contained
commonly at least two brecciated flows. Typically, the Troy flow
was one of these brecciated flows. The Troy flow is usually the
thickest flow measured and explosion structures are better developed
within this flow. The collection of measurements from explosion
structures indicates a definite relationship between the total
thickness of the flow and the vertical breccia interval.

2) Development of explosion structures required: a)

availablity of water and b) a mechanism(s) to trigger interaction of this water with the molten basalt. Water was available at favorable locations in troughs of the pre-eruption topography. These favored locations are reflected in the parallel trends of the central spine of the explosion structures. Sufficient water existed in the troughs that both bases of the first and second cooling units were quenched. Water was trapped between units in the scoriaceous top of the first cooling unit.

3) Models for mechanisms triggering the violent interaction of water with molten basalt are: a) tectonic in origin, b) excessive pressure mechanism from heating, and c) fuel-coolant reactions. Tectonic mechanisms include either fracture of the base of the second unit directly from movement caused by faulting and folding or favorable troughs cut by drainage networks into pre-eruption topography that are controlled by faulting and folding. A pressure mechanism fractures the base of the second cooling unit from excessive water/steam pressure that resulted from the transfer of heat from the flow. Finally, a fuel-coolant mechanism triggered an explosion from instabilities and fragmentation along the water-basalt interface.

4) The violent explosions can act either episodically or as a single event. Episodic formation is less reasonable, because pulses would not produce the vertical stratification in the central spine. Single event formation is more reasonable and can produce the vertical stratification. Violent upward release of steam/water causes mixing and fragmentation during formation of explosion

structures. These two processes produced the unique intraflow zones that are reflected in the petrographic textures, geochemical characteristics and jointing patterns observed within explosion structures.

REFERENCES CITED

Anderson, A. T., 1973, The before-eruption water content of some high-alumina magmas: Bulletin of Volcanology, v. 37, pp. 530-552.

Anderson, A. T., Friedman, J. O., Wood, T. V., and Wyszynski, J., 1982, The fractional crystallization of plagioclase in the Hat Creek Basalt: observations and theory: Journal of Geology, v. 90, pp. 545-558.

Board, S. J., Clarke, A. J., Duffey, R. B., Hall, R. S., and Poole, D. H., 1971, An experimental study of energy transfer processes relevant to thermal explosions: International Journal of Heat and Mass Transfer, v. 14, pp. 1631-1641.

Board, S. J., Hall, R. W., and Hall, R. S., 1975, Detonation of fuel coolant explosions: Nature, v.254, pp. 319-321.

Board, S. J., Farmer, C. L., and Poole, D. H., 1974, Fragmentation in thermal explosions: International Journal of Heat and Mass Transfer, v. 17, pp. 331-339.

Bryan, W. B., 1972, Morphology of quenched crystals in submarine basalts: Journal of Geophysical Research, v. 77, pp. 5812-5819.

Buchanan, D. J., 1974, A model for fuel-coolant interactions: Journal of Physics, Applied Physics, v. 7, pp. 1441-1457.

Buchanan, D. J., and Dullforce, T. A., 1973, Mechanisms for vapor explosions: Nature, v. 245, pp. 32-34.

Burnham, C. W., 1975, Water and magmas: a mixing model: Geochimica et Cosmochimica Acta, v. 39, pp. 1077-1084.

Cox, K. G., Bell, J. D., and Pankhurst, R. J., 1984, The interpretation of igneous rocks: London, George Allen and Unwin, 450 p.

Cummings, M. L., Orzol, L. L., and Trone, P. M., 1987, Characteristic of the Troy flow, Grande Ronde Basalt in the area of thickened flow-top breccias, northeastern Oregon: evidence for mixing [abs.]: Geological Society of America Bulletin, Abstrasts with Programs, v. 19, pp. 369.

Degraff, J .M., and Aydin, A., 1987, Fracture growth directions and inferred thermal regime during solidification of basaltic lava flows [abs.]: Geological Society of America Bulletin, Abstrasts with Programs, v. 19, pp. 371.

Desai, P. J. and Anderson, A. T., 1974, Nature and Origin of microphenocrysts in a basalt: Bulletin of Volcanclogy, v. 38, pp. 65-72.

Dowty, E., Keil, K., and Prinz, M., 1974, Lunar pyroxene-phyric basalts: crystallization under supercooled conditions: Journal of Petrology, v. 15, pp. 419-453.

Drake, M. J.,1976, Plagioclase-melt equilibria: Geochimica et Cosmochimica Acta, v. 40, pp. 457-465.

Fisher, R. V., and Schmincke, H. U., 1984, Pyroclastic rocks: Berlin, Germany, Springer-Verlag, 472 p.

Fuller, R. F., 1931, The aqueous chilling of basaltic lava on the Columbia River Plateau: American Journal of Science, v. 21, pp. 281-300.

Gibb, F. G., 1974, Supercooling and the crystallization of plagioclase from a basaltic magma: Mineralogical Magazine, v. 39, pp. 641-653.

Hamilton, D. L., Burnham, C. W., and Osborn, E. F., 1964, The solubility of water and effects of oxygen fugacity and water content on crystallization in mafic magmas: Journal of Petrology, v. 5, pp. 21-39.

Hoffer, J. M., 1966, Compositional variations of plagioclase feldspar from a basaltic lava flow: The American Mineralogist, v. 51, pp. 807-813.

Hoffer, J. M., 1970, Plagioclase mineralogy of the Rock Creek flow, Columbia River Basalt: in, Gilmour, E.H., and Stradling, D., eds., Proceedings of the second Columbia River Basalt symposium, Cheney, Washington, EWSC Press, pp. 51-54.

Holmgren, D .A., 1968, Origin of subhorizontal platey jointing in the Yakima basalt: Northwest Science, v. 42, p. 35.

Hooper, P .R., and Camp, V. E., 1981, Deformation of the southeast part of the Columbia Plateau: Geology, v. 9, pp. 323-328.

Khitarov, N. I. and Kadik, A. A., 1973, Water and carbon dioxide in magmatic melts and peculiarities of the melting process: Contribution to Mineralogy and Petrology, v. 41, pp. 205-215.

Kirkpatrick, J. R., 1977, Nucleation and growth of plagioclase, Makaopuhi and Alae lava lakes, Kilauea Volcanco, Hawaii: Geological Society of America Bulletin, v. 88, pp. 78-84.

Kokelaar, P., 1986, Magma-water interactions in subaqueous and emergent basaltic volcanism: Bulletin of Volcanology, v. 48, pp. 275-289.

Kouchi, A., Tsuchiyama, A., and Sunagawa, I., 1986, Effect of stirring on crystallization kinetics of basalt: texture and element partitioning: Contribution to Mineralogy and Petrology, v. 93, pp. 429-438.

Lipman, P. W., and Banks, N. G., 1987, AA flow dynamics, Mauna Loa 1984: in Decker, R. W., Wright, T. L., and Stauffer, P. H., eds., United States Geological Survey Professional Paper 1350, pp. 1527-1568.

Lofgren, G. E., 1983, Effect of heterogeneous nucleation on basaltic textures: a dynamic crystallization study: Journal of Petrology, v. 24, pp. 229-255.

Long, P. E., 1987, Review of evidence for quenching origin of entablatures in Columbia River Basalt flows [abs.]: Geological Society of America Bulletin, Abstrasts with Programs, v. 19, pp. 399.

Loomis, T. P.,1979, An empirical model for plagioclase equilibrium in hydrous melts: Geochimica et Cosmochimica Acta, v. 43, pp. 1753-1759.

MacDonald, G. A., 1949, Petrography of the Island of Hawaii: United States Geological Survey Professional Paper 214-D, 95 p.

MacDonald, G. A., 1953, Pahoehoe, aa, and block lava: American Journal of Science, v. 251, pp. 169-191.

MacDonald, G. A., 1963, Physical properties of erupting Hawaiian magmas: Geological Society of America Bulletin, v. 74., pp. 1071-1078.

MacDonald, G. A., 1972, Volcanoes: New Jersey, Prentice-Hall, Inc., 510 p.

Moore, J. G., 1970, Pillow lava in a historic lava flow from Hualallai Volcano, Hawaii: Journal of Geology, v. 78, pp. 239-243.

Moore, J. G., Cristofolini, R., and Lo Giudice, A., 1971, Development of pillows on the submarine extension of recent lava flows, Mount Etna, Sicily: United States Geological Survey Professional Paper 750-C, pp. 89-97.

Moore, J. G., Phillips, R. L., Grigg, R. W., Peterson, D. W., and Swanson, D. A., 1973, Flow of lava into the sea: Geological Society of America Bulletin, v. 84, pp. 537-546.

Murase, T., and McBirney, A. R., 1973, Properties of some common igneous rocks and their melts at high temperatures: Geological Society of America Bulletin, v. 84, pp. 3563-3592.

Myers, C. W. and Price, S. M., 1979, Geologic studies of the Columbia Plateau: a status report: Rockwell Hanford Operations, Richland, Washington, RHO-BWI-ST-4, 454 p.

Orzol, L. L., and Cummings, M. L., 1986, Phreatic structures in flows of the Grande Ronde Basalt, Columbia River Basalt Group, near Troy, Oregon [abs.]: Abstrasts with Programs, Geological Society of America, v. 18, pp. 167-168.

Orzol, L. L., and Cummings, M. L., 1986, Phreatic explosion features in Grande Ronde Basalt near Troy, Oregon [abs.]: Oregon Academy of Science, In Press

Orzol, L. L., and Cummings, M. L., 1987, Distribution of phreatic eruption structures in the Troy flow, Grande Ronde basalt, near Troy, Oregon [abs.]: Oregon Academy of Science, In Press

Osborn, E. F., 1959, Role of oxygen pressure in the crystallization and differentiation of basaltic magmas: American Journal of Science, v. 257, pp. 609-647.

Peck, D. L., Moore, J. G., and Kojima, G., 1964, Temperatures in the crust and melt of Alae Lava Lake, Hawaii, after the August 1963 eruption of Kilauea Volcano-a preliminary report: United States Geological Survey Professional Paper 501-D, pp. 1-7.

Peck, D. L., Wright, T. L., and Moore. J. G., 1966, Crystallization of tholeiitic basalt in Alae Lava Lake, Hawaii: Bulletin of Volcanology, v. 29, pp. 629-656.

Peck, D. L., Hamilton, M. S., and Shaw, H. R., 1977, Numerical analysis lava lake cooling models: part II, application to Alae Lava Lake, Hawaii: American Journal of Science, v. 277, pp. 415-437.

Reid, R. C., 1976, Superheated liquids: American Scientist: v. 64, pp. 146-156.

Reidel, S. P., Tolan, T. L., Anderson, J. L., Beeson, M. H., and Fecht, K. R., 1987, Regional stratigraphy of the Grande Ronde Basalt (GRB) and its tectonic and petrogenetic implications [abs.]: Geological Society of America Bulletin, Abstrasts with Programs, v. 19, pp. 442.

Rowley, P. D., Kuntz, M. A., and MacLeod, N. S., 1981, Pyroclastic-flow deposits, in, Lipman, P. W., and Mullineaux, D. R., eds., The 1980 eruptions of Mount St. Helens, Washington, United States Geological Survey Professional Paper 1250, pp. 489-512.

Ross, M. E., 1975, The structure of Yakima basalts in a portion of the Grande Ronde River region of northeastern Oregon and southeastern Washington: Geological Society of America Abstrasts with Programs, v. 3, pp. 51.

Ross, M. E., 1978, Stratigraphy, structure, and petrology of Columbia River Basalt in a portion of the Grande Ronde River-Blue Mountains area of Oregon and Washington: Richland, Washington, Rockwell Hanford Operations, RHO-SA-58, 460 p.

Ross, M. E., 1980, Tectonic controls of topographic development within Columbia River basalts in a portion of the Grande Ronde River-Blue Mountains region, Oregon and Washington: Oregon Geology, v. 42, pp. 167-174.

Russel, I.C., 1897, A reconnaissance in southeastern Washington: United States Geological Survey Water Supply Paper, pp. 1-76.

Schmincke, H. U., 1967, Stratigraphy and petrography of four upper Yakima basalt flows in south-central Washington: Geological Society of American Bulletin, v. 78, pp. 1385-1422.

Shaw, H. R., Wright, T. L., Peck, D. L., and Okamura, R., 1968, The viscosity of basaltic magma: an analysis of field measurements in Makaopuhi Lava Lake, Hawaii: American Journal of Science, v. 266, pp. 225-264.

Shaw, H. R., 1969, Rheology of basalt in the melting range: Journal of Petrology, v. 10, pp. 510-535.

Shaw, H. R., 1972, Viscosities of magmatic silicate liquids: an empirical method of prediction: American Journal of Science, v. 272, pp. 870-893.

Shaw, H. R., and Swanson, D. A., 1970, Eruption and flow rates of flood basalts: in, Gilmour, E.H., and Stradling, D., eds., Proceedings of the second Columbia River Basalt Symposium, Cheney, Washington, EWSC Press, pp. 271-300.

Shaw, H. R., Hamilton, M. S., and Peck, D. L., 1977, Numerical analysis of lava lake cooling models: part I, Description of the method: American Journal of Science, v. 277, p. 384-414.

Sheridan, M. F., and Wohletz, K. H., 1983, Hydrovolcanism: Basic considerations and review: Journal of Volcanology and Geothermal Research, v. 17, pp. 1-29.

Silver, L., and Stolper, E., 1985, A thermodynamic model for hydrous silicate melts: Journal of Geology, v. 93, pp. 161-178.

Smith, R. L., 1960, Ash flows: Geological Society of American Bulletin, v. 71, pp. 795-842.

Stoffel, K. L., 1981, Preliminary report on the geology of the Grande Ronde lignite field, Asotin County, Washington: State of Washington, Division of Geology and Earth Resources, Open-File Report 81-6, 30 p.

Stoffel, K. L., 1984, Geology of the Grande Ronde lignite field Asotin County, Washington: State of Washington, Division of Geology and Earth Resources, Report of Investigations 27, 79 p.

Swanson, D. A., 1967, Yakima basalt of the Tieton River area, south-central Washington: Geological Society of America Bulletin, v. 78, pp. 1077-1110.

Swanson, D. A., and Wright, T. L., and Helz, R. T., 1975, Linear vent systems and estimated rates of magma production and eruption for the Yakima Basalt on the Columbia Plateau: American Journal of Science, v. 275, pp. 877-905.

Swanson, D. A., and Wright, T. L., Hooper, P. R., and Bently, R. D., 1979, Revisions in stratigraphic nomenclature of the Columbia River Basalt Group: United States Geological Survey Bulletin 1457-C, 59 p.

Swanson, D. A., and Wright, T. L., Camp, V. E., Gardner, J. N., Helz, R. T., Price, S. A., and Ross, M. E., 1977, Reconnaissance geologic map of the Columbia River Basalt Group, Pullman and Walla Walla quadrangles, southeast Washington and adjacent Idaho: United States Geological Survey Open File Map, 77-100.

Swanson, D. A., and Wright, T. L., 1981, Guide to geologic field trip between Lewiston, Idaho, and Kimberly, Oregon, emphasizing the Columbia River Basalt Group, in, Johnston, D. A. and Nolan-Donnelly, eds., Guides to some volcanic terranes in Washington, Idaho, Oregon, and Northern California: United States Geological Survey Circular 838, pp. 1-15.

Tolan, T. L., Reidel, S. P., Beeson, M. H., Anderson, J. L., Fecht, K. R., and Swanson, D. A., 1987, Revisions to the areal extent and volume of the Columbia River Basalt Group (CRBG) [abs.]: Geological Society of America Bulletin, Abstrasts with Programs, v. 19, pp. 458

Walker, D., Kirkpatrick, R. J., Longhi, J., and Hays, J. F., 1976, Crystallization history of lunar picritic basalt sample 12002: phase-equilibrium and cooling rates studies: Geological Society of America Bulletin, v. 87, pp. 646-656.

Walker, G. P., 1971, Characteristics of some basaltic pyoclastics: Bulletin of Volcanology, v. 35, pp. 305-317.

Walker, G. W., 1973, Contrasting compositions of the youngest Columbia River basalt flows in Union and Wallowa Counties, northeastern Oregon: Geological Society of American Bulletin, v. 84, pp. 425-430.

Walker, G. W., 1979, Reconnaissance geologic map of the Oregon part of the Grangeville quadrangle, Baker, Union, Umatilla, and Wallowa Counties, Oregon: United States Geological Survey Miscellaneous Investigations Series, Map I-1116, scale 1:250,000.

Waters, A. C., 1955, Volcanic rocks and the tectonic cycle: Geological Society of American, Special Paper 62, pp. 703-722.

Waters, A. C., 1960, Determining direction of flow in basalts: American Journal of Science, v. 258-A, pp. 350-366.

Waters, A. C., 1961, Stratigraphic and lithologic variations in the Columbia River basalt: American Journal of Science, v. 259, pp. 583-611.

Wentworth, C. K., and MacDonald, G. A., 1953, Structures and forms of basaltic rocks in Hawaii: United States Geological Survey Bulletin 994, 98 p.

Williams, H., Turner, F. J., and Gilbert, C. M., 1982, Petrography: an introduction to the study of rocks in thin sections: San Francisco, W.H. Freeman and Company, 626 p.

Witte, L. C., Cox, J. E., and Bouvier, 1970, The vapor explosion: Journal of Metals, v. 22, pp. 39-44.

Wohletz, K. H., 1983, Mechanisms of hydrovolcanic pyroclast formation: grain-size, scanning electron microscopy, and experimental studies: Journal of Volcanology and Geothermal Research, v. 17, pp. 31-63.

Wohletz, K. H., and Sheridan, M. F., 1983, Hydrovolcanic explosions II. Evolution of basaltic tuff rings and tuff cones: American Journal of Science, v. 283, pp. 385-413.

Wohletz, K. H., and McQueen, R. G., 1984b, Experimental studies of hydromagmatic volcanism: in, Explosive volcanism: Inception, evolution, and hazards, Studies in geophysics: National Academy Press, Washington, DC, pp. 158-169.

Wohletz, K. H., 1986, Explosive magma-water interactions: thermodynamics, explosion mechanisms, and field studies: Bulletin of Volcanology, v. 48, pp. 245-264.

Wright, T. L, and Okamura, R. T., 1977, Cooling and crystallization of tholeiitic basalt, !965 Makaopuhi Lava Lake, Hawaii: United States Geological Survey Professional Paper 1004, 78 p.

Vlasov, K. A., 1966, Geochemistry of rare elements Volume I: ed., Jerusalem, Israel, S. Monson, 688 p.

APPENDIX A

SUMMARY OF STRATIGRAPHIC AND SAMPLE INFORMATION

TABLE XIII

SUMMARY OF LOCATIONS, MAP SYMBOL, FLOW TYPES FOR EACH STRATIGRAPHIC SECTION

Stratigraphic site label	*Map symbol	+Type section	$Total Flows	&Troy Brecciated	Starting Location 7 1/2 minute quadrangles
Eden Bench	EB	VC	6	Y	NE1/4,NW1/4,SE1/4 Sect 5 T5N R43E Troy
Wenaha Camp	WC	V	1	Y	SE1/4,NE1/4,NW1/4 Sect 5 T5N R43E Troy
Wenaha Camp Road	WCR	V	3	Y	SE1/4,NE1/4,NW1/4 Sect 5 T5N R43E Troy
Umatilla	U	VC	4	Y	SE1/4,NE1/4,NE1/4 Sect 1 T6N R42E Eden
Crooked Creek	CC	VC	2	Y	SW1/4,SW1/4,NE1/4 Sect 27 T6N R42E Eden
South Wenaha	SW	V	2	Y	SW1/4,NE1/4,NE1/4 Sect 5 T5N R43E Troy
Wenaha Ravine	WR	V	1	Y	SE1/4,NW1/4,NE1/4 Sect 5 T5N R43E Troy
Elloit Bend	EF	B	$\geq$3	Y	NW1/4,NW1/4,SE1/4 Sect 9 T5N R43E Troy
Grouse Creek	GC	VC	0	0	NE1/4,SW1/4,SW1/4 Sect 24 T5N R43E Troy
Hoodoo Trail	H	VC	3	Y	SE1/4,NE1/4,SW1/4 Sect 29 T6N R42E Eden
Maggie Canyon	MC	B	$\geq$2	Y	NW1/4,SE1/4,NW1/4 Sect 3 T5N R43E Troy
Lighte Flat	LF	B	$\geq$2	Y	NW1/4,SW1/4,NW1/4 Sect 3 T5N R43E Troy
Squaw Canyon #1	SC1	B	$\geq$4	Y	NW1/4,SE1/4,NW1/4 Sect 35 T6N R43E Troy
Squaw Canyon #2	SC2	B	$\geq$2	Y	NE1/4,SW1/4,NE1/4 Sect 35 T6N R43E Troy
Floral Grade	F	V	$\geq$2	C	SE1/4,SW1/4,NW1/4 Sect 1 T5N R43E Troy
South Grande Ronde	SG	B	3	Y	NW1/4,SW1/4,NW1/4 Sect 17 T5N R43E Troy
Saddle Mountain	SM	B	$\geq$2	Y	SE1/4,SW1/4,NE1/4 Sect 29 T7N R43E Saddle Butte
Wenaha River	W	V	$\geq$1	Y	SW1/4,SW1/4,NW1/4 Sect 5 T5N R43E Troy
Cougar Creek	C	V	$\geq$1	Y	NE1/4,NE1/4,NW1/4 Sect 32 T7N R44E Mountain View

* Map Symbols are used to indentify the stratigraphic sections on Plate 1 and used to indentify each section in Appendix A.
+ Type section indicates the method used to measure each stratigraphic section.
    VC - vertical complete section through all flows present at the site.
    V - partial vertical section through selected flows.
    B - lateral section to dtermine horizontal variations through one or more flows.
$ The total number of brecciated flows present.
& Troy Brecciated indicates if the Troy flow contained explosion structures (Y) or lacks explosion structures (0) or the Troy flow was covered (C).

Table XIV

DEFINITIONS FOR SYMBOLS USED IN STRATIGRAPHIC SECTIONS
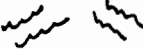
Symbols	Definitions
	Undulating base
	Covered base
	Invasive lobes
	Breccia associated with invasive lobes
	Chilled Pahoehoe base
	Subjacent clay zone
	Flow-top breccia or rubble flow-top
	Distinct first cooling unit
	Vesicular intraflow zones
	Vugy zone
	Inclined vesicles and vug (the plane of elongation is inclined)

Table XIV CONTINUED

DEFINITIONS FOR SYMBOLS USED IN STRATIGRAPHIC SECTIONS
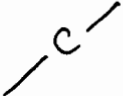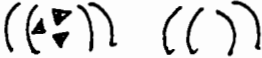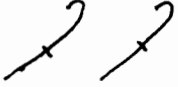
Symbols	Definitions
	Covered interval
	Confining walls with trapped vesicles or breccia and without
	Breccia spine
	Highly fractured zone
	Platey jointing
	Convex-up or convex-down platey jointing
	Columnade jointing
	Blockly jointing
	Platey blocky jointing
	Spheroidal weathering
	Fault planes

Table XIV CONTINUED

DEFINITIONS FOR SYMBOLS USED IN STRATIGRAPHIC SECTIONS

Symbols	Definitions
SU	Stratigraphic formation
UN	Flow name
GR	Grand Ronde Basalt
T	Troy flow
W	Wanapum Basalt
SM	Saddle Mountains Basalt
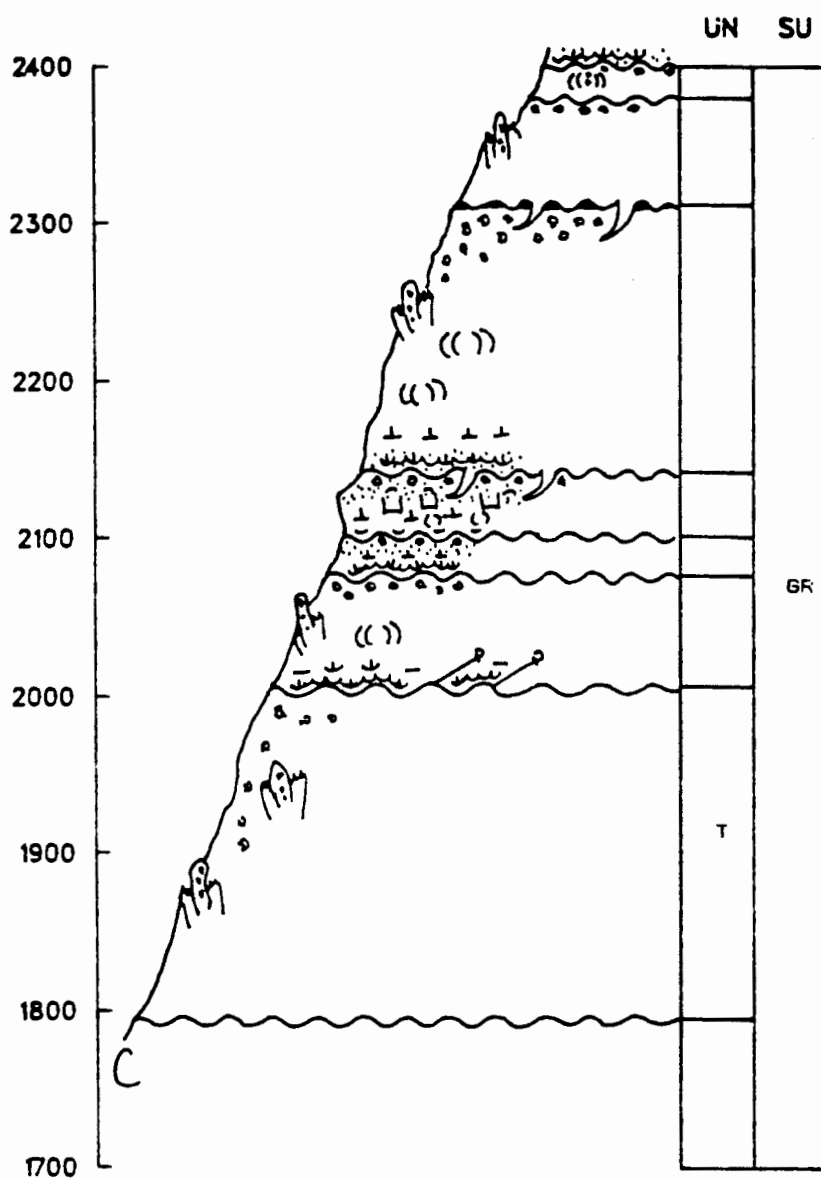
Figure 35. Eden Bench section (EB).
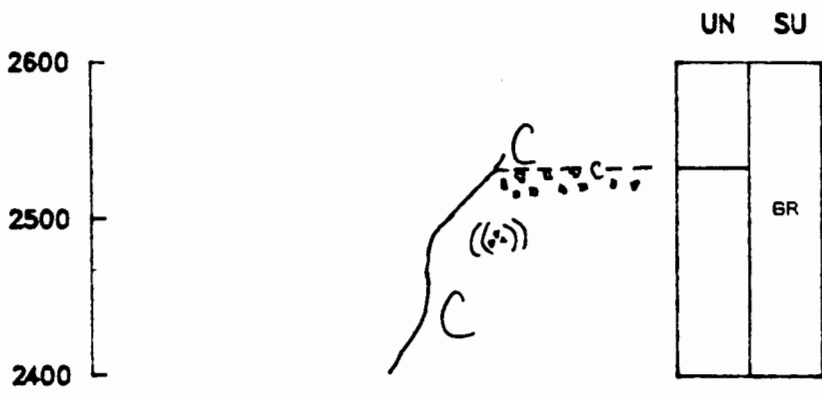
Figure 35. Eden Bench section (EB) continued.
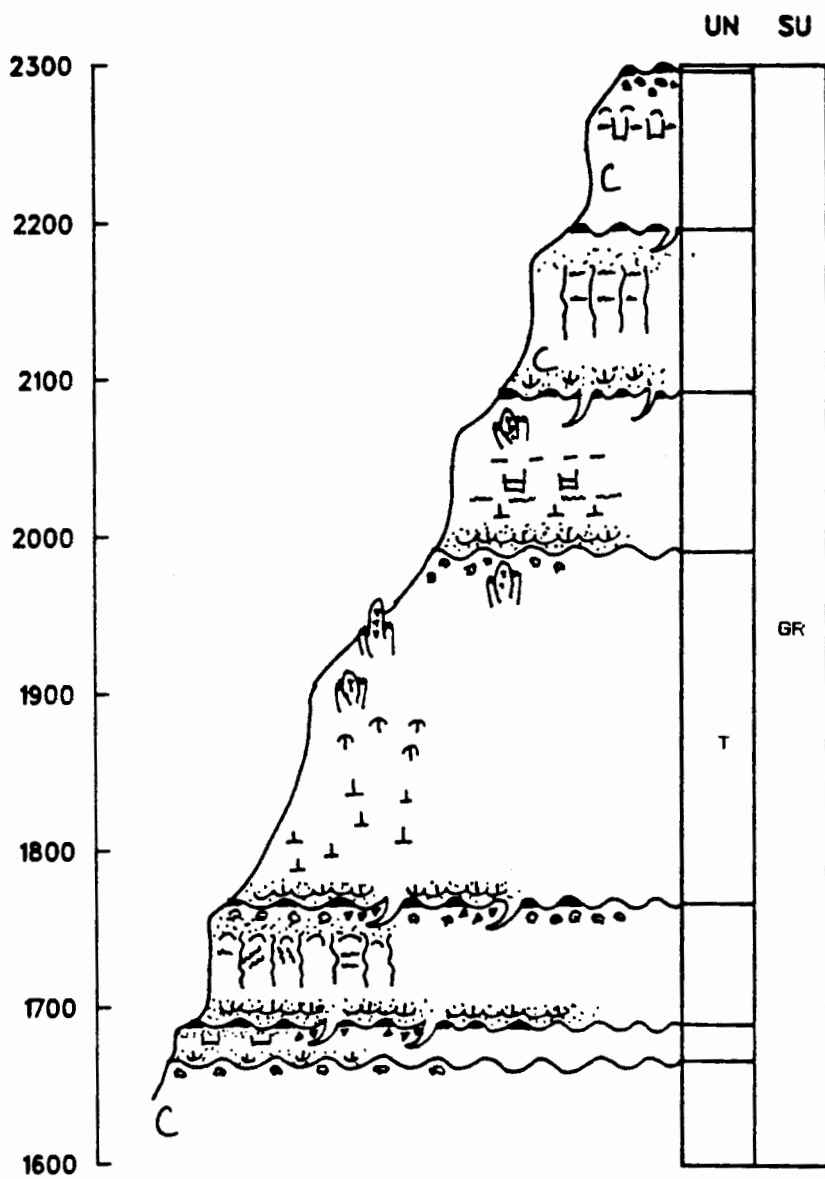
Figure 36. Wenaha Camp section (WC).
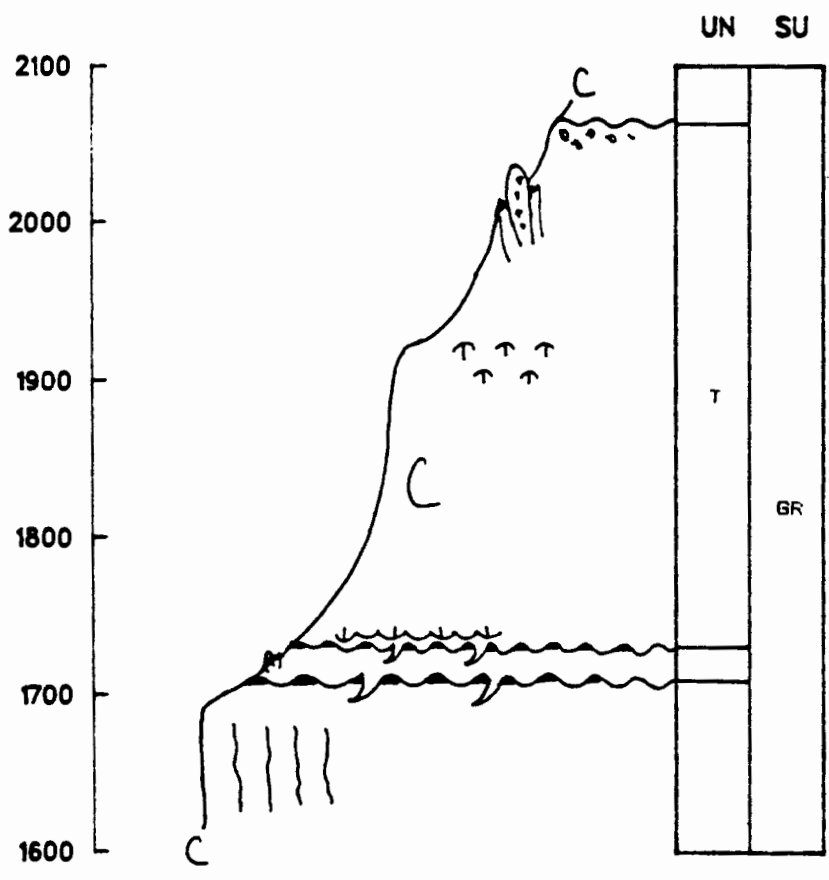
Figure 37. Wenaha Camp Road section (WCR).
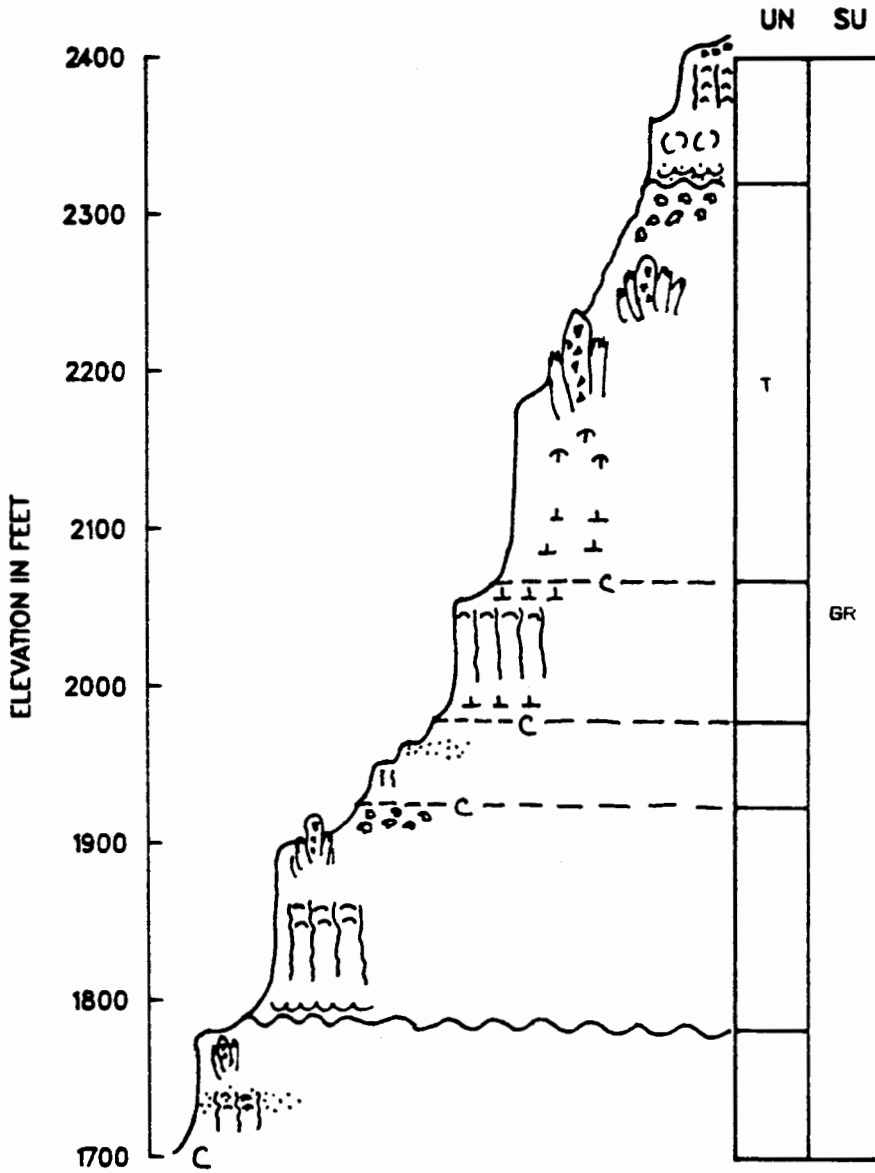
Figure 38. Umatilla section (U).
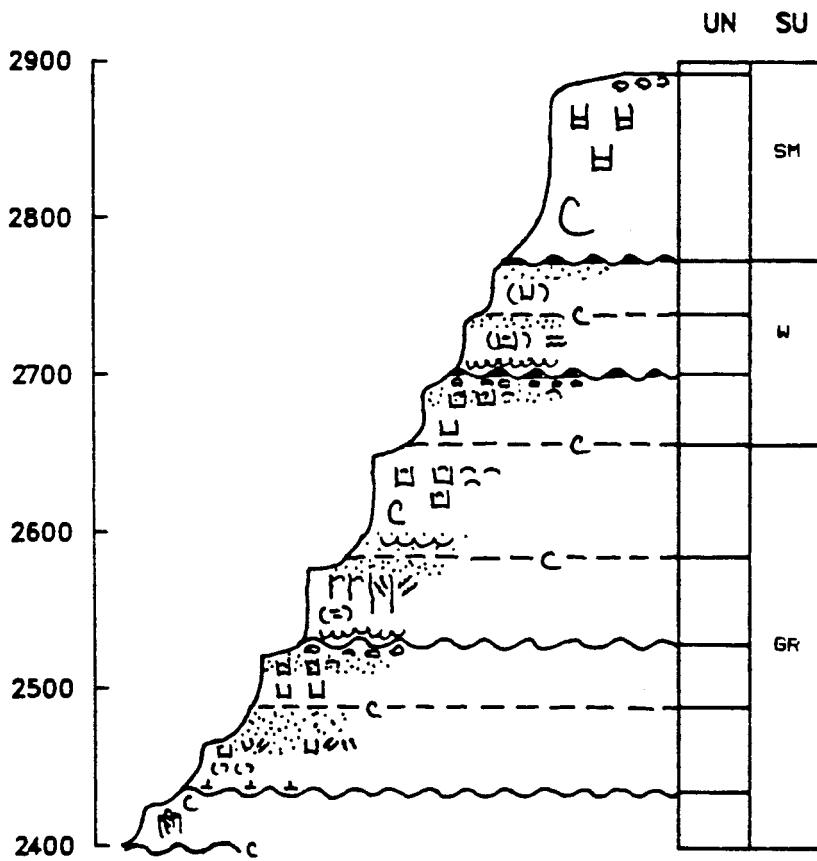
Figure 38. Umatilla section (U) continued.
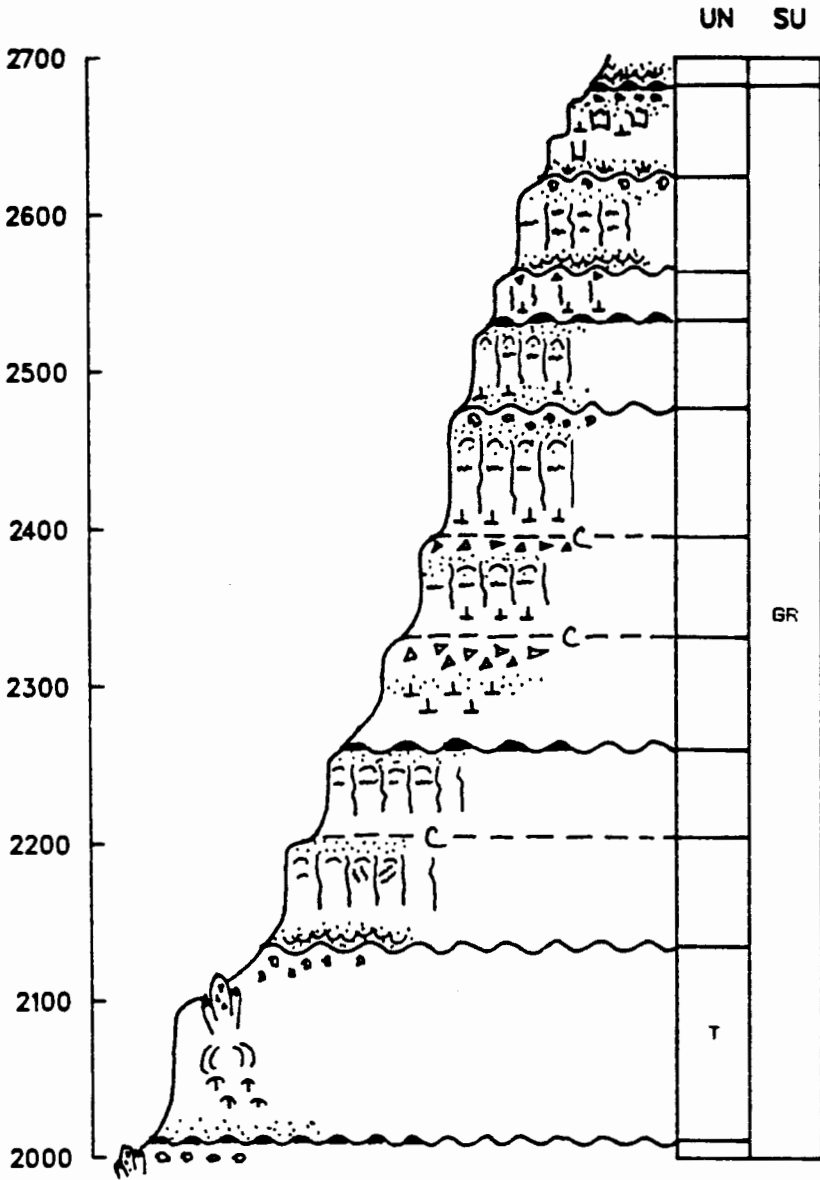
Figure 39. Crooked Creek section (CC).
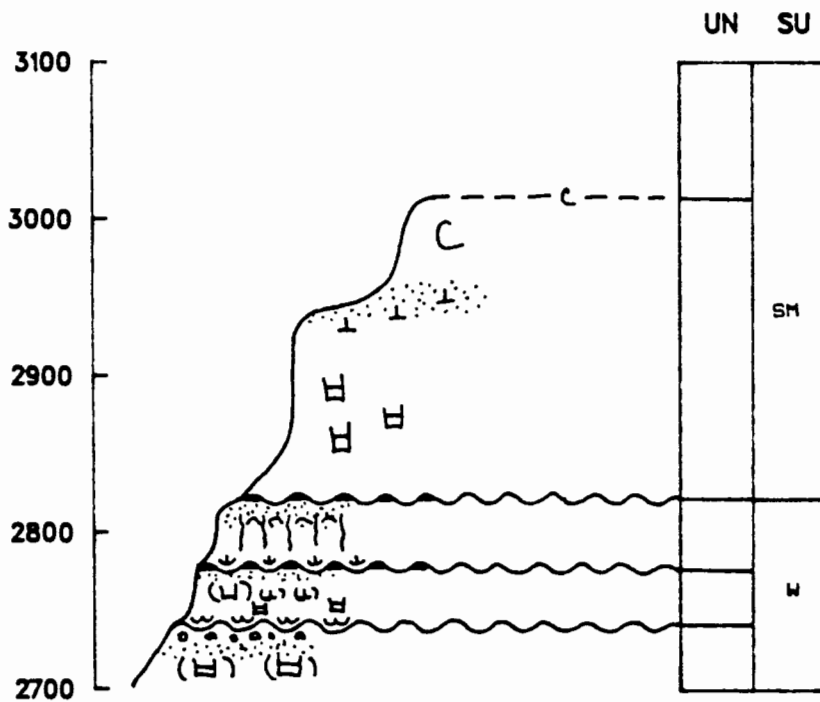
Figure 39. Crooked Creek section (CC) continued.
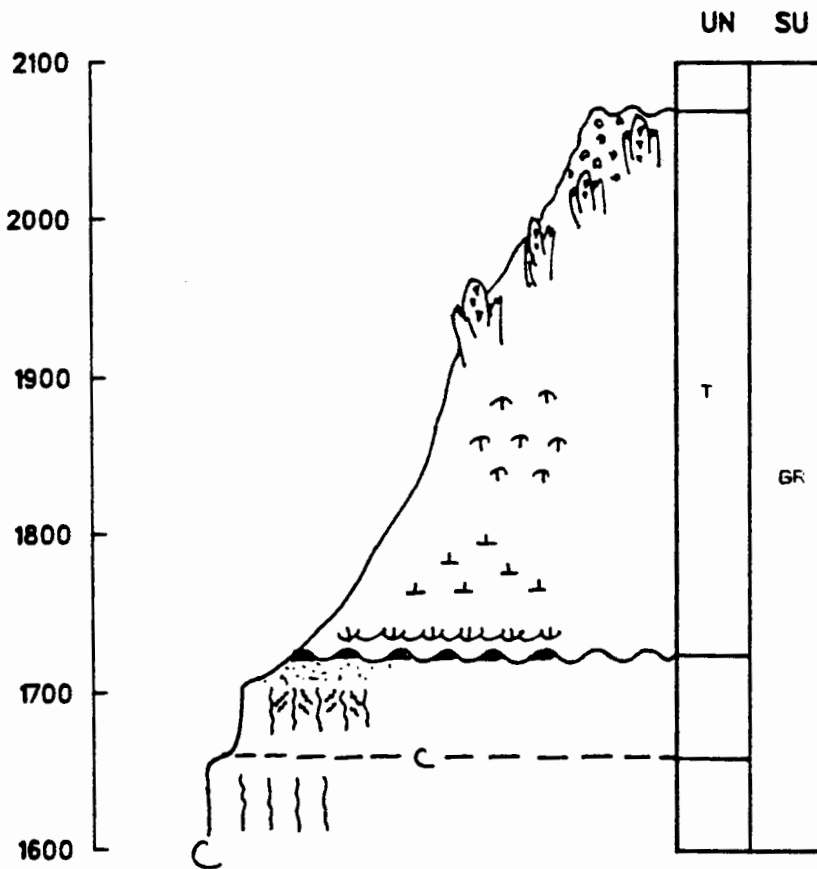
Figure 40. South Wenaha section (SW).
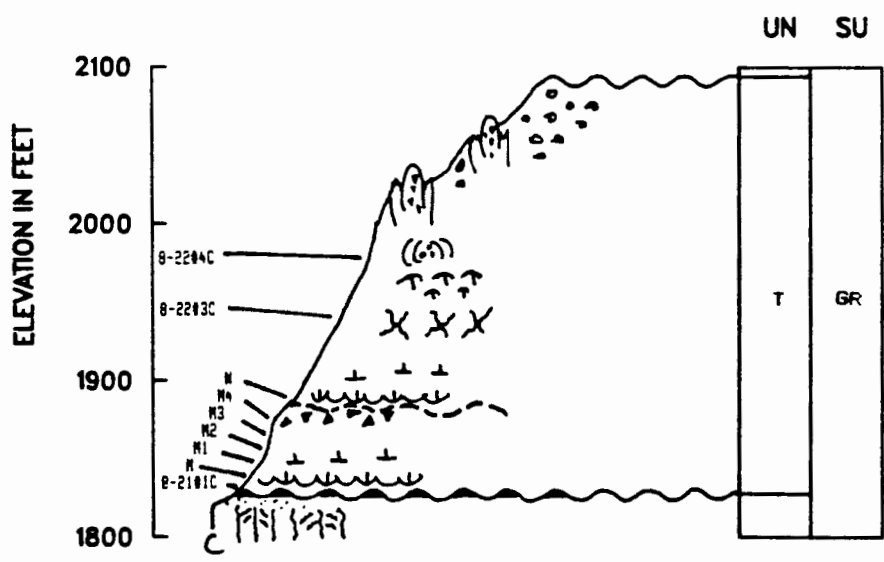
Figure 41. Wenaha Ravine section (W).
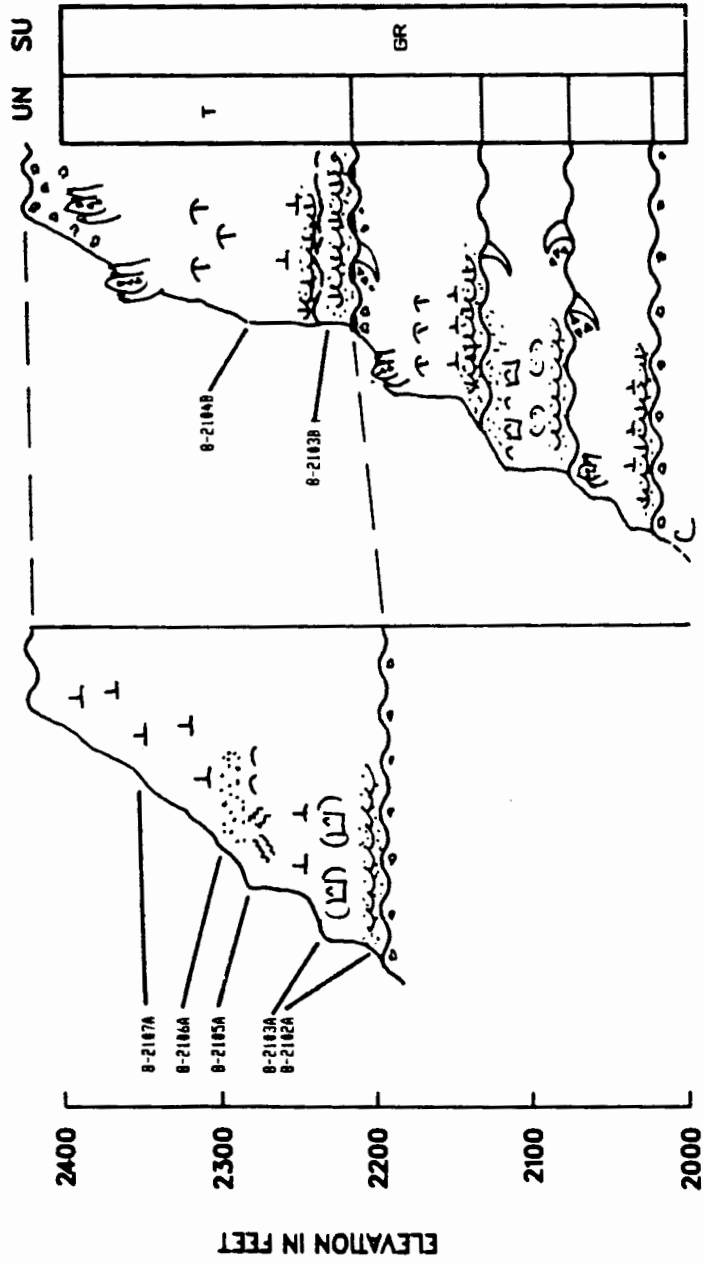
Figure 42. Elloit Farm section (EF).
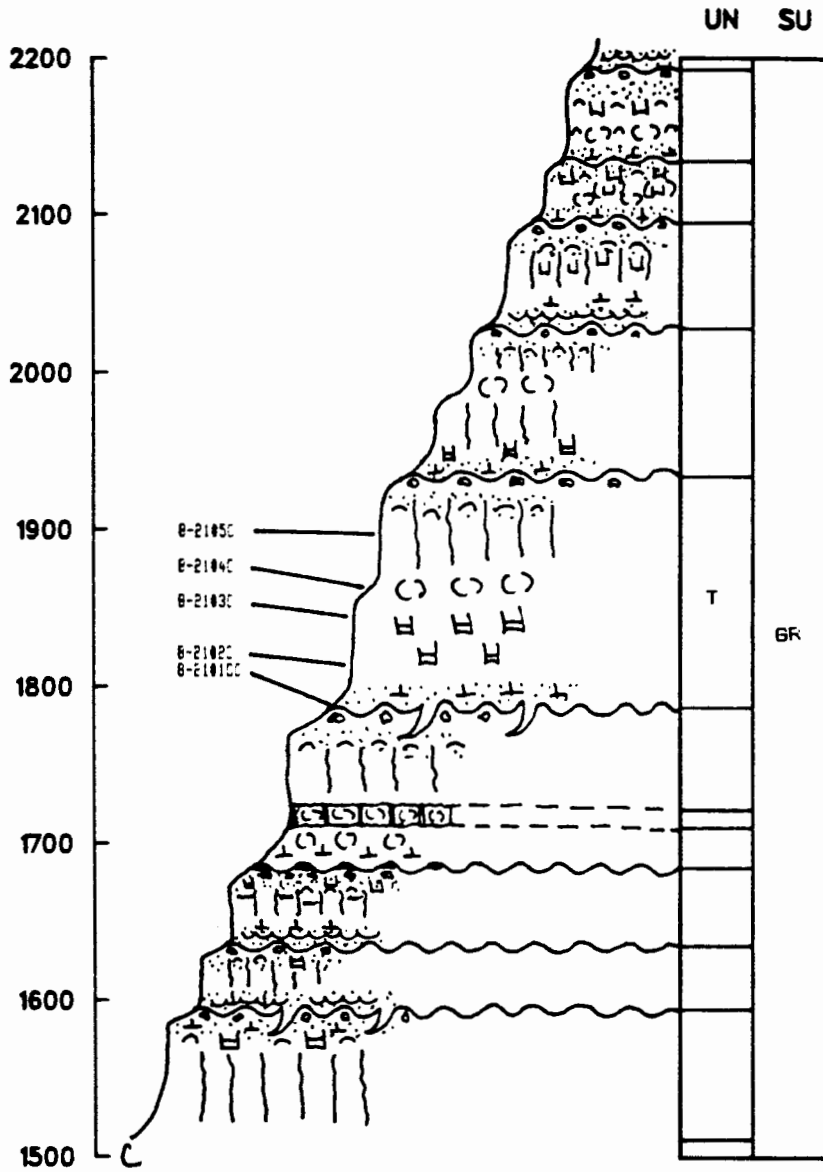
Figure 43. Grouse Creek section (GC).
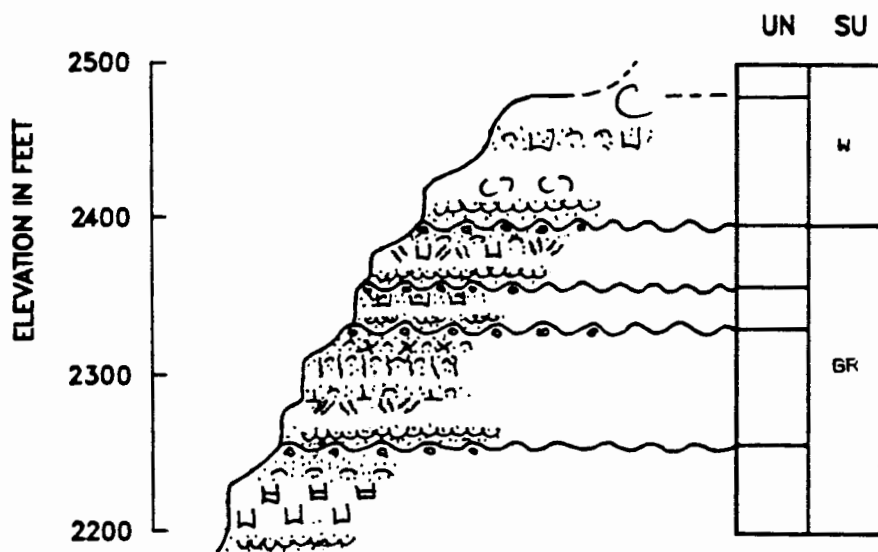
Figure 43. Grouse Creek section (GC).
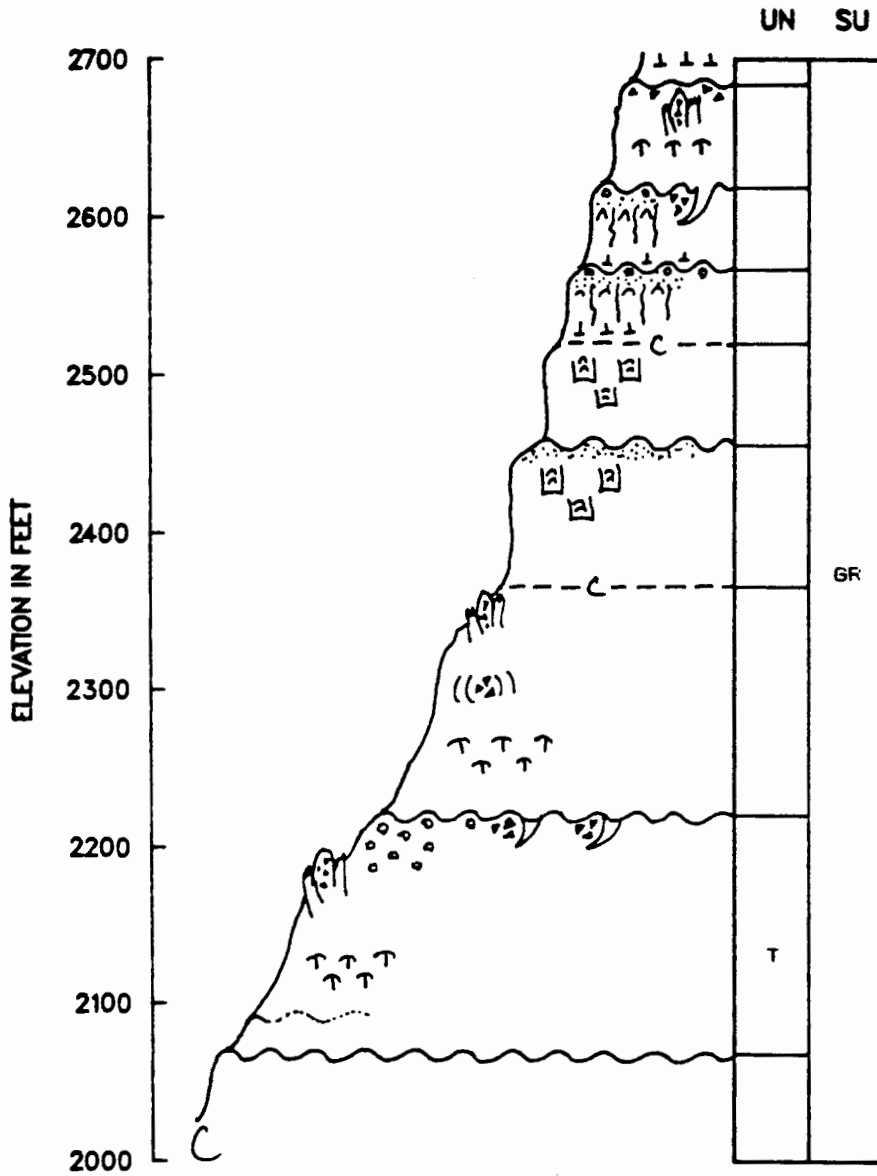
Figure 44. Hoodoo Trail section (H).
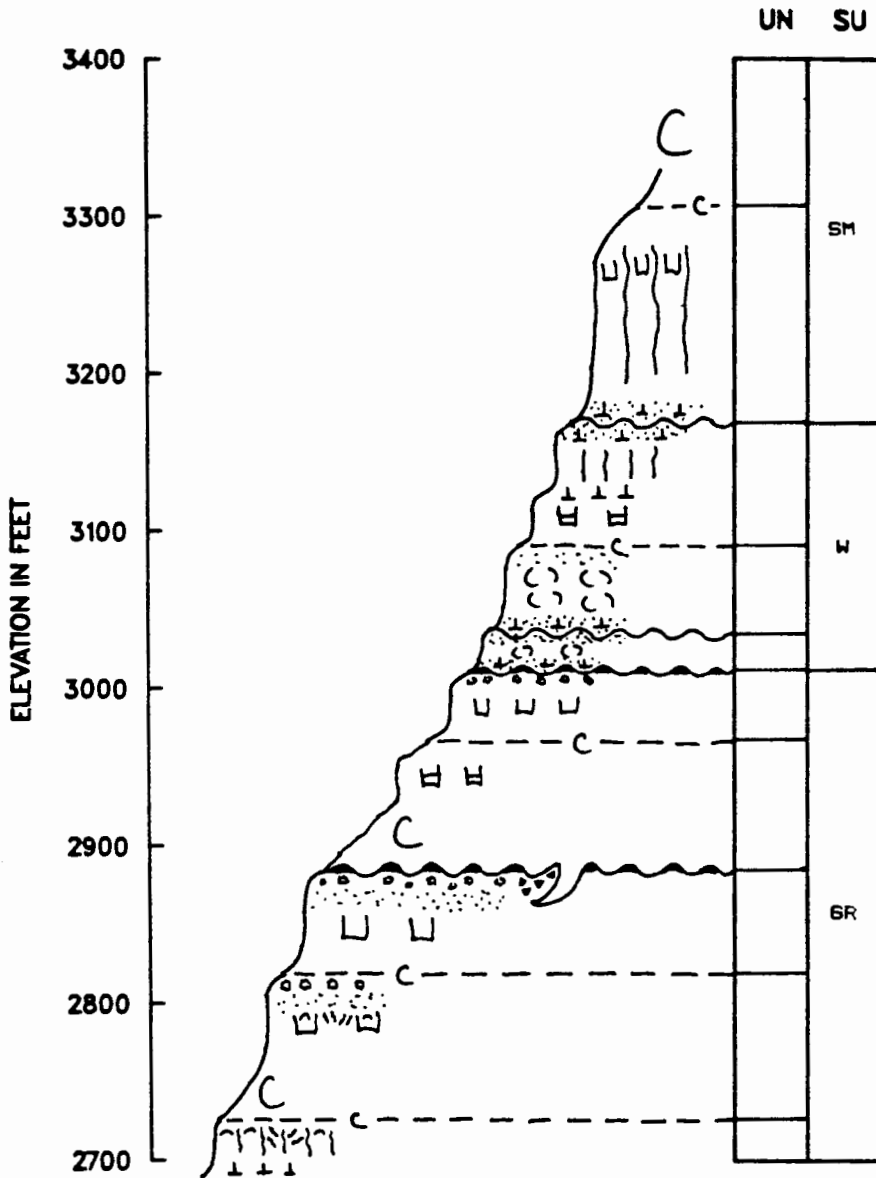
Figure 44. Hoodoo Trail section (H) continued.

135
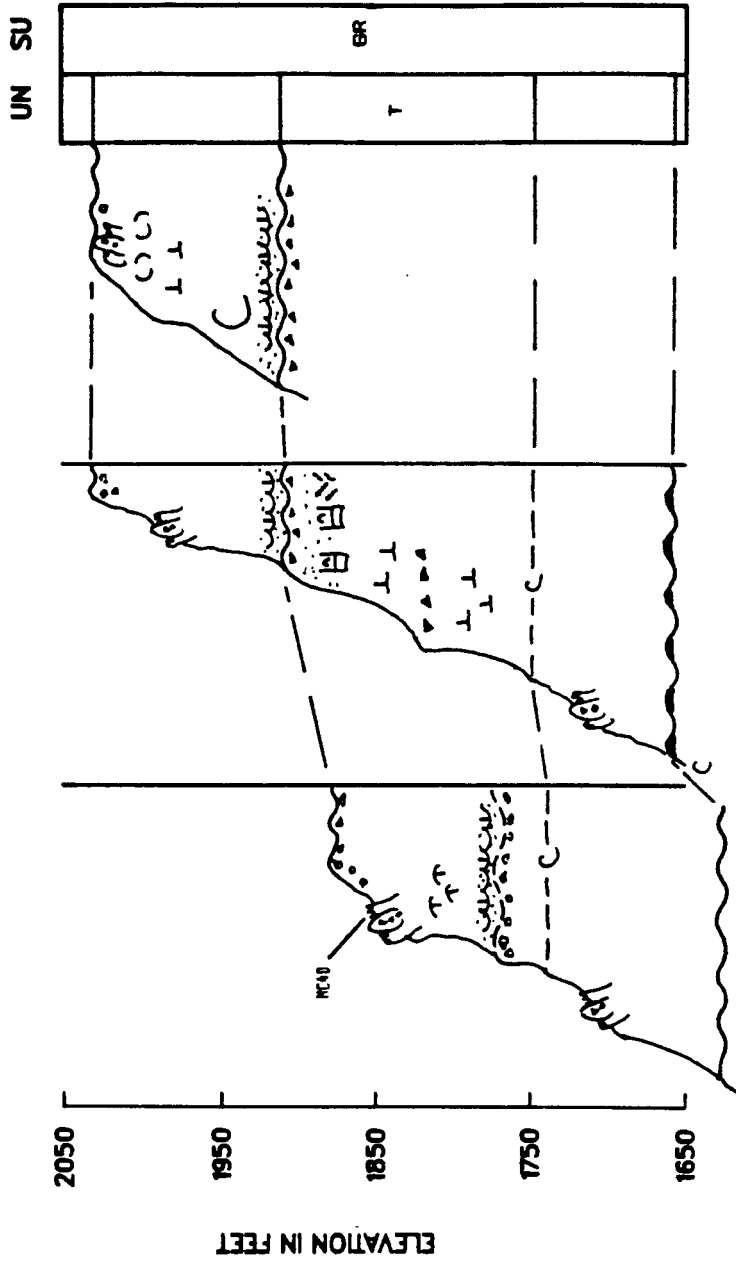
Figure 45. Maggie Canyon section (MC).

Figure 46. Lightle Flat section (LF).

137
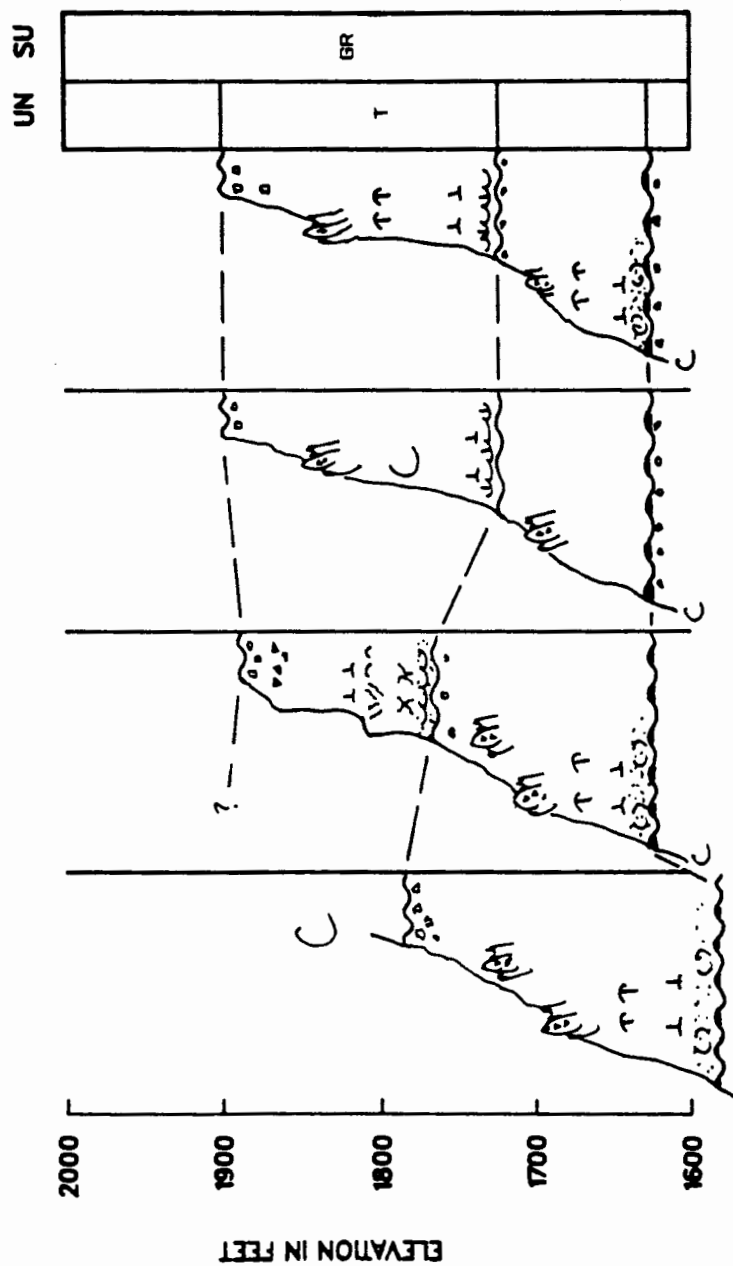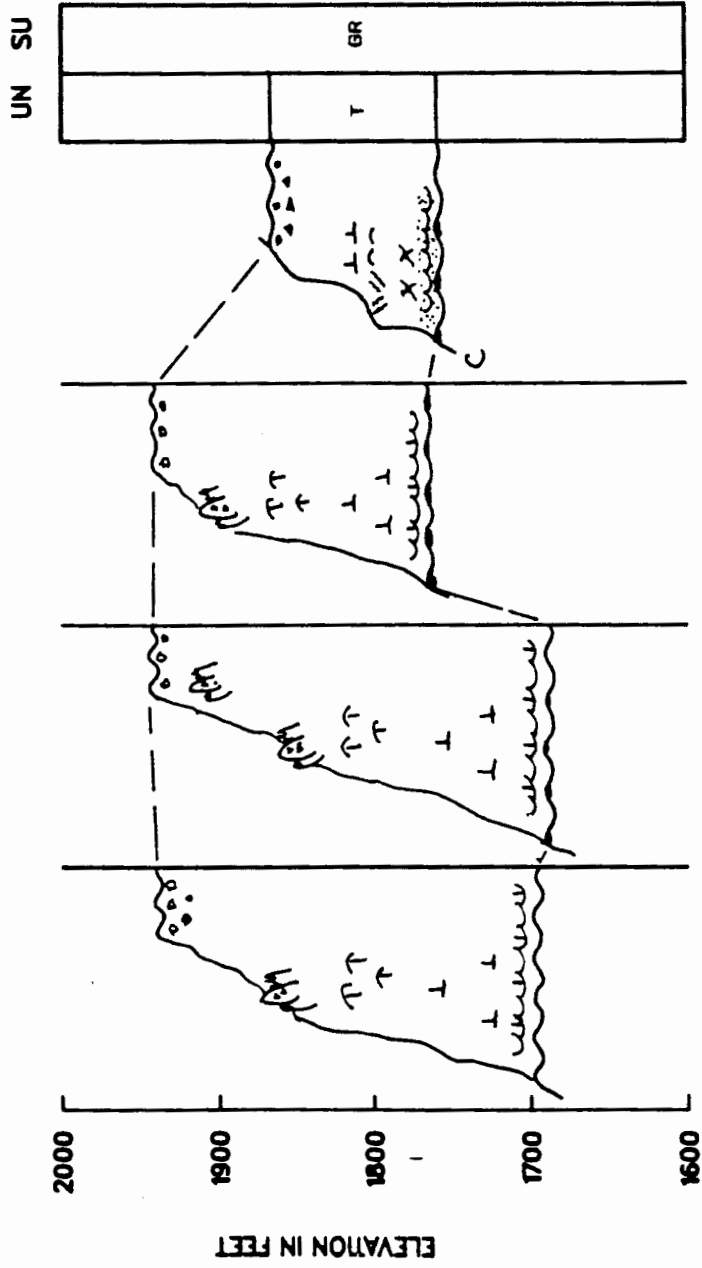
Figure 46. Lightle Flat section (LF) continued.

138
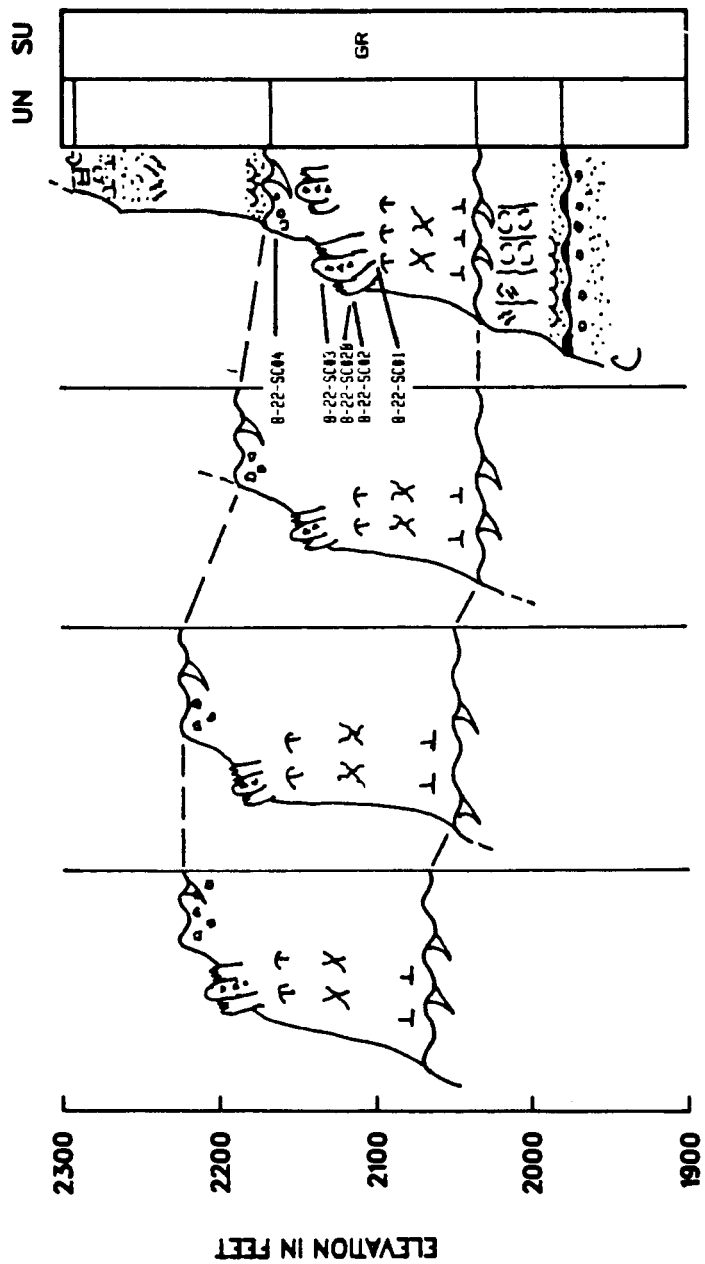
Figure 47. Squaw Canyon #1 section (SC1).
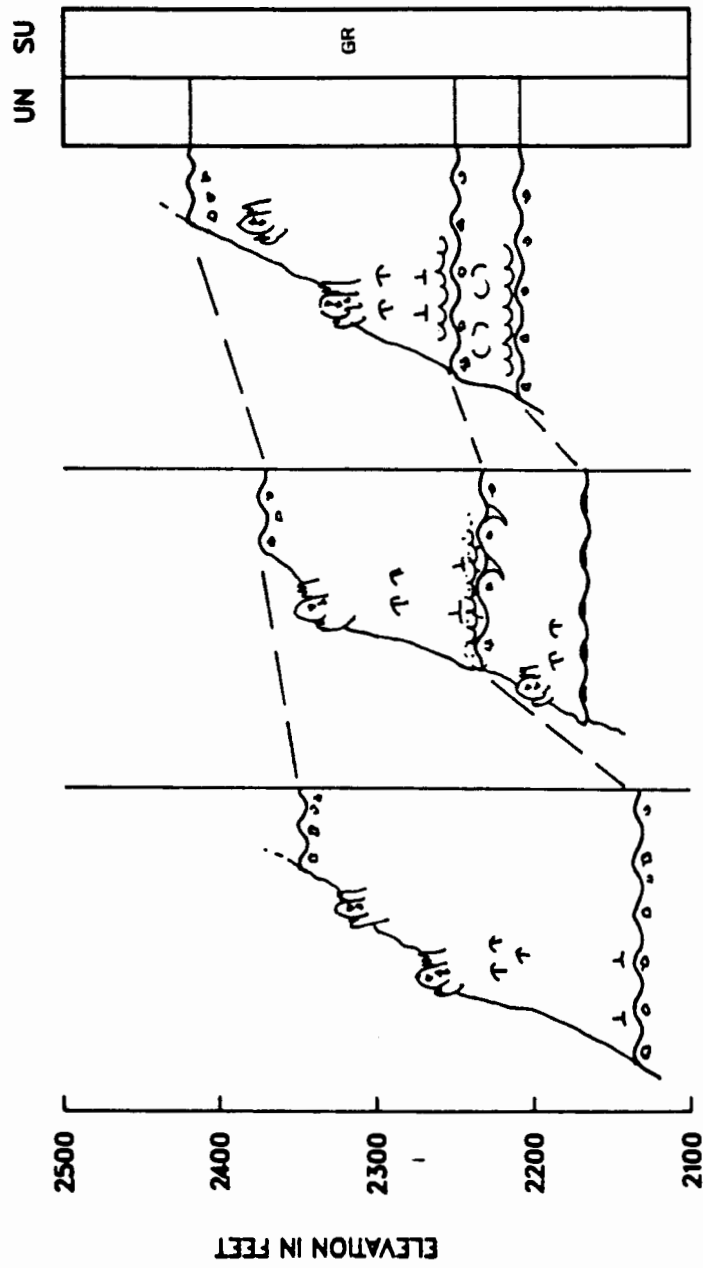
Figure 48. Squaw Canyon #2 section (SC2).
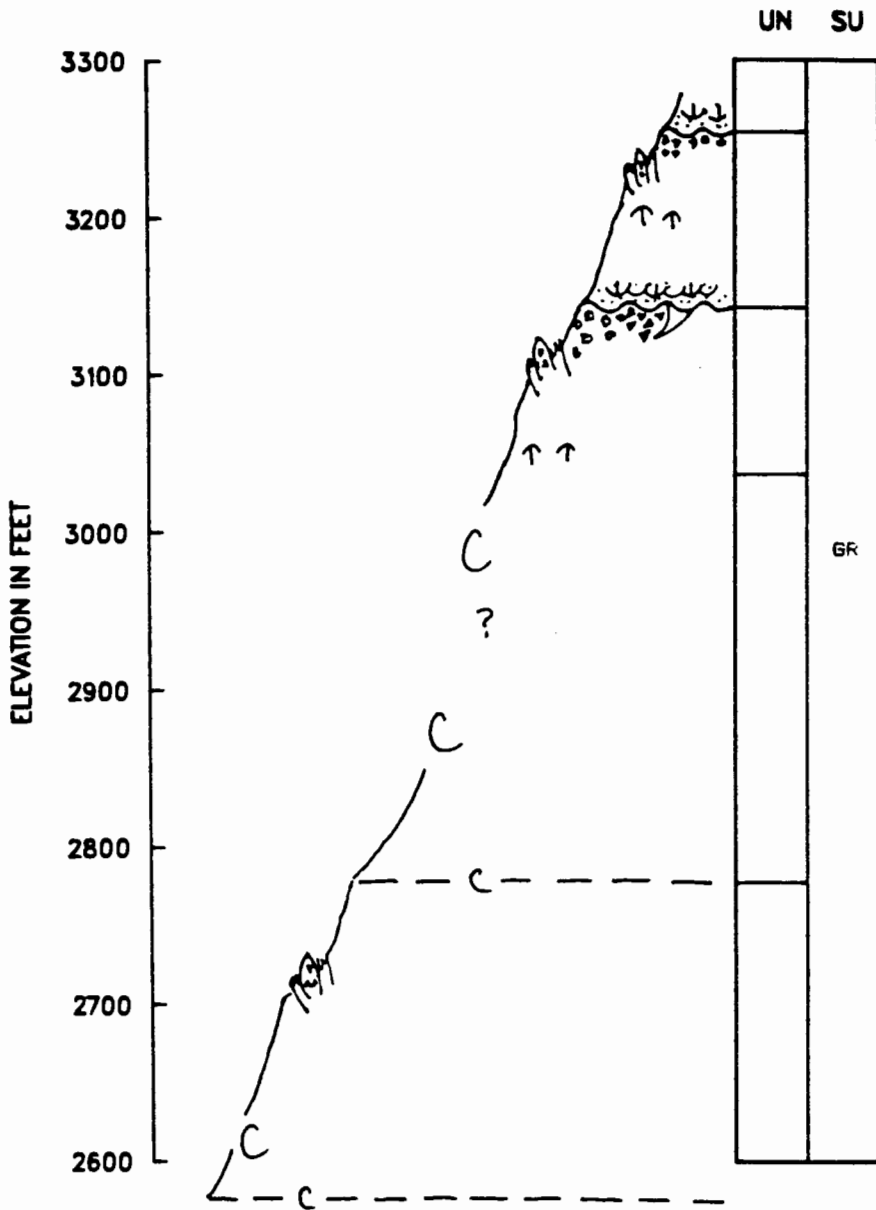
Figure 49. Flora Grade section (F).
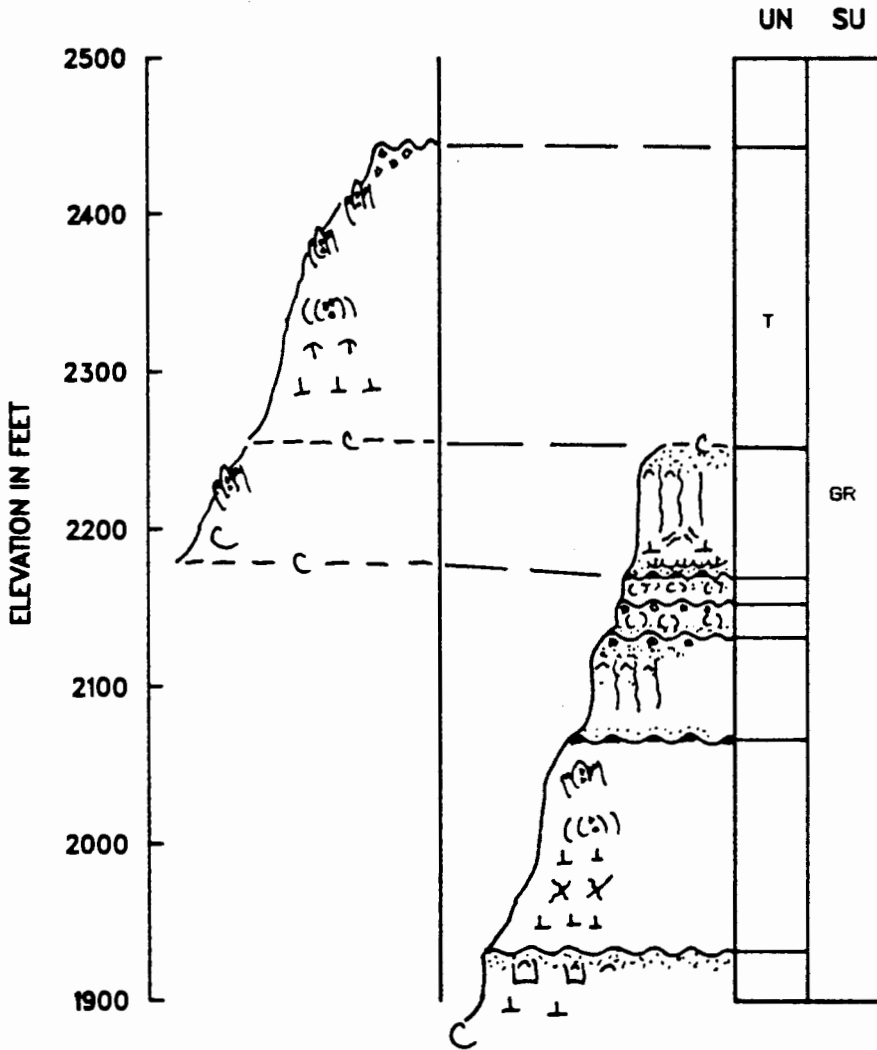
Figure 50. South Grande Ronde section (SG).
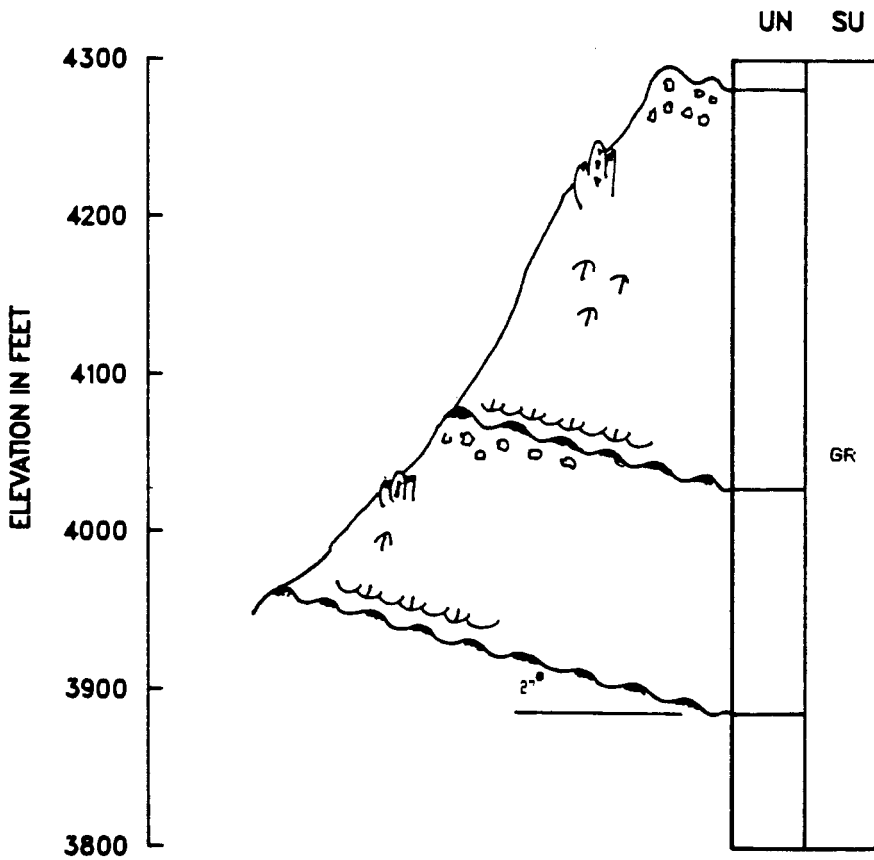
Figure 51. Saddle Mountain section (SM).
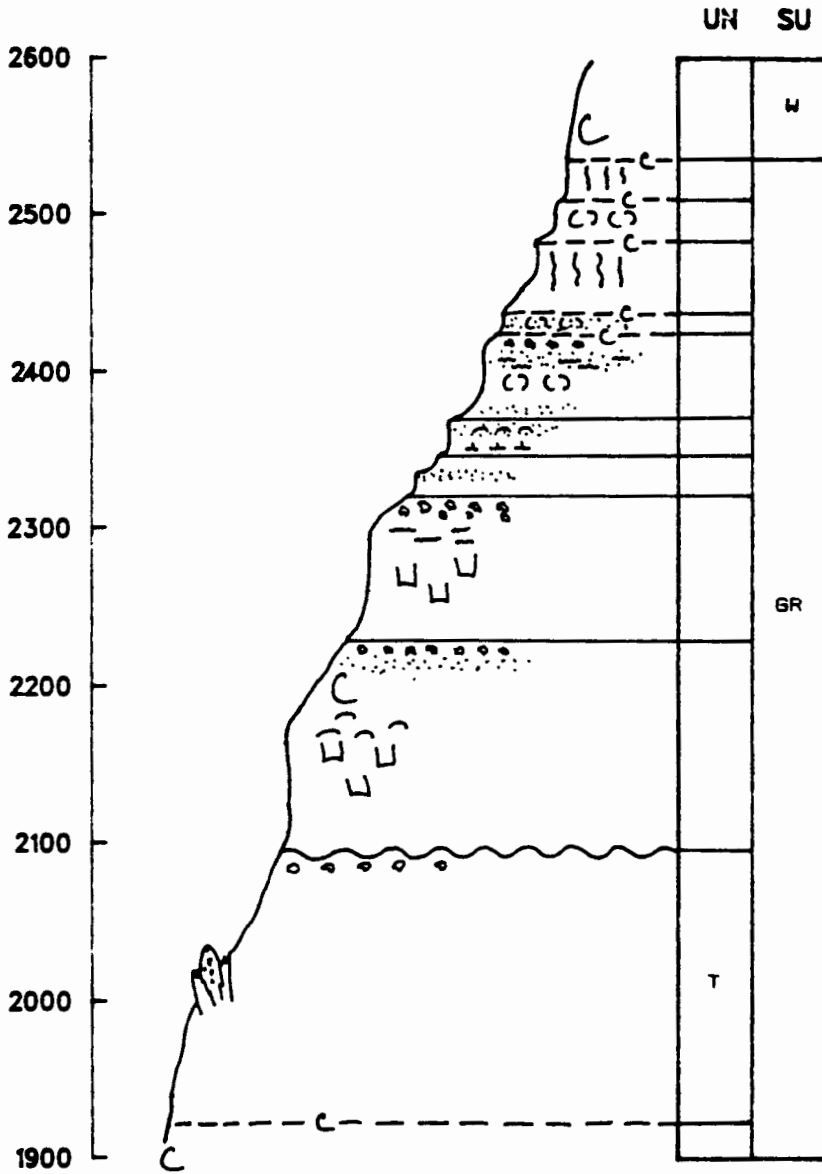
Figure 52. Wenaha River section (W).
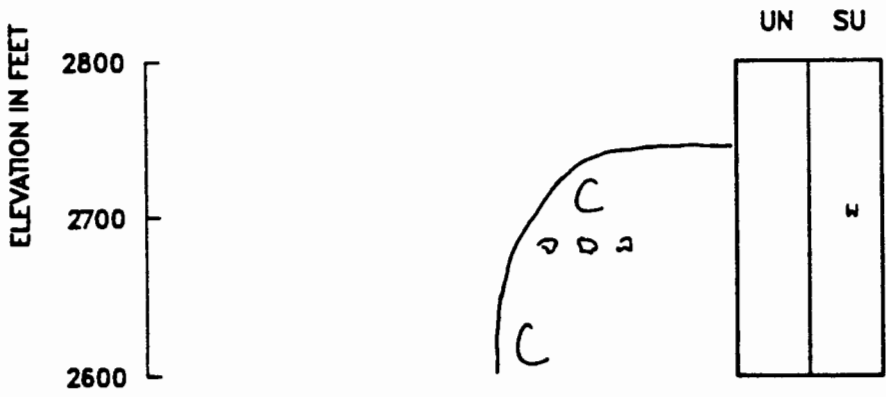
Figure 52. Wenaha River section (W) continued.
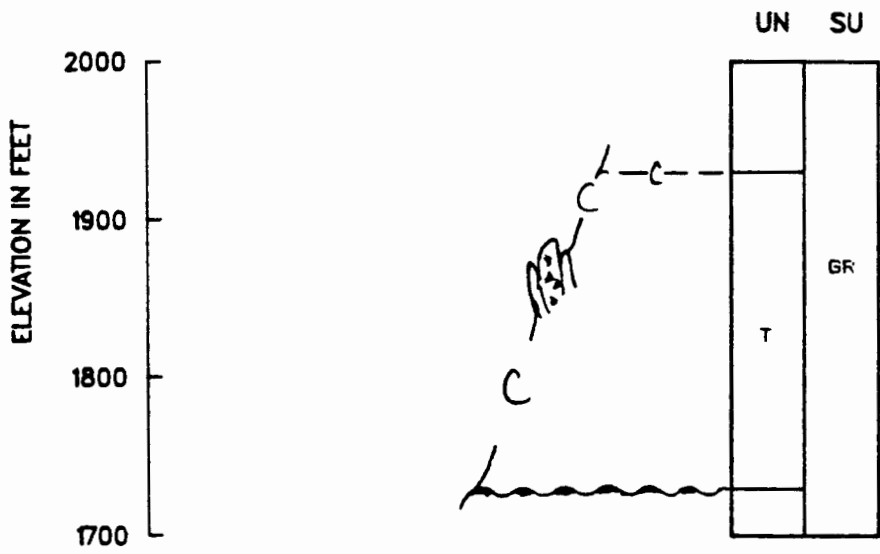
Figure 53. Cougar Creek section (C).

APPENDIX B

SUMMARY OF PETROGRAPHIC INFORMATION

TABLE XV

DEFINITIONS OF TERMS USED FOR GROUNDMASS TERMS

Term	*Definition
vitrophyric	If phenocrysts (microphenocrysts as well) lie in a matrix composed of glass.
intergranular	The angular interstices between the feldspars are occupied by ferro-magnesian granules, usually olivine, pyroxene, or iron-titanium oxides, of random orientation.
intersertal	If interstices are filled with glass, cryptocrystalline material, or non-granular deuteric and secondary materials, such as serpentine, smectite, or others.
trachytic	Microlites of feldspars are dis-posed in a subparallel manner as a result of flow and their interstices are occupied by micro- or cryptocrystalline material.
pilotaxitic	Similar to trachytic, but the subparallel manner is less pronounced.
hyaloophitic	Intersertal texture in which glass and nongranular minerals begin to envelop the feldspars.
banded	Banding of different textural layers within the basalt rocks such as intergranular and vitrophyric layers. The bands have a sub-parallel orientations to each other and a planar orientation.
crenulate bands	Banding of different layers as above (banding) ,but the contact between each other as well as the layer itself have a crenulated form.

* Definitions taken from Williams, Gilbert, and Turner (1982).

TABLE XVI

DEFINITIONS USED FOR PHENOCRYSTS AND MICROPHENOCRYSTS

Term	Definition
microphenocrysts	Microphenocrysts are less than 1 mm in size.
phenocrysts	Phenocrysts are greater than 1 mm in size.
equant	Microphenocrysts and phenocrysts grains have equal dimensions.
prismatic	Individual grain has grown longer in one direction than the other directions.
sharp	Grain boundaries are distinct.
irregular	The boundary of the mineral crystal has irregular undulations with the surrounding grains.
fractured	Phenocrysts or microphenocrysts have been broken into smaller fragments.
glomero-	Phenocrysts or microphenocrysts are gathered in distinct clusters.
cross-shaped	Mineral grains which have crossed shaped appearances, that is not due to twinning.
remnant	Remnant shadow texture of an original cystal, which now no longer exists.
swallow-tailed	A quench texture in which the peripheral edges (lath or prism shaped grains) grow at a faster rate than the interior resulting in v-shaped terminal form.
symplectite	Growth of a mineral grain at a favorable location on a different mineral grain. Growth of these grains is simultaneous. This growth behavior results in skewed cross-shaped grains.
2V	The measured "2V" angle of clinopyroxene is first described positive or negative followed by the extinction angle with the c-axis then the measured "2V" angle.
An content	The An content of plagioclase was measured using the Michel-Levy method for phenocrysts, microphenocrysts, and microlites (under respective columns). The An content for microphenocrysts occurring within different colored bands or different textural types of basalt was measured separately for certain thin sections.
plagioclase zoning	Plagioclase zoning was recorded under the respective columns for phenocrysts and microphenocrysts.

TABLE XVII

DEFINITIONS OF TERMS USED FOR VESICLES

Term	Definition
spherical	Spherical shaped vesicles.
planar	Planar shaped vesicles, that the size of the length dimension is greater than 5 times the width dimension.
enlongated	Elongated-shaped vesicles, that the size of the length dimension is less than 5 times its width dimension, but still is greater than its width.
irregular	Irregularly shaped vesicles where the peripheral surface is marked by sharp undulations of projecting crystalline material from the basalt.
crenulated	Crenulated-shaped vesicles where the vesicles have been flattened, but the overall form has been crinkled.
filled	These vesicles are filled with secondary materials such as zeolites or opal/quartz.
large	These vesicles are unusually large compared to the relative sizes (greater than 5 mm in diameter) found in other thin sections described in this section.
random	These vesicles are found in a random pattern within the rock as observed in thin sections.
zones	Concentrations of vesicles are found in zones across the thin section.

TABLE XVIII

SYMBOLS AND DEFINITIONS FOR ADJECTIVES USED

Symbol	Term	Definition
N	not counted	Phenocrysts or microphenocrysts were observed, but were not included during the counting process.
W	well developed	The adjective emphasizes the texture term is relatively better developed as compared to the same texture in other thin sections.
P	poorly developed	The opposite of well-developed. The term is relative to other thin sections.
R/R	specific banding	A specific type of color banding in which the layers are both red colored when observed with the nake eye.
R/B	specific banding	A specific type of color banding similar to the above banding, but the layers vary from black colored to red colored.
B/B	specific banding	A specific type of color banding similar to the above banding, but the layers colored black.
R	rare	A term which describes the relative proportion as being rare compared to other thin sections.
V	very	A prefix used to emphasize.
r	remnant	A term describing a feature observed within the groundmass of the thin section consisting of a concentration of microlitic plagioclase. The microlitic concentration forms a shape resembling a phenocryst lath of plagioclase. An eariler formed plagioclase phenocrysts probably reacted with the surrounding melt that resulted in these plagioclase micolites. Ross (1978) noted similar remnant plagioclase features.

TABLE XIX

THIN SECTION DESCRIPTION FOR SAMPLE : M

| | Phenocrysts and microphenocrysts | | | | Groundmass | | Vesicles | |
| | Clinopyroxene | | Plagioclase | | | | | |
	Pheno-crysts	Micropheno-crysts	Pheno-crysts	Micropheno-crysts				
Modal percent	.2	.8	.1	3.1	Modal percent	89.5	Modal percent	4.6
Anhedral		X			vitrophyric	X		
Subhedral		X			intergranular		spherical	X
Euhedral	X	X	X	X	intersertal		planar	
Equant		X		X	trachytic	X	elongated	
Prismatic	X		X	X	pilotaxitic		irregular	X
Sharp			X	X			crenulated	
Irregular	X	X		X	hyaloophitic		filled	X
Fractured							partially filled	X
Glomero-				R	banded		large	
Cross-shaped		R			crenulated bands		random	X
Swallow-tailed				X			zones	X
Symplectite		R		R				
2V angle +	approx. 45							
An content				57		54		
Plagioclase zoning				Osc				

Comments:
  Several distinct zones grade from the surface towards the interior of this thin section. The textural zones are separated from each other by the vesicle pattern. Vesicles are absent along the contact margin and increase in number towards the interior. Arrangement of vesicles is random within these textural zones. Reddish-colored quench cracks penetrate as much as 5 mm inward. Traverse lines for modal counting are perpendicular to the surface contact.

TABLE XX

THIN SECTION DESCRIPTION FOR SAMPLE : M1

	Clinopyroxene Phenocrysts	Clinopyroxene Micropheno-crysts	Plagioclase Phenocrysts	Plagioclase Micropheno-crysts	Groundmass		Vesicles	
Modal percent		N		.1	Modal percent	99.6	Modal percent	.3
Anhedral		X			vitrophyric			
Subhedral					intergranular		spherical	X
Euhedral				X	intersertal	X	planar	
Equant		R		R	trachytic		elongated	
Prismatic		X		X	pilotaxitic	X	irregular	
Sharp				X			crenulated	
Irregular		X		X	hyaloophitic		filled	X
Fractured		X		X			partially filled	
Glomero-					banded		large	
Cross-shaped					crenulated bands		random	X
Swallow-tailed							zones	
Symplectite								
2V angle +		approx. 50 ^ c						
An content			65		57			
Plagioclase zoning			Osc					

Comments:
Clinopyroxene microphenocrysts observed during point counting, but the crystal did not fall under the cross hair. Vesicles are filled with reddish-brown-colored material. Remanent plagioclase grains are visible as a concentration of plagioclase microlites that are grouped in the shape of a microphenocryst lath of plagioclase.

TABLE XXI

THIN SECTION DESCRIPTION FOR SAMPLE : M2

| | Phenocrysts and microphenocrysts | | | | Groundmass | | Vesicles | |
| | Clinopyroxene | | Plagioclase | | | | | |
	Pheno- crysts	Micropheno- crysts	Pheno- crysts	Micropheno- crysts				
Modal percent		2.2		8.9	Modal percent	81.1	Modal percent	7.8
Anhedral					vitrophyric			
Subhedral		X		X	intergranular		spherical	
Euhedral				X	intersertal	X	planar	X
Equant		X		R	trachytic		elongated	
Prismatic		X		X	pilotaxitic	X	irregular	
Sharp							crenulated	X
Irregular		X		X	hyaloophitic	X	filled	X
Fractured		X		X			partially filled	X
Glomero-					banded		large	X
Cross-shaped				R	crenulated bands		random	
Swallow-tailed							zones	X
Symplectite		R		R				
2V angle + (45 ^ c)		approx. 50-60						
An content				58		49		
Plagioclase Zoning				Osc				

Comments:
A reddish-brown-colored rind extending into the groundmass surrounds each vesicle. Planar trend of vesicles parallels alignment of microphenocrysts and microlites. A large microphenocrysts of clinopyroxene has a curved possibly broken fractured shape. Plagioclase microphenocrysts have a seriate texture.

TABLE XXII

THIN SECTION DESCRIPTION FOR SAMPLE : M3

| | Phenocrysts and microphenocrysts | | | | Groundmass | Vesicles |
| | Clinopyroxene | | Plagioclase | | | |
	Pheno-crysts	Micropheno-crysts	Pheno-crysts	Micropheno-crysts		
Modal percent	N	N		1.3	Modal percent 75.7	Modal percent 23.0
Anhedral	X				vitrophyric	
Subhedral				X	intergranular VP to P	spherical X
Euhedral		X	X	X	intersertal	planar
Equant		X	X	X	trachytic	elongated
Prismatic		X	X	X	pilotaxitic	irregular X
Sharp						crenulated
Irregular		X	X	X	hyaloophitic	filled
Fractured						partially filled
Glomero-					banded	large
Cross-shaped					crenulated bands	random
Swallow-tailed						zones X
Synplectic						
2V angle + 40 ^ c						
An content			54			
Plagioclase Zoning			Osc			

Comments:
Smaller vesicles are observed in the very poorly developed intergranular textured zones, while larger vesicles are found in the poorly developed intergranular textured zones. Vesicles are surrounded by reddish-colored groundmass.

TABLE XXIV

THIN SECTION DESCRIPTION FOR SAMPLE : N

| | Phenocrysts and microphenocrysts | | | | Groundmass | | Vesicles | |
| | Clinopyroxene | | Plagioclase | | | | | |
	Pheno- crysts	Micropheno- crysts	Pheno- crysts	Micropheno- crysts				
Modal percent	.2			.3	Modal percent	97.9	Modal percent	1.6
Anhedral					vitrophyric			
Subhedral	X			X	intergranular		spherical	X
Euhedral				X	intersertal	X	planar	R
Equant	X			X	trachytic		elongated	
Prismatic	X			X	pilotaxitic	X	irregular	
Sharp							crenulated	X
Irregular	X			X	hyaloophitic	X	filled	X
Fractured							partially filled	
Glomero-	X			X	banded		large	X
Cross-shaped	R			R	crenulated bands		random	
Swallow-tailed	R				secondary alteration		zones	X
Symplectite	R			R				
2V angle + 51 ^ c approx. 60								
An content			64			59		
Plagioclase Zoning			Osc					

Comments:

Vesicles are concentrated in one area of the slide and are surrounded by reddish-brown rind of secondary minerals. One large planar vesicle displays a crenulated shape and is filled by yellowish-brown material. Microphenocrysts of plagioclase occur as fragments. Also the terminal ends may have many small projecting points (clinopyroxenes as well). Clinopyroxene grains are fractured predominantly perpendicular to the c-axis and cracks are irregular in form. Opaques are distributed in small clusters of anhedral to subhedral grains.

TABLE XXV

THIN SECTION DESCRIPTION FOR SAMPLE : 8-22#4C

| | Phenocrysts and microphenocrysts | | | | Groundmass | | Vesicles | |
| | Clinopyroxene | | Plagioclase | | | | | |
	Pheno-crysts	Micropheno-crysts	Pheno-crysts	Micropheno-crysts				
Modal percent	1.3	N		2.7	Modal percent	96.0	Modal percent	N
Anhedral					vitrophyric	X		
Subhedral	X			X	intergranular	VP	spherical	
Euhedral	X	X		X	intersertal	X	planar	
Equant	R			R	trachytic		enlongated	
Prismatic	X	X		X	pilotaxitic	X	irregular	X
Sharp							crenulated	
Irregular	X			X	hyaloophitic	X	filled	X
Fractured		X					partially filled	
Glomero-	R			X	banded	B/B	large	
Cross-shaped	R				crenulated bands	B/B	random	
Swallow-tailed							zones	X
Symplectite	R			R				
2V angle +43 ^ c approx. 40-50								
An content		67	61	vitrophyric 58	intersertal 57	intergranular		
Plagioclase Zoning		Osc	Osc					

Comments:

Textures vary from vitrophyric to very poorly developed intergranular. Textural bands can pinch and swell, twist, or swirl. Sharp and gradational boundaries exist between different textural types. A single phenocryst of plagioclase is broken, but the adjacent fragments are optically continuous.

TABLE XXVI

THIN SECTION DESCRIPTION FOR SAMPLE : MC-4D

| | Phenocrysts and microphenocrysts | | | | Groundmass | | Vesicles |
| | Clinopyroxene | | Plagioclase | | | | |
	Pheno-crysts	Micropheno-crysts	Pheno-crysts	Micropheno-crysts			
Modal percent		.3		1.5	Modal percent	98.2	Modal percent
Anhedral					vitrophyric	X	
Subhedral		X			intergranular	VP	spherical
Euhedral				X	intersertal	X	planar
Equant				X	trachytic	X	elongated
Prismatic		X		X	pilotaxitic		irregular
Sharp				X			crenulated
Irregular		X		X	hyaloophitic	X	filled
Fractured		X					partially filled
Glomero-					banded	B/B	large
Cross-shaped					crenulated bands	B/B	random
Swallow-tailed							zones
Symplectite		R		R			
2V angle + 51 ^ c		approx. 45					
An content				58			
Plagioclase Zoning				Osc			

Comments:
    Groundmass textures vary from vitrophyric to poorly developed intergranular and groundmass
    colors range from dark black (vitrophyric) to grey (poorly developed intergranular).
    Individual textural types appear as crenulated bands that terminate into a swirl pattern.
    Often contrasting textures can be observed in alternating patterns. Boundaries between
    contrasting textural zones can be either sharp or gradational. Microphenocrysts, where
    present, and microlites parallel these boundaries between textural zones. Microphenocrysts
    grains have pointed terminations.

TABLE XXVII

THIN SECTION DESCRIPTION FOR SAMPLE : 8-22-T1A1

| | Phenocrysts and microphenocrysts | | | | Groundmass | | Vesicles | |
| | Clinopyroxene | | Plagioclase | | | | | |
	Pheno-crysts	Micropheno-crysts	Pheno-crysts	Micropheno-crysts				
Modal percent	.5		1.3		Modal percent	92.0	Modal percent	6.2
Anhedral	X				vitrophyric	X		
Subhedral	X			X	intergranular		spherical	X
Euhedral				X	intersertal	X	planar	X
Equant	X			X	trachytic		elongated	
Prismatic	X			X	pilotaxitic	X	irregular	X
Sharp			X^{black}				crenulated	X
Irregular	X		X^{red}		hyaloophitic	X	filled	
Fractured							partially filled	X
Glomero-					banded	R/R R/B	large	
Cross-shaped			R		crenulated bands	R/R R/B	random	X^{red}
Swallow-tailed							zones	X
Symplectite	R		R					
2V angle + 42 ^ c approx. 40-60								
An content			57^{black} 60^{red}			51		
Plagioclase Zoning			Osc					

Comments:
     A complete variety of black-colored, vitrophyric to intersertal-textured basalt to reddish-brown-colored, poorly intergranular basalt. Interwoven patterns of different textured basalt with swirled, twisted, and crenulated shapes. Sharp to gradational boundaries exist between the different textures. These different colored and textured zones can be as thin as .01 mm. Vesicles are found in en echelon sets in the reddish-brown-colored basalt. Each vesicle is crenulated parallel or perpendicular to the adjacent textural boundary. En echelon vesicles are as small as .01 mm. Some vesicles are spherical and are grouped in dark red-colored basalt zones. In these spherical vesicles, microphenocrystss and microlites are present. Clinopyroxene grains have fuzzy dark outlines that contain high birefringence material and opaques.

TABLE XXVIII

THIN SECTION DESCRIPTION FOR SAMPLE : 8-22-T1A2

| | Phenocrysts and microphenocrysts | | | | Groundmass | | Vesicles | |
| | Clinopyroxene | | Plagioclase | | | | | |
	Pheno-crysts	Micropheno-crysts	Pheno-crysts	Micropheno-crysts				
Modal percent .4		1.9	.1	1.9	Modal percent	91.0	Modal percent 5.5	
Anhedral		X			vitrophyric			
Subhedral	X	X	X	X	intergranular	X^{red}	spherical	
Euhedral			X	X	intersertal	X^{black}	planar	
Equant		X		R	trachytic		elongated	X
Prismatic	X	X		X	pilotaxitic	X	irregular	X
Sharp		X					crenulated	X
Irregular	X	X		X	hyaloophitic		filled	
Fractured							partially filled	X
Glomero-		R		R	banded R/R R/B B/B		large	
Cross-shaped					crenulated bands R/R R/B B/B random			
Swallow-tailed							zones	X
Symplectite		R		R				
2V angle + 44 ^ c		approx. 30-40						
An content			61^{black} 59^{red}			51		
Plagioclase Zoning			Osc					

Comments:
    Thin section cut perpendicular to the plane of the interface between black and red-colored
    textures. A fractured clinopyroxene phenocrysts encloses a lath of plagioclase. Textures
    vary from red-colored, very poorly intergranular to black-colored intersertal bands, layers,
    or spheres. The different textures can be twist, swirl, pinch or swell. Textures within
    the individual colored basalt also vary within each textural type. Vesicles occur only in
    the red-colored textures and can be as small 1 mm in diameter. Ragged crenulated vesicles
    are observed in the red-colored textures and often are found adjacent to the boundaries
    between opposing textural types. Abrupt boundaries separate the different textural types.
    Clinopyroxene grains have fuzzy dark outlines and have been altered to high birefringence
    material and opaques.

TABLE XXIX

THIN SECTION DESCRIPTION FOR SAMPLE : 8-22-T1A3

	Clinopyroxene Pheno-crysts	Clinopyroxene Micropheno-crysts	Plagioclase Pheno-crysts	Plagioclase Micropheno-crysts	Groundmass		Vesicles	
Modal percent		0.5		1.1	Modal percent	98.4	Modal percent	0.0
Anhedral		X			vitrophyric			
Subhedral		X		X	intergranular	VP	spherical	
Euhedral				X	intersertal	X	planar	
Equant		X		R	trachytic		elongated	
Prismatic				X	pilotaxitic	X	irregular	
Sharp							crenulated	
Irregular		X		X	hyaloophitic		filled	
Fractured							partially filled	
Glomero-				R	banded	B/B	large	
Cross-shaped		R			crenulated bands	B/B	random	
Swallow-tailed							zones	
Symplectite		R		R				
2V angle + 51 ^ c								
An content				61				
Plagioclase Zoning				Osc				

Comments:
Intercalated bands that have varying textures that are crenulated, twisted, or swirled. Textures vary from veryly poorly developed intergranular to intersertal. All textural bands or spheres are black in color. Some bands are truncated abruptly often by another set of bands at an acute angle. Some textures are observed in the form of a sphere around which the other textures pinch and swell. Microphenocrysts within the spherical textures have random orientations, while those in the adjacent bands are parallel the boundary between the textural types.

TABLE XXX

THIN SECTION DESCRIPTION FOR SAMPLE : 8-22-T1B

| | Phenocrysts and microphenocrysts | | | | Groundmass | | Vesicles |
| | Clinopyroxene | | Plagioclase | | | | |
	Pheno-crysts	Micropheno-crysts	Pheno-crysts	Micropheno-crysts			
Modal percent		.8		2.0	Modal percent	97.2	Modal percent
Anhedral		X			vitrphyric		
Subhedral		X		X	intergranular	VP	spherical
Euhedral		R		X	intersertal	X	planar
Equant		R		R	trachytic		elongated
Prismatic		X		X	pilotaxitic	X	irregular
Sharp		R		R			crenulated
Irregular		X		X	hyaloophitic		filled
Fractured		R		R			partially filled
Glomero-		R		R	banded	B/B	large
Cross-shaped				R	crenulated bands	B/B	random
Swallow-tailed							zones
Symplectite		R		R			
2V angle	+ 43 ^ c	approx. 30-40					
An content				60			
Plagioclase Zoning				Osc			

Comments:
   Textures vary from intersertal to very poorly intergranular and typically gradational boundaries exist between different textures. The bands of textures can be twisted, swirled, and pinch and swell. Textures and forms of bands are similar to those in thin section 8-22-T1A1.

TABLE XXXI

THIN SECTION DESCRIPTION FOR SAMPLE : 8-22-T1C

	Clinopyroxene Phenocrysts	Clinopyroxene Microphenocrysts	Plagioclase Phenocrysts	Plagioclase Microphenocrysts	Groundmass		Vesicles	
Modal percent		1.1		1.7	Modal percent	89.9	Modal percent	7.3
Anhedral		X			vitrphyric			
Subhedral				X	intergranular	VP	spherical	X
Euhedral				X	intersertal	X	planar	
Equant				R	trachytic		elongated	X
Prismatic				X	pilotaxitic	X	irregular	X
Sharp							crenulated	X
Irregular		X		X	hyaloophitic		filled	
Fractured							partially filled	X
Glomero-				R	banded	B/B	large	
Cross-shaped					crenulated bands	B/B	random	
Swallow-tailed							zones	X
Symplectite		R		R				
2V angle + 33 ^ c								
An content			59					
Plagioclase Zoning			Osc					

Comments:

Textures in crenulated black-colored bands vary from intersertal to very poorly intergranular. Bands are as much as 20 mm thick. Vesicles near the boundaries separating the different textural bands are elongated parallel to these boundaries. Microphenocrysts and microlites, where present near the boundaries, also are aligned parallel to the boundaries. Vesicle tears in the intergranular textures can be less than 1 mm, while larger tears greater than 1 mm are perpendicular to these boundaries. A yellowish-brown-colored groundmass surrounds all vesicles.

TABLE XXXII

THIN SECTION DESCRIPTION FOR SAMPLE : 8-22-SC#1

| | Phenocrysts and microphenocrysts | | | | Groundmass | | Vesicles | |
| | Clinopyroxene | | Plagioclase | | | | | |
	Pheno-crysts	Micropheno-crysts	Pheno-crysts	Micropheno-crysts				
Modal percent	2.5		4.0		Modal percent	92.9	Modal percent	.7
Anhedral	X				vitrphyric			
Subhedral	X				intergranular	X	spherical	
Euhedral			X		intersertal		planar	X
Equant	X		X		trachytic		elongated	X
Prismatic	X		X		pilotaxitic	X	irregular	
Sharp			X				crenulated	X
Irregular	X		X		hyaloophitic		filled	X
Fractured	X						partially filled	
Glomero-	R		R		banded		large	X
Cross-shaped			R		crenulated bands		random	
Swallow-tailed							zones	
Symplectite	R		R					
2V angle + 42 ^ c	approx. 30							
An content			57			53		
Plagioclase Zoning			Osc					

Comments:
Opaques are approximately 1/2 the size of the microphenocrysts. Opaques are randomly spaced in the groundmass, but concentrated around and among the plagioclase and clinpyroxene grains.

TABLE XXXIII

THIN SECTION DESCRIPTION FOR SAMPLE : 8-22-SC#2

| | Phenocrysts and microphenocrysts | | | | Groundmass | | Vesicles | |
| | Clinopyroxene | | Plagioclase | | | | | |
	Pheno-crysts	Micropheno-crysts	Pheno-crysts	Micropheno-crysts				
Modal percent		3.7		4.4	Modal percent	78.9	Modal percent 13.0	
Anhedral	X				vitrphyric			
Subhedral				X	intergranular VP to P		spherical	
Euhedral				X	intersertal		planar	X
Equant	X			X	trachytic		elongated	
Prismatic	X			X	pilotaxitic	X	irregular	X
Sharp				X			crenulated	X
Irregular	X			X	hyaloophitic		filled	X
Fractured	X						partially filled	X
Glomero-				R	banded	R/B	large	X
Cross-shaped				R	crenulated bands	R/B	random	
Swallow-tailed							zones	
Symplectite	R			R				
2V angle + 44 ^ c approx. 30-40								
An content			60 black 61 red					
Plagioclase Zoning			Osc					

Comments:
The thin section was cut perpendicular to the plane of the interface between black-colored, poorly developed intergranular-textured basalt and the reddish-brown-colored, better developed intergranular-textured basalt. Microlites in the black-colored basalt are smaller than in the reddish-brown-colored basalt. Opaques in the reddish-brown basalt are reddish and anhedral. Parallel alignment of microphenocrysts and microlites cuts the plane of the vesicles at approximately 45 degrees. The plane of the interface between the two colored basalts is parallel to the alignment of microphenocrysts and microlites. Secondary minerals surround microphenocrysts of plagioclase and clinpyroxene in the reddish-brown basalt. Vesicle filling is yellowish-brown to clear in color and has a high birefringence.

TABLE XXIV

THIN SECTION DESCRIPTION FOR SAMPLE : 8-22-SC#3

| | Phenocrysts and microphenocrysts | | | | Groundmass | | Vesicles | |
| | Clinopyroxene | | Plagioclase | | | | | |
	Pheno-crysts	Micropheno-crysts	Pheno-crysts	Micropheno-crysts				
Modal percent	2.5	N		5.1	Modal percent	86.9	Modal percent	5.5
Anhedral	X				vitrphyric			
Subhedral	X			X	intergranular	X	spherical	
Euhedral		X		X	intersertal		planar	
Equant	X			X	trachytic		elongated	
Prismatic	X	X		X	pilotaxitic	X	irregular	X
Sharp		X					crenulated	X
Irregular	X			X	hyaloophitic		filled	
Fractured		X					partially filled	
Glomero-	R			R	banded	R/R	large	
Cross-shaped	R			R	crenulated bands	R/B	random	
Swallow-tailed							zones	X
Symplectite	R			R				
2V angle + 57 ^ c								
An content			70	54black 59red				
Plagioclase Zoning		Osc		Osc				

Comments:
Zones of differently developed intergranular textures are observed as swirled to twisted, layers or clots. Some zones grade into adjacent textural zones, but have sharp distinct boundaries. Often irregular-shaped vesicles border between the different textural zones. Clinopyroxene grains have fuzzy dark outlines that are composed of high birefringence material and opaques.

TABLE XXXV

THIN SECTION DESCRIPTION FOR SAMPLE : 8-21#3B

| | Phenocrysts and microphenocrysts | | | | Groundmass | Vesicles |
| | Clinopyroxene | | Plagioclase | | | |
	Pheno-crysts	Micropheno-crysts	Pheno-crysts	Micropheno-crysts		
Modal percent		.2		.5	Modal percent 98.1	Modal percent 1.2
Anhedral					vitrophyric	
Subhedral		X		X	intergranular X	spherical X
Euhedral				X	intersertal	planar
Equant					trachytic	enlongated
Prismatic				X	pilotaxitic VP	irregular
Sharp						crenulated
Irregular		X		X	hyaloophitic	filled X
Fractured		X		X		partially filled
Glomero-		R		X	banded	large
Cross-shaped					crenulated bands	random
Swallow-tailed						zones
Synplectic						
2V angle + 47 ^ c approx. 20-30						
An content				61		
Plagioclase Zoning				Osc		
Comments:						

TABLE XXXVI

THIN SECTION DESCRIPTION FOR SAMPLE : 8-21#4B

| | Phenocrysts and microphenocrysts | | | | Groundmass | | Vesicles |
| | Clinopyroxene | | Plagioclase | | | | |
	Pheno-crysts	Micropheno-crysts	Pheno-crysts	Micropheno-crysts			
Modal percent	1.0		1.7		Modal percent	97.3	Modal percent
Anhedral					vitrophyric		
Subhedral	X				intergranular	X	spherical
Euhedral			X		intersertal		planar
Equant			R		trachytic		enlongated
Prismatic	X		X		pilotaxitic	X	irregular
Sharp							crenulated
Irregular			X		hyaloophitic		filled
Fractured	X		X				partially filled
Glomero-					banded		large
Cross-shaped					crenulated bands		random
Swallow-tailed							zones
Synplectic							
2V angle + 41 ^ c approx. 30-40							
An content			59				
Plagioclase Zoning			Osc				

Comments:

TABLE XXXVII

THIN SECTION DESCRIPTION FOR SAMPLE : 8-20#2

| | Phenocrysts and microphenocrysts | | | | Groundmass | | Vesicles | |
	Clinopyroxene Pheno-crysts	Clinopyroxene Micropheno-crysts	Plagioclase Pheno-crysts	Plagioclase Micropheno-crysts				
Modal percent		.4	N	1.8	Modal percent	95.5	Modal percent	1.8
Anhedral		X			vitrophyric			
Subhedral		X		X	intergranular	VP	spherical	
Euhedral			X	X	intersertal	X	planar	
Equant		R		R	trachytic		elongated	X
Prismatic		X	X	X	pilotaxitic	X	irregular	X
Sharp			X				crenulated	X
Irregular					hyaloophitic		filled	
Fractured							partially filled	
Glomero-		R		R	banded	B/B	large	
Cross-shaped				R	crenulated bands	B/B	random	
Swallow-tailed							zones	X
Symplectite		R		R				
2V angle + 44 ^ c approx. 35-45								
An content			59	59				
Plagioclase Zoning			Osc					

Comments:
Intercalated bands or spheres of varying textures, very poorly developed intergranular to intersertal textures, that are crenulated, twisted, pinched, and swelled. Bands of textures pinch and swell around sphere. Vesicles are adjacent to sharp and gradational boundaries between opposing textural types.

TABLE XXXVIII

THIN SECTION DESCRIPTION FOR SAMPLE : 8-20#3

| | Phenocrysts and microphenocrysts | | | | Groundmass | Vesicles |
| | Clinopyroxene | | Plagioclase | | | |
	Pheno-crysts	Micropheno-crysts	Pheno-crysts	Micropheno-crysts		
Modal percent		.3		1.5	Modal percent 85.1	Modal percent 13.1
Anhedral		X			vitrophyric	
Subhedral		X		X	intergranular VP to P	spherical X
Euhedral				X	intersertal X	planar
Equant				R	trachytic	elongated X
Prismatic		X		X	pilotaxitic X	irregular X
Sharp						crenulated X
Irregular		X		X	hyaloophitic	filled
Fractured						partially filled X
Glomero-					banded B/B	large
Cross-shaped				R	crenulated bands B/B	random X
Swallow-tailed						zones X
Synplectite	R			R		
2V angle + 40 ^ c approx. 40-60						
An content				58		
Plagioclase Zoning				Osc		

Comments:
Intercalated bands or spheres of varying textures, very poorly developed intergranular to intersertal textures, that are crenulated, twisted, pinched, and swelled. Vesicles away from boundaries between oppposing textural types are enlongated to spherical, while vesicles adjacent to boundaries form ragged tears. Ragged vesicles are abundant in intersertal textures. Boundaries are sharp to gradational in character. A yellowish-brown alteration rind is observed adjacent to most vesicles within the groundmass surrounding these vesicles.

TABLE XXXIX

THIN SECTION DESCRIPTION FOR SAMPLE : 8-20#4

	Phenocrysts and microphenocrysts				Groundmass		Vesicles	
	Clinopyroxene		Plagioclase					
	Pheno-crysts	Micropheno-crysts	Pheno-crysts	Micropheno-crysts				
Modal percent	N			1.0	Modal percent	83.2	Modal percent 15.6	
Anhedral	X				vitrophyric	X		
Subhedral				X	intergranular		spherical	
Euhedral					intersertal	X	planar	X
Equant	R			R	trachytic		elongated	X
Prismatic				X	pilotaxitic	X	irregular	X
Sharp							crenulated	X
Irregular	X			X	hyaloophitic	X	filled	X
Fractured	X						partially filled X	
Glomero-					banded	R/R R/B	large	
Cross-shaped					crenulated bands R/R R/B random			
Swallow-tailed							zones	X
Symplectite								
2V angle + 47 ^ c								
An content				60				
Plagioclase Zoning				Osc				

Comments:

Intercalated bands or spheres of varying textures that vary from intersertal to vitrophyric. Bands are crenulated, twisted, pinched and swelled, or swirled. Textural bands are colored from red for intersertal textures to black for vitrophyric basalt. Vesicular tears are concentrated in the red colored intersertal basalt. Vesicles are interlocked and are extremely ragged in appearances. Boundaries between opposing textures are abrupt. In the one area where vesicles tears are abundant, individual clasts are interwoven with one another in the center of a band. Rare clasts are broken into fragments. Vesicles are partly filled with a high birefringence material. The peripheral margins of this clast-filled band have small vesicle tears parallel to the adjacent boundaries of vitrophyric textures. This clast-filled band pinches and swell. Clast sizes range from 2 mm in diameter to .5 mm. Clast types vary from vesicular to nonvesicular basalt that are colored either black or organish-red. Larger vesicle tears occur in the vitrophyric bands.

TABLE XL

THIN SECTION DESCRIPTION FOR SAMPLE : 8-20#5

| | Phenocrysts and microphenocrysts | | | | Groundmass | | Vesicles | |
| | Clinopyroxene | | Plagioclase | | | | | |
	Pheno-crysts	Micropheno-crysts	Pheno-crysts	Micropheno-crysts				
Modal percent		.7		1.0	Modal percent	93.4	Modal percent	4.9
Anhedral					vitrophyric	X		
Subhedral		X		X	intergranular	VP	spherical	X
Euhedral				X	intersertal	X	planar	X
Equant		X		X	trachytic		elongated	X
Prismatic		X		X	pilotaxitic		irregular	X
Sharp							crenulated	X
Irregular		X			hyaloophitic	X	filled	
Fractured							partially filled	X
Glomero-		R		R	banded	X	large	
Cross-shaped				R	crenulated bands R/R R/B B/B		random	
Swallow-tailed		R					zones	X
Symplectite		R		R				
2V angle + 42 ^ c								
An content		54 intergranular		59 intersertal	56 vitrophyric			
Plagioclase Zoning				Osc				

Comments:
   Intercalated bands or spheres of varying textures. Textures range from very poorly
   developed intergranular to intersertal to vitrpophyric and are crenulated, twisted, pinched
   and swelled, or swirled. Intergranular textures are colored red or black. Intersertal and
   vitrophyric textures are colored black. Vesicular tears are concentrated within the
   intergranular bands and within the distinct vesicular clasts. Sharp distinct boundaries
   separate these clasts from the surrounding basalt. Boundaries between the textural bands
   are less abrupt. Microphenocrysts abundance varies between and within the different
   textural bands and clasts.

TABLE XLI

THIN SECTION DESCRIPTION FOR SAMPLE : 8-21#2A

| | Phenocrysts and microphenocrysts | | | | Groundmass | | Vesicles | |
| | Clinopyroxene | | Plagioclase | | | | | |
	Pheno-crysts	Micropheno-crysts	Pheno-crysts	Micropheno-crysts				
Modal percent	3.5	N		13.5	Modal percent	67.4	Modal percent	15.6
Anhedral	X				vitrophyric			
Subhedral	X			X	intergranular		spherical	X
Euhedral				X	intersertal	X	planar	
Equant	X			R	trachytic		elongated	X
Prismatic		r		X	pilotaxitic	X	irregular	X
Sharp				X			crenulated	
Irregular	X			R	hyaloophitic		filled	X
Fractured							partially filled	X
Glomero-					banded	X	large	
Cross-shaped				R	crenulated bands	R/B	random	X
Swallow-tailed							zones	
Symplectite	R			R				
2V angle + 44 ^ c								
An content				58				
Plagioclase Zoning				Osc				

Comments:

Irregular vesicles found along boundaries between red and black-colored textural bands. Vesicles can be partly filled to filled with yellowish-green material. Microphenocrysts of plagioclase form a seriate pattern. Clinopyroxene in the red-colored bands has a fuzzy dark outline that is composed of highly birefringent material and opaques.

TABLE XLII

THIN SECTION DESCRIPTION FOR SAMPLE : 8-21#3A

| | Phenocrysts and microphenocrysts | | | | Groundmass | | Vesicles | |
| | Clinopyroxene | | Plagioclase | | | | | |
	Pheno-crysts	Micropheno-crysts	Pheno-crysts	Micropheno-crysts				
Modal percent	.9	N		3.6	Modal percent	95.2	Modal percent	.3
Anhedral					vitrophyric			
Subhedral					intergranular	X	spherical	X
Euhedral	X			X	intersertal		planar	
Equant				X	trachytic		elongated	
Prismatic	X	r		X	pilotaxitic		irregular	
Sharp				X			crenulated	
Irregular	X			X	hyaloophitic		filled	
Fractured				R			partially filled	
Glomero-					banded		large	
Cross-shaped				R	crenulated bands		random	X
Swallow-tailed							zones	
Symplectite								
2V angle + 38 ^ c approx. 35-45								
An content			55					
Plagioclase Zoning			Osc					

Comments:
Microlites of clinopyroxene are larger than plagioclase microlites.

TABLE XLIII

THIN SECTION DESCRIPTION FOR SAMPLE : 8-21#5A

	Clinopyroxene Phenocrysts	Clinopyroxene Micropheno-crysts	Plagioclase Phenocrysts	Plagioclase Micropheno-crysts	Groundmass	Vesicles
Modal percent	.8	N		2.3	Modal percent 92.8	Modal percent 4.1
Anhedral					vitrophyric	
Subhedral	X				intergranular	spherical
Euhedral				X	intersertal	planar
Equant	X				trachytic	elongated X
Prismatic		r		X	pilotaxitic	irregular
Sharp	X			X		crenulated
Irregular					hyaloophitic	filled X
Fractured	X			X		partially filled
Glomero-	R			R	banded	large X
Cross-shaped					crenulated bands	random
Swallow-tailed						zones
Symplectite						
2V angle + 44 ^ c approx. 30 -40						
An content				60		
Plagioclase Zoning				Osc		

Comments:
   Opaques are concentrated in layers or bands. One larger vesicle filled with greenish-blue
   material is observed in the thin section.

TABLE XLIV

THIN SECTION DESCRIPTION FOR SAMPLE : 8-21#7A

	Clinopyroxene Pheno-crysts	Clinopyroxene Micropheno-crysts	Plagioclase Pheno-crysts	Plagioclase Micropheno-crysts	Groundmass		Vesicles
Modal percent		.6	N	3.5	Modal percent	95.9	Modal percent
Anhedral		X			vitrophyric		
Subhedral		X		X	intergranular	X	spherical
Euhedral				X	intersertal		planar
Equant		X		R	trachytic		elongated
Prismatic			r	X	pilotaxitic	X	irregular
Sharp							crenulated
Irregular		X		X	hyaloophitic		filled
Fractured		X					partially filled
Glomero-					banded		large
Cross-shaped					crenulated bands		random
Swallow-tailed							zones
Symplectite							
2V angle + 50 ^ c							
An content				59		57	
Plagioclase Zoning				Osc			
Comments:							

TABLE LXV

THIN SECTION DESCRIPTION FOR SAMPLE : 8-21#3C

| | Phenocrysts and microphenocrysts | | | | Groundmass | | Vesicles |
| | Clinopyroxene | | Plagioclase | | | | |
	Pheno-crysts	Micropheno-crysts	Pheno-crysts	Micropheno-crysts			
Modal percent		.8	N	2.1	Modal percent	97.1	Modal percent
Anhedral		X			vitrophyric		
Subhedral				X	intergranular	X	spherical
Euhedral				X	intersertal		planar
Equant				R	trachytic		enlongated
Prismatic			r	X	pilotaxitic		irregular
Sharp							crenulated
Irregular		X		X	hyaloophitic		filled
Fractured		X					partially filled
Glomero-					banded		large
Cross-shaped					crenulated bands		random
Swallow-tailed							zones
Symplectite		R		R			
2V angle + 46 ^ c approx. 35-45							
An content				58			
Plagioclase Zoning				Osc			
Comments:							

TABLE LXV

THIN SECTION DESCRIPTION FOR SAMPLE : 8-21#3C

| | Phenocrysts and microphenocrysts | | | | Groundmass | | Vesicles |
| | Clinopyroxene | | Plagioclase | | | | |
	Pheno- crysts	Micropheno- crysts	Pheno- crysts	Micropheno- crysts			
Modal percent	.3	N		1.3	Modal percent	98.4	Modal percent
Anhedral	X				vitrophyric		
Subhedral	X			X	intergranular	X	spherical
Euhedral				X	intersertal		planar
Equant				R	trachytic		enlongated
Prismatic			r	X	pilotaxitic		irregular
Sharp							crenulated
Irregular	X			X	hyaloophitic		filled
Fractured				X			partially filled
Glomero-					banded		large
Cross-shaped					crenulated bands		random
Swallow-tailed							zones
Symplectite	R			R			
2V angle + 45 ^ c approx. 30-40							
An content				57			
Plagioclase Zoning				Osc			
Comments:							

TABLE LXVI

THIN SECTION DESCRIPTION FOR SAMPLE : 8-21#5C

| | Phenocrysts and microphenocrysts | | | | Groundmass | | Vesicles | |
| | Clinopyroxene | | Plagioclase | | | | | |
	Pheno-crysts	Micropheno-crysts	Pheno-crysts	Micropheno-crysts				
Modal percent		1.1		3.0	Modal percent	95.0	Modal percent	.9
Anhedral		X			vitrophyric			
Subhedral		X		X	intergranular	W	spherical	
Euhedral				X	intersertal		planar	
Equant		X		R	trachytic		enlongated	X
Prismatic		X		X	pilotaxitic		irregular	
Sharp							crenulated	
Irregular		X		X	hyaloophitic		filled	
Fractured		X					partially filled	
Glomero-				X	banded		large	X
Cross-shaped					crenulated bands		random	
Swallow-tailed							zones	
Symplectite								
2V angle + 47 ^ c approx. 40-50								
An content				61		59		
Plagioclase Zoning				Osc				

Comments:

Opaques are equal in size with microlites of plagioclase and clinopyroxene. Plagioclase sizes are in a seriate manner.

APPENDIX C

SUMMARY OF TRAVERSE INFORMATION
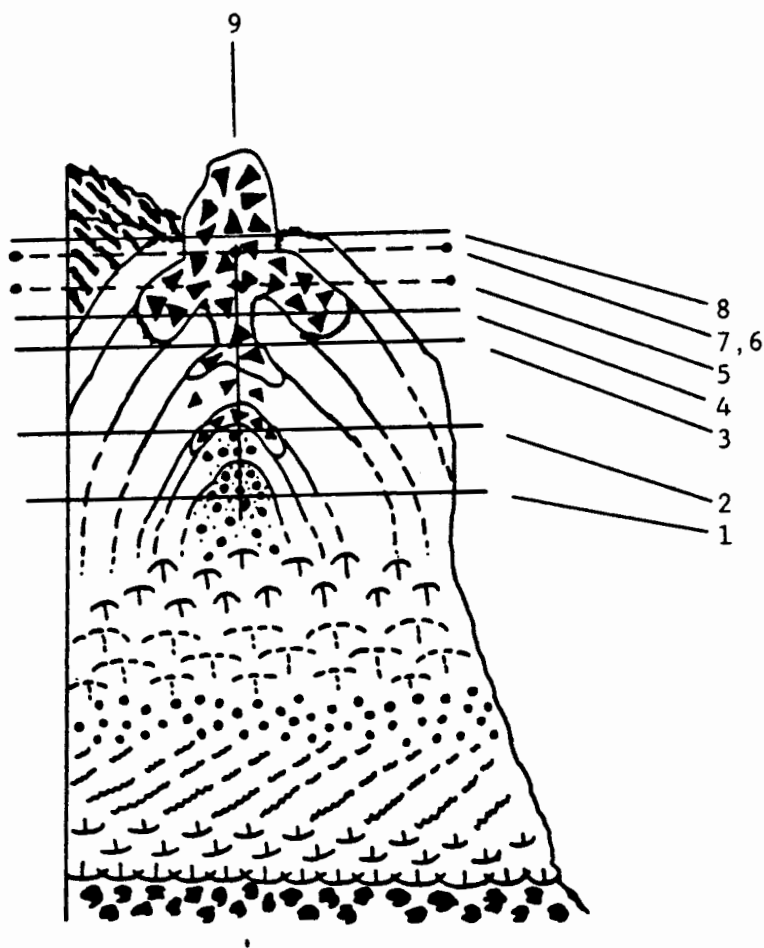
Figure 54. The position of each transverse are shown relative to the intraflow zones of the second cooling unit of the Troy flow. Each transverse label corresponds to a title label in the following tables of collected data. The solid circles at the ends of certain lines indicates the transverses were parallel to the plane of the central spine.

TABLE XLVII

DEFINITIONS AND SYMBOLS FOR HORIZONTAL AND VERTICAL TRAVERSES

<u>Definitions and general characteristics</u> :

<u>Region 1</u> · Region 1 consists of black, glassy-textured basalt, that is vertically jointed with joints spaced one or two per two foot interval. Differential weathering has accentuated the visible alignment of microphenocrysts of plagioclase, which are parallel to the inner dipping breccia of the structure. Rock within this region fractures conchoidally. In the upper portions of an explosion structure, region 1 rock will form inward curving confining walls of black glassy-textured basalt that are parallel and surround region 2 rock and or the breccia of region 3. The confining walls can narrow to a single projecting arm of region 1 basalt (called hereafter as a basaltic arm) that penetrates into region 2 basalt and or the breccia of region 3. Typically an individual arm or basaltic arm can be traced back in a portion of the confining walls as a single layer of region 1 basalt separated by joint traces form the remaining basalt. Gradational contact with region 2.

<u>Region 2</u> · Region 2 is comprised of isolated vesicular clasts/pockets (see definitions section) or groups of vesicular clasts/pockets that are within a black glassy-textured basaltic matrix. Vesicles commonly compose less than 50 % of the clasts/pockets and the vesicles can be stretched or spherical. Obvious boundaries are not visible in hand samples. Clasts/pockets sizes increase towards region 3. A sharp visble contact exists against region 3 and the vertical joints begin to tilt towards the contact with region 3.

<u>Region 3</u> · Region 3 contains convex upward jointing with its margins continuing in common orientation with that within region 2 (commonly the trace of the joint can be followed from region 3, where the trace is horizontal into and through regions 2 and 1, where the trace has swung to vertical). The rock is made up of 80-90 % clasts of various types (see table ? for data) and are colored from black to reddish-purple. The sharp contact with region 2 is marked by stretched clasts; elongation is parallel to the trace of the contact. Clast sizes increase away from the trace of the contact with region 2 and breccia grades from a peripheral outer matrix-supported zone to an inner clast-supported zone.

<u>Symbols</u> : Used in the following transverse and vertical transverse tables

- B · Breccia count not made here.

- G · Breccia clasts or vesicular clasts/pockets were counted by grid method, where a 2x2 ft square grid was centered on a selected point and the number of clasts/pockets were counted.

- + · Center of a 2x2 square grid that concidence with a selected point on the 100 foot tape (hereafter called an interval mark).

- C · Covered

- N · Vesicular clasts/pockets were not counted.

TABLE XLVIII

HORITZONTAL GRID TRAVERSE 1 THROUGH STRUCTURES

Distance from starting point	Number of clasts	Comments
0+	0G	Region 1: Joint trend N55E 82NW.
10+	0G	Region 1: Joint trending change to N55E 43NW.
20+	7G	Region 2: Largest vesicular clasts/pockets to 20 mm in size.
30+	10G	Region 2:
40+	41G	Region 3: Abrupt increase in the size of clasts that become up to 40 mm in diameter and matrix supported.
50+	47G	Region 3: Large clasts up to 150 mm in diameter, but commonly 40 mm in diameter. Majority of clasts are colored black.
60+	C	Covered

TABLE XLIX

HORIZONTAL TRAVERSE 2 THROUGH AN EXPLOSION STRUCTURE

Distance from starting point	Number of clasts	Comments
0-30	0	Region 1.
30-40	N	Region 2: Predominantly convex up joints and joint traces are separated by 40 to 150 mm. Joint traces may pinch out towards previous interval of region 1-type rock. Joint traces undulate similar to small ripple marks with amplitudes of 10 to 20 mm and wavelengths of up to 500 mm. Vesicles are small in diameter, < 1 mm, and filled with reddish brown material.
40-50	N	Region 2: Contains vesicular or scoriaceous clasts/pockets and the vesicles may be filled with either brownish yellow to greenish yellow, but commonly reddish brown material. Clasts/pockets have distinct boundaries of brownish red rims of 1 to 2 mm thick within a black basaltic matrix. Larger-sized clasts/pockets often consist of more than one vesicular to scoriaceous clasts/pockets welded together as a single clast with reddish brown rims separating each individual clast/pocket. Predominantly convex up jointing with irregular thicknesses separating individual joint traces by 50 to 500 mm. Similar small undulating surfaces are observed as in interval 30-40.
50-60	N	Region 2: Contains similar clasts/pockets patterns, except reddish brown rims were observed to surround nonvesicular basalt clasts as well. Number of clasts/pockets increases upward and grades into region 3. Similar jointing and surface patterns on joints as with interval 40-50.
60-70	N	Region 3: Contains clasts of vesicular, scoriaceous, and aphyric basalt surrounded in a reddish-purple-colored basaltic matrix. Convex up jointing less pronounced and rock appears more massive (non-jointed).
70-80	G	Region 3: Grid count was performed on breccia face perpendicular to this interval. Clasts counts are complied in TABLE LII. Clasts counts: 13 clasts >60mm, 88+ clasts <60mm; 9 clasts >60mm and 1 clast > 400mm, 50+ clasts <60mm; 9 clasts >60mm, 80+ clasts <60mm; 5 clasts >60mm, 80+ clasts <60mm.
80+	C	Section discontinued because of cliff.

TABLE L

HORITZONTAL TRAVERSE 3 THROUGH AN EXPLOSION STRUCTURE

Distance from starting point	Number of clasts	Comments
0-1	8	Region 2: Vesicular clasts/pockets up to 150 mm in diameter. Abrupt contact trace with abjacent region 3.
1-7	B	Region 3: Grades inward to more open breccia and grades downward into region 2 type rock with convex-up jointing.
7-10	B	Region 3: Composed of extremely small-sized clasts of breccia, less than 20 mm. Rare vesicular clasts have milky-white to clear-colored opal filled vesicles. Grades downward into region 2-type rock that consist of chaotic elongated plate-shaped fragments. Vesicular clasts/pockets are in a black blasaltic matrix and vesicles are filled by blue-green material. Isolated reddish-purple-colored basalt surround open voids within this region 2-type rock. Region 3-type rock grades upward into larger sized clasts similar to the previous interval (1-7).
11-15	B	Region 3: Larger sized clasts of breccia similar to interval (1-7). This interval grades downward into elongated plate-shaped fragments that are fractured along convex-up joints. Joints are coated with clear-colored, mammillary-shaped material. Plate-shaped fragments are commonly 5 to 20 mm thick,but may be up to 70 mm thick and commonly 50 to 60 mm long, but may be up to 250 mm in length. Plate-shaped fragments pinch and swell and the outer surfaces have ripple-like patterns.
15-32	N	Region 2: Elongated plate-shaped fragments are observed, but the prominance diminishes downward from this interval.
32-35c	B	Region 3.
35-54	C	Covered section.
54-60	31	Region 3: Grades into a clast-supported zone where clast size increases and void space between clasts increases. Clast-supported zone marked by a large v-shaped notch in the breccia spine, some 100 feet deep into slope of the valley walls and approximately 50 feet wide at the opening of the v shaped mouth. Clast-supported zone is less resistant to weathering. Line count of this interval resulted in 27 clasts less than 60 mm in size and 4 clasts over 60 mm. Clasts in the v-shaped notch of clasts-supported breccia increase to rare blocks up to 1 m in diameter. A horizontal transverse was completed along the western arm of this notch and is horizontal transverse number 4 (see this transverse for details).

TABLE LI

HORITZONTAL TRAVERSE 4 THROUGH AN EXPLOSION STRUCTURE

Distance from starting point	! Number ! of clasts !	Comments	! !
0-13	9	Region 2: Includes a 4 ft thick interval of reddish purple vesicular clasts.	
13-15	11	Region 2: Jointed with dip of joints towards adjacent region 3.	
16-29	B	Region 3: Clasts have interlocking pattern and welded character.	
29-39	8	Region 2: Jointed with dip towards last interval (16-29).	
39-76	0	Region 1.	
76-102	37G	Region 2: Grid counts at interval mark* 81 were 30 vesicle clasts/pockets, at interval mark 86 the total was 11, and finally at interval mark 91, the total was 12.	
102-148	0	Region 1: An interval (120-122) that is colored reddish purple and containes no clasts. Surface textures observed at intervals 105 and 134 are rippled. Surface appearance is similar to small sedimentary ripple marks (< 2cm in amplitude). Three successive layers of basalt with the rippled surface texture overlie each other and each layer is 30 to 40 mm thick.	
148-156	26G	Region 2: Rare clasts/pockets up to 120 mm in diameter and the number of clasts/pockets increases towards the next interval; 156-162. Grid count at interval mark 152 with total at 39 clasts.	
156-162	B	Region 3: Rare clasts up to 200 mm in diameter but commonly less than 40 mm in diameter.	
162-169	14	Region 2: Joints end abruptly into overlying region 3. Clast sizes increase towards overlying region 3.	
169-178c	B	Region 3: Covered after interval mark 178.	

* interval mark is at point along the 100 foot tape the 2 by 2 foot square grid was centered on.

TABLE LII

DESCRIPTIONS FOR CLAST TYPES USED DURING COUNTING TRAVERSES

CLAST TYPES :

BVA - Clast is a composite of clasts or fragments of black vesicular or non-vesicular, vitrophyric to intergranular-textured basalt with a reddish purple colored basaltic matrix. The matrix can be twisted, swirled, or stretched into layers that can be cracked or fractured. The cracks can contain very small fragments of rock, $\leq$ 1 mm in size. Some block-sized clasts are coated with a fused layer, up to 1 mm thick, of finely brecciated black-colored basalt and reddish-purple-colored matrix. Shapes of clasts range from sharp angular to planar to agglutinated froms. Rare empty interclast voids.

S - Clast composed of black or reddish colored scoriaceous basalt. Scoriaceous clasts show two types of either randomly placed vesicles through the clast or vesicles are concentrated in inflated vesicular margins. Shapes of clasts range from subrounded forms for the random vesicle type to plate-shaped forms for the inflated type of clast.

PAH - Clast composed of vesicular basalt with vesicles that are elongated and twisted parallel to the surface shape of the clast. Vesicles are up to 50 mm long, 2 to 3 mm thick, and up to 20 mm wide with vesicles often filled along the peripheral surface by dark green material. Clasts are colored blue gray internally and grade outward from yellow green to an orange-brown rim. Clasts have ropy surface texture. Clast shapes have generally plate-like forms.

SP - Measurement of void space difficult to measure with 100 foot line method.

TABLE LVII

CLAST COUNTING GRID FOR HORITZONTAL TRAVERSE 2

THROUGH A CENTRAL SPINE

Position Label	All types of clasts	
	<64mm	>64mm
1	88	13
2	50	9
3	80	9
4	80	5
TOTALS:	278	36
Percentage(%)	89	11

TABLE LIV

HORITZONTAL TRAVERSE 5 CLAST GRID COUNTING THROUGH A STEEPLY DIPPING BRECCIA ZONE

Position Label	Type of clast							
	BVA		S		PAH		SP	
	<64mm	>64mm	<64mm	>64mm	<64mm	>64mm	<64mm	>64mm
1	- -	8	- -	2	- -	0	- -	- -
2	220	6	12	9	0	1	- -	- -
3	176	10	12	2	0	1	- -	- -
4	248	7	28	13	0	0	- -	- -
5	200	6	8	8	0	4	- -	- -
6	140	8	8	7	0	0	- -	- -
TOTALS:	984	45	68	41	0	6	- -	- -
Percentage(%)	86	4	6	4	0	1	- -	- -

TABLE LV

HORITZONTAL LINE COUNTING TRAVERSES 6 AND 7 IN A CENTRAL SPINE

Position Label	Type of clast							
	BVA		S		PAH		SP	
	<64mm	>64mm	<64mm	>64mm	<64mm	>64mm	<64mm	>64mm
5	89	22	29	3	0	1	5	1
6	141	11	42	17	1	8	0	2
TOTALS:	230	33	71	20	1	9	5	3
Percentage(%)	62	9	19	5	0	2	1	1

TABLE LVI

HORIZONTAL GRID TRAVERSE 8 THROUGH AN EXPLOSION STRUCTURE

Distance from starting point	Number of clasts	Comments
C0-5	B	Region 3: no horizontal or vertical jointing pattern (massive) as observed in other region 3-type rock. Clast types range from black nonvesicular to vesicular basalt to scoriaceous clasts in a reddish-purple basaltic matrix. Further upslope, approximately 15 to 30 feet, an isolated outcrop of region 1 basalt is exposed. This region 1 has no dominant jointing pattern but has fractures that weather spheroidally into irregular-sized cobbles and pebbles.
5-7	0	Region 1: a sharp contact trace with region 3 and is vertically jointed. No region 2-type rock was seen here, but instead a transformation between region 1 and region 3-type rocks.
7-19	B	Region 3: forms resistant ridges between intervening cover.
19-34	0	Region 1: vertical joints that, where fractured, break along spherical fractures into small spheres or fluted spheroids, $\geq$ 10 mm in diameter. Distinct, darker black matrix surrounds broken spheres.
34-40	0	Region 2: similar fracture patterns of spheres, but with diameters only up to 5 mm. Streaks of reddish-purple-colored basalt intermixed within black basalt and vesicular clasts/pockets observed within these colored streaks. Vesicles of clasts/pockets can be filled with greenish-yellow material and vesicle shapes range from circular to elongated and $\leq$ 2 mm in diameter.
40-66	C	Covered interval overlies region 3 of transverse 2 field number.
66-78	0	Region 1: similar spheroidal fracture pattern, but breaks into sharp angular forms. Poorly developed vertical joints.
78-98C	B	Region 3 for 2 feet then covered.
98-118	0	Region 1: irregular wavy vertical and platy joints, that fracture into spheroidal forms commonly $\leq$ 20 mm in diameter, but may be up to 30 mm in diameter.
118-131	B	Region 3: individual clasts composed of single clasts or a fused group of clasts that form one welded, distinct individual clast. Breccia is clast-supported with a thin coating of black aphyric basalt or reddish-purple-colored basalt.
131+	C	Intervening cliff ended transverse.

TABLE LVII

VERTICAL LINE TRAVERSE 9 THROUGH AN EXPLOSION STRUCTURE

Distance from starting point	Number of clasts	Comments
0-10	0	Region 1: Irregular wavy platy jointing, spaced up to 250 mm, but commonly less than 70 mm. Strong NW joint pattern. No breccia or vesicular clasts/pockets observed.
10-20	0	Region 1: Containing random microphenocrysts. Platy jointed with large plates, up to 400 mm in length but commonly 100 mm.
20-30	0	Region 1: Predominant vertical joints lacking horizontal jointing.
30-40	0	Region 1: Containing vertically jointed basalt that breaks into small irregular fragments. Greenish-colored streaks produced by deuteric alteration.
40-50	0	Region 1: Tilted joints towards near adjacent breccia zone. Similar deuteric alteration observed.
50-60	C	Region 1: For approximately 1 m with tilted vertical joints toward superjacent region 2. Region 2 for approximately 2.5 m with horitzonal joints and vesicular clasts/pockets. Vesicular clasts/pockets commonly one or two per foot and increasing in number upwards. Vesicles filled with reddish brown material.
60-70	C	Region 2: Horizontal joints and increasing number of clasts/pockets. Vesicles filled with reddish-brown material.
70-80	C	Region 2: Breaks into very angular fragments. Vesicular clasts/pockets in black basalt with microphenocrysts of plagioclase. Individual layers of basalt separated by joints (basalt arms) that tilt towards horizontal as each arm nears the trace of the region 3 breccia.
80-90+	B	Region 3: Basalt arms of region 2 penetrate and fragment within the breccia layers.

TABLE LVIII

SUMMARY OF BRECCIA TRENDS AND LOCATIONS

Location or stratigraphic label	Flow	Measurement of bearings
NE1/4,SE1/4,SE1/4 Sect 31 T5N R43E Troy 71/2	Troy	N30E,N25E,N45E,N60E,N32E,N45E,N60E,N32E,N25E,N30E N55E,N32E,N28E,N23E,N20E,N45E,N45E
WR WR	Troy LGR	N87W,N70E,N80W,N82W,N70E N55W
U U U	UGR Troy LGR	N30W,N10W N32W,N14W N32W,N15W,N14W
WC	Troy	N30E,N35E
MC MC MC	UGR Troy LGR	N5E,N7E,N5E,N40E N78E,N60E,N64E,N70E,N65E,N65E,N85E N60E,N80E,N70E,N72E,N62E,N70E,N30E,N35E
LF	Troy LGR	N5E,N10E N55W,N38W
EF EF	Troy LGR	N10E,N25E,N38E,N22E,N47E,N36E,N38E,N45E,N27E,N37E N16E,N37E,N18E,N15E,N43E,N7E,N5W,N12W,N2W,N55E,N29E N35W,N49W,N36W,N38W,N28W,N56W
F	UGR	N60E,N45E,N20E,N38E
SG	Troy	N30E,N40E
SC1 SC1	UGR1 UGR2	 N50E,N53E,N52E,N49E,N45E,N77E,N55E,N52E,N65W,N3E N70E,N85W,N85E,N2W,N48E,N35E,N20W,N18W,N45W,N78E N38E,N60E,N90E,N80W,N74W,N10E,N65W,N10W,N45E,N8E N60E,N45E,N61E,N68E,N85E,N84E,N63E,N72E,N64E,N70E N84W,N72E,N68E,N78E,N72E,N78E,N48E,N30E,N40E,N80E N47E,N62E,N90E,N42E,N82E,N6E,N70E,N38E,N50E,N38W N86E,N42E,N57E,N69E,N40W N75W,N75W,N65W,N30W,N50W,N44W,N56W,N51W,N61W,N74W N65W,N66W,N80E,N71W,N72W,N88W,

TABLE LVIII CONTINUED

SUMMARY OF BRECCIA TRENDS AND LOCATIONS

Location or stratigraphic label	Flow	Measurement of bearings
SC2	UGR1	N55E,N71E,N51E,N71E,N87W,N8E,N68W,N67W,N88W,N88E N60E,N60W,N78W,N80W,N85W,N79W,N78W,N89W,N74E,N67E N80W,N88E,N80E
SC2	UGR2	N88W,N64W,N74W,N60W.N90W
NW1/4,SE1/4,NE1/4 Sect 9 T5N R43E Troy QUAD	LGR	N47W,N40W,N22W,N20W
SW1/4,NW1/4,NE1/4 Sect 9 T5N R43E Troy Quad	Troy	N20E
NE1/4,NE1/4,NW1/4 Sect 9 T5N R43E Troy Quad	Troy	N2E
NE1/4,NW1/4,NW1/4 Sect 9 T5N R43E Troy Quad	Troy	N20E,N57E,N40E,N65E,N55E
NW1/4,SE1/4,NW1/4 Sect 10 T5N R43E Troy Quad	Troy	N41E,N23E,N47E,N15E,N29E,N7E,N31E
SE1/4,SE1/4,NE1/4 Sect 15 T5N R43E Troy Quad	LGR1 LGR2	N35E,N28E,N33E,N19E,N23E,N30E,N25E,N31E N42E,N21E

APPENDIX D

SUMMARY OF GEOCHEMICAL INFORMATION

Summary of sample preparation

Each selective sample was treated in the following manner:

<u>1)</u> A sample was broken into several fragments and one fragment selected for thin section (to avoid any containation from cutting oils or water during the cutting/polishing operation).

<u>2)</u> Remaining fragments were separated in two groups. The first group of fragments was saved and the second group was then chipped (rock chipper).

<u>3)</u> Any chips with possible hammer marks or crusher marks were removed. Also precautions for special samples listed in TABLE LIX were initiated at this point. Sample chips marked by symbol ($) were separated from altered or weathered chips. Sample chips marked by symbol (*) were separated, because these chips were red in color and were samples containing breccia.

<u>4)</u> Next, the chips were randomly separated into three splits (approximately equal) and each split went to one of the three following analyzes: INAA, XRF, Mossbauer.

TABLE LIX

SUMMARY OF SAMPLE LOCATION AND SAMPLE LABORATORY ANALYTICAL METHODS

Stratigraphic section label	Location 7 1/2 minute quadrangle	Sample label	Labatory analytical method			
			Thin section	INAA	XRF	Mossbaurer
SC1	NW1/4SE1/4NW1/4 Sect 35 T6N R43E Troy	8-22-SC#1	Y	Y		
		8-22-SC#2	Y	Y		
		*8-22-SC#2B		Y		
		8-22-SC#3	Y	Y		
		8-22-SC#4		Y		
Wenaha.C	SE1/4SE1/4SE1/4 Sect 31 T6N R43E Troy	8-20#1		Y		
		8-20#2	Y	Y		
		8-20#3	Y	Y		
		8-20#4	Y	Y		
		8-20#5	Y	Y		
Wenaha.B	NE1/4SE1/4SE1/4 Sect 31 T6N R43E Troy	8-22-T1A1	Y	Y		Y
		*8-22-T1AR		Y		
		8-22-T1A2	Y			
		8-22-T1A3	Y	Y		Y
		8-22-T1B	Y	Y		
		8-22-T1C	Y	Y		Y
WR	SE1/4NW1/4NE1/4 Sect 5 T5N R43E Troy	$M	Y	Y	Y	
		M1	Y	Y		
		M2	Y	Y		
		M3	Y	Y		
		M4		Y		
		$N	Y	Y	Y	
		8-22#1C		Y		
		8-22#3C		Y	Y	
		8-22#4C	Y	Y	Y	
MC	NW1/4SE1/4NW1/4 Sect 3 T5N R43E Troy	&MC4D	Y	Y		
GC	NE1/4SW1/4SW1/4 Sect 24 T5N R43E Troy	8-21#1CC		Y		
		8-21#2C		Y		
		8-21#3C	Y	Y		
		8-21#4C		Y		
		8-21#5C	Y	Y		
EF	NW1/4NW1/4SE1/4 Sect 9 T5N R43E Troy	$8-21#2A	Y	Y	Y	
		8-21#3A	Y	Y	Y	
		8-21#5A	Y	Y	Y	
		8-21#6A		Y	Y	
		8-21#7A	Y	Y	Y	
EF	NW1/4NW1/4SE1/4 Sect 9 T5N R43E Troy	8-21#3B		Y		
		8-21#4B		Y		

Symbol * -- Selected red colored chips within breccia sample
Symbol $ -- Selected fresh chips
Symbol & -- Included in WR sample set

TABLE LX

INAA VALUES, EQUIVALENT DEPTHS, DEPTH IN FLOW, ELEVATION OF

SAMPLES FROM SAMPLE SET ELLOIT FARM (EF)

SAMPLE LABELS	*DEPTH IN FLOW	$ELEVATION IN FLOW	LA	CE	SM
8-21#2A	&(100)330.00	2095	36.10	70.00	9.59
8-21#3A	(98)325.00	2110	32.60	68.00	8.40
8-21#5A	(83)320.00	2122	31.00	67.00	8.35
8-21#6A	(67)315.00	2127	30.70	65.00	8.40
8-21#7A	(19)260.00	2179	30.60	66.00	7.83

LABELS			EU	TB	YB
8-21#2A			2.85	1.70	5.70
8-21#3A			2.63	1.50	5.40
8-21#5A			2.54	1.70	5.10
8-21#6A			2.52	1.70	5.00
8-21#7A			2.43	1.40	4.80

LABELS			LU	BA	CO
8-21#2A			0.66	720.00	0.00
8-21#3A			0.61	500.00	24.00
8-21#5A			0.61	620.00	22.00
8-21#6A			0.60	550.00	20.00
8-21#7A			0.59	520.00	19.00

LABELS			+FEO	+K_2O	HF
8-21#2A			8.19	3.30	6.80
8-21#3A			11.63	1.60	6.20
8-21#5A			11.13	2.10	6.40
8-21#6A			10.99	2.50	5.90
8-21#7A			11.63	2.30	6.20

LABELS			+NA_2O	RB	SC
8-21#2A			3.69	73.00	34.79
8-21#3A			3.64	48.00	31.98
8-21#5A			3.52	61.00	32.41
8-21#6A			3.59	49.00	31.38
8-21#7A			3.48	63.00	31.69

LABELS			TA	TH	
8-21#2A			0.58	6.90	
8-21#3A			0.51	6.60	
8-21#5A			0.53	6.60	
8-21#6A			0.55	6.20	
8-21#7A			0.48	7.20	

&(xx) enclose equivalent depths used to compare concentrations against another sample set in a hypothetical flow of 100 feet thick.

* Depth in flow is calculated from field elevations during measurement of stratigraphic section

$ Elevation of the sample within the flow was measured during stratigraphic section or traverse measurements

+ Oxides concentrations in weight percent (iron is in total FeO) and remaining concentrations in part per million

TABLE LXI

INAA VALUES, EQUIVALENT DEPTHS, DEPTH IN FLOW, ELEVATION OF

SAMPLES FROM SAMPLE SET GROUSE CREEK (GC)

SAMPLE LABELS	*DEPTH IN FLOW	$SELEVATION IN FLOW	LA	CE	SM
8-21#1CC	&(100)170.00	1784	33.00	68.00	8.47
8-21#2C	(98)165.00	1787	31.80	68.00	8.26
8-21#3C	(83)142.00	1814	29.50	65.00	7.83
8-21#4C	(67)115.00	1841	30.30	63.00	7.76
8-21#5C	(19) 33.00	1923	29.40	61.00	7.66

LABELS			EU	TB	YB
8-21#1CC			2.59	1.50	4.20
8-21#2C			2.61	1.70	5.60
8-21#3C			2.34	1.50	4.10
8-21#4C			2.41	1.40	4.80
8-21#5C			2.28	1.60	5.40

LABELS			LU	BA	CO
8-21#1CC			0.46	600.00	15.00
8-21#2C			0.62	540.00	20.00
8-21#3C			0.57	600.00	29.00
8-21#4C			0.57	630.00	25.00
8-21#5C			0.61	590.00	28.00

LABELS			+FEO	+K_2O	HF
8-21#1CC			9.48	2.70	6.30
8-21#2C			11.65	2.30	6.30
8-21#3C			11.93	2.00	5.70
8-21#4C			12.08	2.20	6.10
8-21#5C			11.76	1.90	5.90

LABELS			+NA_2O	RB	SC
8-21#1CC			3.45	90.00	32.77
8-21#2C			3.51	64.00	32.20
8-21#3C			3.47	54.00	32.47
8-21#4C			3.47	41.00	33.17
8-21#5C			3.47	48.00	33.32

LABELS			TA	TH	
8-21#1CC			0.52	6.30	
8-21#2C			0.49	6.10	
8-21#3C			0.43	6.70	
8-21#4C			0.51	6.80	
8-21#5C			0.34	6.90	

&(xx) enclose equivalent depths used to compare concentrations against another sample set in a hypothetical flow of 100 feet thick.

* Depth in flow is calculated from field elevations during measurement of stratigraphic section

$ Elevation of the sample within the flow was measured during stratigraphic section or traverse measurements

+ Oxides concentrations in weight percent (iron is in total FeO) and remaining concentrations in part per million

TABLE LXII

INAA VALUES, EQUIVALENT DEPTHS, DEPTH IN FLOW, ELEVATION OF

SAMPLES FROM SAMPLE SET WENAHA RAVINE (WR)

SAMPLE LABELS	*DEPTH IN FLOW	$ELEVATION IN FLOW	LA	CE	SM
8-22#1C	&(98)284.00	1830	32.30	65.00	8.53
M	(83)235.00	1879	31.60	69.00	8.63
M1	(81)230.00	1884	31.00	66.00	8.30
M2	(80)228.00	1886	32.70	67.00	8.47
M3	(78)221.00	1893	32.30	64.00	8.19
M4	(76)214.00	1900	31.80	68.00	8.27
N	(73)206.00	1908	37.30	66.00	10.10
8-22#3C	(36) 92.00	2022	30.60	62.00	8.05
8-22#4C	(30) 85.00	2029	31.90	64.00	8.25
MC4D	(6) 0.00	2114	30.10	63.00	7.71

LABELS			EU	TB	YB
8-22#1C			2.67	1.80	5.50
M			2.65	1.80	5.50
M1			2.63	1.50	5.00
M2			2.55	1.50	5.90
M3			2.49	1.70	4.60
M4			2.50	1.60	5.80
N			2.88	2.20	5.60
8-22#3C			2.47	1.50	5.10
8-22#4C			2.49	1.60	6.00
MC4D			2.48	1.60	4.00

LABELS			LU	BA	CO
8-22#1C			0.62	640.00	14.00
M			0.57	570.00	13.00
M1			0.58	590.00	25.00
M2			0.74	680.00	20.00
M3			0.60	620.00	16.00
M4			0.59	630.00	20.00
N			0.71	750.00	19.00
8-22#3C			0.55	550.00	25.00
8-22#4C			0.61	640.00	23.00
MC4D			0.55	540.00	27.00

&(xx) enclose equivalent depths used to compare concentrations against another sample set
     in a hypothetical flow of 100 feet thick.
* Depth in flow is calculated from field elevations during measurement of stratigraphic
     section
$ Elevation of the sample within the flow was measured during stratigraphic section or
     traverse measurements
+ Oxides concentrations in weight percent (iron is in total FeO) and remaining
   concentrations in part per million

TABLE LXII CONTINUED

INAA VALUES, EQUIVALENT DEPTHS, DEPTH IN FLOW, ELEVATION OF

SAMPLES FROM SAMPLE SET WENAHA RAVINE (WR)

LABELS	+FEO	+K$_2$O	HF
8-22#1C	11.56	2.50	6.50
M	10.45	2.30	6.40
M1	11.82	2.40	6.60
M2	11.29	2.30	6.50
M3	11.16	2.00	6.00
M4	11.49	1.90	6.30
N	10.67	2.30	6.60
8-22#3C	11.03	1.80	6.20
8-22#4C	11.30	2.80	6.20
MC4D	11.60	2.00	5.90

LABELS	+NA$_2$O	RB	SC
8-22#1C	3.49	48.00	31.96
M	3.59	54.00	33.06
M1	3.57	40.00	26.41
M2	3.48	52.00	31.66
M3	3.45	69.00	30.72
M4	3.53	58.00	30.81
N	3.23	68.00	31.95
8-22#3C	3.56	53.00	32.28
8-22#4C	3.61	70.00	31.61
MC4D	3.27	42.00	32.46

LABELS	TA	TH
8-22#1C	0.50	6.40
M	0.54	6.40
M1	0.55	6.70
M2	0.51	6.80
M3	0.36	6.50
M4	0.54	6.20
N	0.53	6.70
8-22#3C	0.49	6.30
8-22#4C	0.49	6.90
MC4D	0.46	6.60

&(xx) enclose equivalent depths used to compare concentrations against another sample set
    in a hypothetical flow of 100 feet thick.
* Depth in flow is calculated from field elevations during measurement of stratigraphic
    section
$ Elevation of the sample within the flow was measured during stratigraphic section or
    traverse measurements
+ Oxides concentrations in weight percent (iron is in total FeO) and remaining
  concentrations in part per million

TABLE LXIII

INAA VALUES, EQUIVALENT DEPTHS, DEPTH IN FLOW, ELEVATION OF

SAMPLES FROM SAMPLE SET WENAHA RAVINE (WR)

SAMPLE LABELS	*DEPTH IN FLOW	$ELEVATION IN FLOW	LA	CE	SM
8-22-T1A1	1.00	2200	30.40	62.00	7.71
8-22-T1A1R	2.00	2199	31.40	63.00	7.80
8-22-T1A2	3.00	2198	30.90	65.00	7.97
8-22-T1A3	4.00	2197	31.40	61.00	8.04
8-22-T1B	5.00	2196	30.20	65.00	7.87
8-22-T1C	6.00	2195	30.50	62.00	7.77

LABELS			EU	TB	YB
8-22-T1A1			2.31	1.60	4.50
8-22-T1A1R			2.33	1.40	4.50
8-22-T1A2			2.45	1.80	5.20
8-22-T1A3			2.39	1.60	5.20
8-22-T1B			2.45	1.40	5.10
8-22-T1C			2.44	1.60	4.90

LABELS			LU	BA	CO
8-22-T1A1			0.56	500.00	19.00
8-22-T1A1R			0.63	640.00	20.00
8-22-T1A2			0.54	630.00	23.00
8-22-T1A3			0.60	720.00	30.00
8-22-T1B			0.68	660.00	17.00
8-22-T1C			0.56	550.00	24.00

&(xx) enclose equivalent depths used to compare values against another sample set in a hypothetical flow of 100 feet thick.
* Depth in flow was not measured for this sample set.
$ Elevation of the sample within the flow was measured during stratigraphic section or traverse measurements
+ Oxides concentrations in weight percent (iron is in total FeO) and remaining concentrations in part per million

TABLE LXIII CONTINUED

INAA VALUES, EQUIVALENT DEPTHS, DEPTH IN FLOW, ELEVATION OF

SAMPLES FROM SAMPLE SET WENAHA RAVINE (WR)

LABELS	+FEO	+K$_2$O	HF
8-22-T1A1	11.52	2.60	5.80
8-22-T1A1R	11.39	2.40	5.70
8-22-T1A2	11.78	2.20	6.40
8-22-T1A3	11.01	2.60	5.80
8-22-T1B	11.27	2.00	6.00
8-22-T1C	10.56	2.10	5.70

LABELS	+NA$_2$O	RB	SC
8-22-T1A1	3.48	59.00	30.07
8-22-T1A1R	3.75	54.00	30.20
8-22-T1A2	3.45	66.00	31.80
8-22-T1A3	3.47	56.00	25.05
8-22-T1B	3.47	66.00	31.18
8-22-T1C	3.32	39.00	30.19

LABELS	TA	TH
8-22-T1A1	0.46	6.60
8-22-T1A1R	0.52	6.20
8-22-T1A2	0.51	7.10
8-22-T1A3	0.37	6.40
8-22-T1B	0.48	6.80
8-22-T1C	0.47	6.50

&(xx) enclose equivalent depths used to compare values against another sample set in a
     hypothetical flow of 100 feet thick.
* Depth in flow was not measured for this sample set.
$ Elevation of the sample within the flow was measured during stratigraphic section or
     traverse measurements
+ Oxides concentrations in weight percent (iron is in total FeO) and remaining
  concentrations in part per million

TABLE LXIV

INAA VALUES, EQUIVALENT DEPTHS, DEPTH IN FLOW, ELEVATION OF

SAMPLES FROM SAMPLE SET WENAHA RAVINE (WR)

SAMPLE LABELS	*DEPTH IN FLOW	$ELEVATION IN FLOW	LA	CE	SM
8-20#1	&(6)325.00	2158	32.30	68.00	8.15
8-20#2	(15)300.00	2133	30.50	62.00	8.00
8-20#5	(20)290.00	2123	31.50	63.00	8.08
8-20#4	(25)240.00	2073	31.90	62.00	8.10
8-20#3	(30)250.00	2083	31.40	64.00	8.09

LABELS			EU	TB	YB
8-20#1			2.44	1.60	5.90
8-20#2			2.44	1.60	5.70
8-20#5			2.42	1.40	5.10
8-20#4			2.39	1.70	6.10
8-20#3			2.46	1.70	4.80

LABELS			LU	BA	CO
8-20#1			0.55	570.00	32.00
8-20#2			0.52	610.00	29.00
8-20#5			0.54	570.00	20.00
8-20#4			0.60	490.00	17.00
8-20#3			0.53	610.00	16.00

LABELS			+FEO	+K_2O	HF
8-20#1			11.07	1.90	6.60
8-20#2			11.62	2.30	6.10
8-20#5			11.68	2.10	6.40
8-20#4			10.89	2.20	5.70
8-20#3			11.06	2.30	6.40

LABELS			+NA_2O	RB	SC
8-20#1			3.22	41.00	31.45
8-20#2			3.41	47.00	31.83
8-20#5			3.28	64.00	31.84
8-20#4			3.37	46.00	29.00
8-20#3			3.47	49.00	32.77

LABELS			TA	TH	
8-20#1			0.61	7.10	
8-20#2			0.49	7.00	
8-20#5			0.55	6.90	
8-20#4			0.47	6.20	
8-20#3			0.54	7.20	

&(xx) enclose equivalent depths used to compare values against another sample set in a
     hypothetical flow of 100 feet thick.
* Depth in flow was not measured for this sample set.
$ Elevation of the sample within the flow was measured during stratigraphic section or
     traverse measurements
+ Oxides concentrations in weight percent (iron is in total FeO) and remaining
  concentrations in part per million

TABLE LXV

INAA VALUES, EQUIVALENT DEPTHS, DEPTH IN FLOW, ELEVATION OF

SAMPLES FROM SAMPLE SET WENAHA RAVINE (WR)

SAMPLE LABELS	*DEPTH IN FLOW	$ELEVATION IN FLOW	LA	CE	SM
8-22-SC#1	(33)82.00	2087	26.90	58.00	7.18
8-22-SC#2	(30)72.00	2097	26.60	56.00	6.83
8-22-SC#2B	(28)71.50	2097.5	25.80	52.00	7.08
8-22-SC#3	(25)71.00	2098	24.00	50.00	6.38
8-20-SC#4	(6)0.00	2169	26.40	56.00	7.10

LABELS			EU	TB	YB
8-22-SC#1			2.32	1.50	5.00
8-22-SC#2			2.24	1.40	6.10
8-22-SC#2B			2.30	1.20	4.70
8-22-SC#3			2.01	1.20	4.20
8-20-SC#4			2.38	1.30	4.90

LABELS			LU	BA	CO
8-22-SC#1			0.54	550.00	28.00
8-22-SC#2			0.53	480.00	24.00
8-22-SC#2B			0.59	660.00	25.00
8-22-SC#3			0.45	470.00	20.00
8-20-SC#4			0.53	610.00	27.00

LABELS			+FEO	+K_2O	HF
8-22-SC#1			12.45	1.80	5.20
8-22-SC#2			12.12	1.80	5.20
8-22-SC#2B			12.73	1.70	5.20
8-22-SC#3			10.89	1.80	5.10
8-20-SC#4			11.77	2.00	5.40

LABELS			+NA_2O	RB	SC
8-22-SC#1			3.44	47.00	36.32
8-22-SC#2			4.21	47.00	33.19
8-22-SC#2B			3.07	32.00	34.98
8-22-SC#3			3.09	42.00	31.76
8-20-SC#4			2.98	60.00	34.71

LABELS			TA	TH	
8-22-SC#1			0.49	5.70	
8-22-SC#2			0.44	5.20	
8-22-SC#2B			0.51	5.30	
8-22-SC#3			0.29	5.40	
8-20-SC#4			0.51	5.60	

&(xx) enclose equivalent depths used to compare values against another sample set in a
   hypothetical flow of 100 feet thick.
* Depth in flow was not measured for this sample set.
$ Elevation of the sample within the flow was measured during stratigraphic section or
   traverse measurements
+ Oxides concentrations in weight percent (iron is in total FeO) and remaining
   concentrations in part per million

Figure 55. Mossbauer spectrum of sample 8-22-TlAl. The minerals containing ferric and ferrous iron are indicated on the spectrum with their appropriate percentage of the sample.
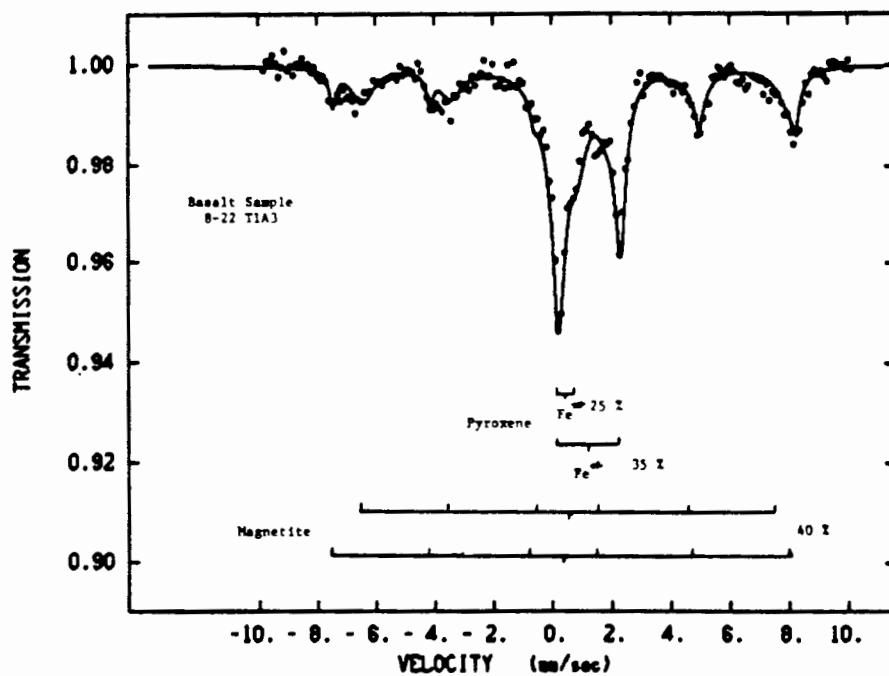
Figure 56. Mossbauer spectrum of sample 8-22-T1A3.
The minerals containing ferric and ferrous iron are indicated
on the spectrum with their appropriate percentage of the
sample.
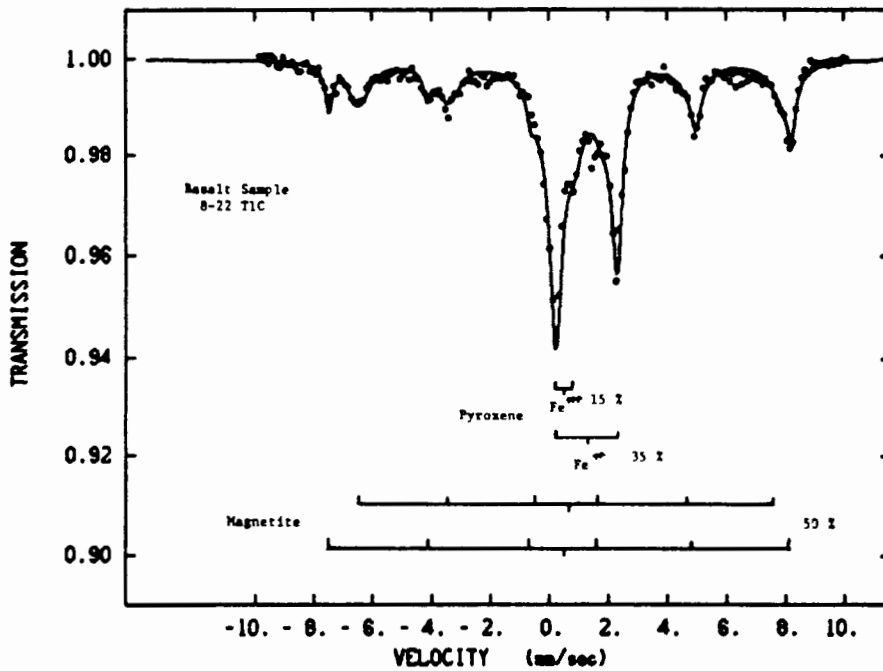
Figure 57. Mossbauer spectrum of sample 8-22-T1C.
The minerals containing ferric and ferrous iron are indicated
on the spectrum with their appropriate percentage of the
sample.

TABLE LVI

INNA DATA FROM 1ST COUNT FOR CERTAIN ELEMENTS FOLLOWED BY ITS ERROR

SAMPLE	SM		CE		LU		LA	
8-20#1	8.15	0.09	58.00	11.00	0.60	0.13	32.30	0.70
8-20#2	8.00	0.08	65.00	12.00	0.70	0.13	30.50	0.70
8-20#3	8.09	0.09	56.00	14.00	0.62	0.13	31.40	0.70
8-20#4	8.10	0.09	50.00	11.00	0.73	0.13	31.90	0.70
8-20#5	8.08	0.09	62.00	11.00	0.60	0.13	31.50	0.70
8-22-SC#1	7.18	0.08	57.00	16.00	0.00	0.00	26.90	0.70
8-22-SC#2	6.83	0.08	50.00	11.00	0.59	0.13	26.60	0.70
8-22-SC#2B	7.08	0.08	51.00	10.00	0.54	0.12	25.80	0.70
8-22-SC#3	6.38	0.08	0.00	0.00	0.44	0.11	24.00	0.60
8-22-SC#4	7.10	0.08	53.00	10.00	0.63	0.12	26.40	8-70
8-22-T1A1	7.71	0.09	57.00	11.00	0.50	0.12	30.40	0.70
8-22-T1A2	7.97	0.09	56.00	11.00	0.00	0.00	30.90	0.80
8-22-T1A3	8.04	0.09	55.00	11.00	0.60	0.12	31.40	0.70
8-22-T1A1R	7.80	0.10	68.00	11.00	0.66	0.12	31.40	0.70
8-22-T1B	7.87	0.09	64.00	11.00	0.65	0.13	30.20	0.70
8-22-T1C	7.77	0.09	61.00	11.00	0.64	0.12	30.50	0.70
8-21#2A	9.59	0.10	67.00	11.00	0.90	0.14	36.10	0.80
8-21#3A	8.40	0.10	63.00	11.00	0.60	0.12	32.60	0.70
8-21#5A	8.35	0.10	53.00	10.00	0.53	0.12	31.00	0.70
8-21#6A	8.40	0.10	51.00	11.00	0.58	0.12	30.70	0.70
8-21#7A	7.83	0.09	69.00	16.00	0.72	0.12	30.60	0.70
8-21#3B	8.32	0.09	48.00	10.00	0.66	0.12	31.50	0.80
8-21#4B	8.14	0.09	52.00	10.00	0.67	0.12	29.90	0.70
8-21#1CC	8.47	0.10	52.00	10.00	0.41	0.11	33.00	0.80
8-21#2C	8.26	0.09	72.00	12.00	0.52	0.12	31.80	0.70
8-21#3C	7.83	0.12	59.00	10.00	0.56	0.12	29.50	0.70
8-21#4C	7.76	0.09	49.00	10.00	0.55	0.12	30.30	0.70
8-21#5C	7.66	0.09	66.00	11.00	0.58	0.12	29.40	0.70
M	8.63	0.10	69.00	12.00	0.52	0.11	31.60	0.80
M1	8.30	0.09	57.00	10.00	0.74	0.12	31.00	0.70
M2	8.47	0.09	54.00	10.00	0.70	0.12	32.70	0.70
M3	8.19	0.09	67.00	11.00	0.58	0.11	32.30	0.80
M4	8.27	0.09	65.00	11.00	0.69	0.12	31.80	0.80
N	10.10	0.11	61.00	10.00	0.74	0.12	37.30	0.80
8-22#1C	8.53	0.09	59.00	10.00	0.62	0.11	32.30	0.70
8-22#3C	8.05	0.12	56.00	10.00	0.56	0.11	30.60	0.70
8-22#4C	8.25	0.09	58.00	10.00	0.60	0.11	31.90	0.70
MC4D	7.71	0.11	57.00	10.00	0.54	0.11	30.10	0.70
*PSU-CR-1	6.63	0.06	55.00	7.00	0.53	0.07	26.40	0.50
+W-2	3.31	0.03	23.00	3.00	0.33	0.04	10.40	0.20

* Portland State Standard used for counting.
+ U.S.G.S. Standard

TABLE LXVI CONTINUED

INNA DATA FROM 1ST COUNT FOR CERTAIN ELEMENTS FOLLOWED BY ITS ERROR

SAMPLE	SC		FE		CO		NA	
8-20#1	31.10	0.50	11.20	0.50	32.00	4.00	3.22	0.01
8-20#2	30.90	0.40	11.20	0.50	29.00	4.00	3.41	0.01
8-20#3	32.20	0.40	10.40	0.50	16.00	4.00	3.47	0.01
8-20#4	28.90	0.40	10.30	0.40	17.00	4.00	3.37	0.01
8-20#5	31.60	0.40	11.50	0.50	20.00	4.00	3.28	0.01
8-22-SC#1	35.50	0.40	12.30	0.40	28.00	4.00	3.44	0.01
8-22-SC#2	32.50	0.40	11.70	0.50	24.00	4.00	4.21	0.01
8-22-SC#2B	34.00	0.40	12.00	0.40	25.00	4.00	3.07	0.01
8-22-SC#3	31.00	0.40	10.90	0.40	20.00	4.00	3.09	0.01
8-22-SC#4	34.30	0.40	12.00	0.40	27.00	4.00	2.98	0.01
8-22-T1A1	30.60	0.40	11.70	0.40	19.00	4.00	3.48	0.01
8-22-T1A2	31.00	0.40	11.60	0.40	23.00	5.00	3.45	0.01
8-22-T1A3	31.00	0.40	10.70	0.40	30.00	4.00	3.47	0.01
8-22-T1A1R	29.90	0.40	11.20	0.40	20.00	3.00	3.75	0.01
8-22-T1B	30.40	0.50	10.60	0.40	17.00	4.00	3.47	0.01
8-22-T1C	30.20	0.40	10.70	0.40	24.00	5.00	3.32	0.01
8-21#2A	34.40	0.40	8.50	0.40	0.00	0.00	3.69	0.01
8-21#3A	31.60	0.40	11.50	0.40	24.00	4.00	3.64	0.01
8-21#5A	31.80	0.50	11.00	0.40	22.00	4.00	3.52	0.01
8-21#6A	31.80	0.40	10.50	0.40	20.00	4.00	3.59	0.01
8-21#7A	31.20	0.40	11.20	0.40	19.00	4.00	3.48	0.01
8-21#3B	31.50	0.40	10.90	0.40	26.00	4.00	3.52	0.01
8-21#4B	31.30	0.40	11.10	0.40	17.00	4.00	3.51	0.01
8-21#1CC	32.50	0.40	9.30	0.40	15.00	3.00	3.45	0.01
8-21#2C	31.10	0.40	11.30	0.40	20.00	5.00	3.51	0.01
8-21#3C	30.70	0.40	11.20	0.40	29.00	3.00	3.47	0.01
8-21#4C	32.00	0.50	11.40	0.40	25.00	3.00	3.47	0.01
8-21#5C	32.30	0.40	11.40	0.40	28.00	3.00	3.47	0.01
M	32.50	0.40	10.20	0.40	13.00	3.00	3.59	0.01
M1	31.10	0.50	11.70	0.40	25.00	4.00	3.57	0.01
M2	31.10	0.40	11.60	0.40	20.00	3.00	3.48	0.01
M3	30.10	0.40	11.00	0.40	16.00	3.00	3.45	0.01
M4	30.40	0.40	11.20	0.40	20.00	3.00	3.53	0.01
N	32.00	0.40	10.70	0.40	19.00	3.00	3.23	0.01
8-22#1C	32.20	0.40	11.50	0.40	14.00	3.00	3.49	0.01
8-22#3C	32.30	0.40	10.40	0.40	25.00	4.00	3.56	0.01
8-22#4C	30.50	0.40	11.10	0.40	23.00	3.00	3.61	0.01
MC4D	31.40	0.40	11.80	0.40	27.00	3.00	3.27	0.01
*PSU-CR-1	33.70	0.20	11.80	0.20	24.20	1.90	3.32	0.01
+W-2	35.70	0.15	9.03	0.14	43.10	1.20	2.20	0.00

* Portland State Standard used for counting.
+ U.S.G.S. Standard

TABLE LXVI CONTINUED

INNA DATA FROM 1ST COUNT FOR CERTAIN ELEMENTS FOLLOWED BY ITS ERROR

SAMPLE	K	
8-20#1	1.90	0.30
8-20#2	2.30	0.30
8-20#3	2.30	0.40
8-20#4	2.20	0.40
8-20#5	2.10	0.40
8-22-SC#1	1.80	0.30
8-22-SC#2	1.80	0.30
8-22-SC#2B	1.70	0.30
8-22-SC#3	1.80	0.30
8-22-SC#4	2.00	0.40
8-22-T1A1	2.60	0.40
8-22-T1A2	2.20	0.40
8-22-T1A3	2.60	0.40
8-22-T1A1R	2.40	0.40
8-22-T1B	2.00	0.30
8-22-T1C	2.10	0.40
8-21#2A	3.30	0.50
8-21#3A	1.60	0.30
8-21#5A	2.10	0.40
8-21#6A	2.50	0.40
8-21#7A	2.30	0.40
8-21#3B	2.10	0.40
8-21#4B	2.30	0.40
8-21#1CC	2.70	0.40
8-21#2C	2.30	0.40
8-21#3C	2.00	0.40
8-21#4C	2.20	0.40
8-21#5C	1.90	0.40
M	2.30	0.40
M1	2.40	0.40
M2	2.30	0.40
M3	2.00	0.40
M4	1.90	0.40
N	2.30	0.40
8-22#1C	2.50	0.40
8-22#3C	1.80	0.40
8-22#4C	2.80	0.50
MC4D	2.00	0.40
*PSU-CR-1	1.70	0.30
+W-2	0.63	0.11

* Portland State Standard used for counting.
+ U.S.G.S. Standard

TABLE LXVII

INNA DATA FROM 2ND COUNT FOR CERTAIN ELEMENTS FOLLOWED BY ITS ERROR

SAMPLE	SC		CE		LU		EU	
8-20#1	31.45	0.14	68.00	3.00	0.55	0.09	2.44	0.08
8-20#2	31.83	0.14	62.00	4.00	0.52	0.06	2.44	0.08
8-20#3	32.77	0.12	64.00	4.00	0.53	0.07	2.46	0.08
8-20#4	29.00	0.13	62.00	3.00	0.60	0.07	2.39	0.08
8-20#5	31.84	0.14	63.00	4.00	0.54	0.07	2.42	0.08
8-22-SC#1	36.32	0.13	58.00	3.00	0.54	0.07	2.32	0.08
8-22-SC#2	33.19	0.12	56.00	3.00	0.53	0.09	2.24	0.08
8-22-SC#2B	34.98	0.16	52.00	3.00	0.59	0.07	2.30	0.08
8-22-SC#3	31.76	0.14	50.00	3.00	0.45	0.06	2.01	0.07
8-22-SC#4	34.71	0.13	56.00	3.00	0.53	0.09	2.38	0.08
8-22-T1A1	30.07	0.13	62.00	3.00	0.56	0.07	2.31	0.08
8-22-T1A2	31.80	0.14	65.00	4.00	0.54	0.07	2.45	0.08
8-22-T1A3	25.05	0.06	61.00	3.00	0.60	0.08	2.39	0.08
8-22-T1A1R	30.20	0.13	63.00	4.00	0.63	0.08	2.33	0.08
8-22-T1B	31.18	0.14	65.00	4.00	0.68	0.09	2.45	0.08
8-22-T1C	30.19	0.13	62.00	4.00	0.56	0.07	2.44	0.08
8-21#2A	34.79	0.13	70.00	4.00	0.66	0.07	2.85	0.09
8-21#3A	31.98	0.14	68.00	4.00	0.61	0.07	2.63	0.09
8-21#5A	32.41	0.14	67.00	4.00	0.61	0.07	2.54	0.09
8-21#6A	31.38	0.14	65.00	4.00	0.60	0.07	2.52	0.09
8-21#7A	31.69	0.14	66.00	4.00	0.59	0.07	2.43	0.08
8-21#3B	31.61	0.14	64.00	4.00	0.64	0.07	2.52	0.08
8-21#4B	32.19	0.14	64.00	4.00	0.58	0.07	2.58	0.08
8-21#1CC	32.77	0.12	68.00	4.00	0.46	0.06	2.59	0.09
8-21#2C	32.20	0.14	68.00	4.00	0.62	0.07	2.61	0.09
8-21#3C	32.47	0.15	65.00	4.00	0.57	0.07	2.34	0.09
8-21#4C	33.17	0.12	63.00	3.00	0.57	0.07	2.41	0.08
8-21#5C	33.32	0.12	61.00	3.00	0.61	0.07	2.28	0.08
M	33.06	0.12	69.00	4.00	0.57	0.07	2.65	0.09
M1	26.41	0.07	66.00	4.00	0.58	0.07	2.63	0.09
M2	31.66	0.14	67.00	4.00	0.74	0.08	2.55	0.08
M3	30.72	0.14	64.00	4.00	0.60	0.07	2.49	0.08
M4	30.81	0.14	68.00	4.00	0.59	0.07	2.50	0.08
N	31.95	0.14	66.00	4.00	0.71	0.09	2.88	0.09
8-22#1C	31.96	0.14	65.00	4.00	0.62	0.07	2.67	0.09
8-22#3C	32.28	0.14	62.00	3.00	0.55	0.07	2.47	0.08
8-22#4C	31.61	0.14	64.00	4.00	0.61	0.07	2.49	0.08
MC4D	32.46	0.15	63.00	3.00	0.55	0.07	2.48	0.10
*PSU-CR-1	34.61	0.10	54.00	3.00	0.54	0.06	2.10	0.06
+W-2	35.70	0.10	23.40	1.50	0.33	0.04	1.12	0.04

* Portland State Standard used for counting.
+ U.S.G.S. Standard

TABLE LXVII CONTINUED

INNA DATA FROM 2ND COUNT FOR CERTAIN ELEMENTS FOLLOWED BY ITS ERROR

SAMPLE	HF		FE		TA		TB	
8-20#1	6.60	0.50	11.07	0.09	0.61	0.07	1.60	0.20
8-20#2	6.10	0.50	11.62	0.09	0.49	0.07	1.60	0.20
8-20#3	6.40	0.50	11.06	0.09	0.54	0.07	1.70	0.30
8-20#4	5.70	0.50	10.89	0.09	0.47	0.06	1.70	0.20
8-20#5	6.40	0.50	11.68	0.09	0.55	0.07	1.40	0.20
8-22-SC#1	5.20	0.50	12.45	0.09	0.49	0.07	1.50	0.20
8-22-SC#2	5.20	0.50	12.12	0.10	0.44	0.06	1.40	0.20
8-22-SC#2B	5.20	0.40	12.73	0.09	0.51	0.07	1.20	0.20
8-22-SC#3	5.10	0.40	10.89	0.09	0.29	0.06	1.20	0.20
8-22-SC#4	5.40	0.50	11.77	0.10	0.51	0.06	1.30	0.20
8-22-T1A1	5.80	0.50	11.52	0.08	0.46	0.06	1.60	0.20
8-22-T1A2	6.40	0.50	11.78	0.10	0.51	0.07	1.80	0.30
8-22-T1A3	5.80	0.50	11.01	0.09	0.37	0.07	1.60	0.20
8-22-T1A1R	5.70	0.50	11.39	0.09	0.52	0.06	1.40	0.20
8-22-T1B	6.00	0.50	11.27	0.09	0.48	0.07	1.40	0.20
8-22-T1C	5.70	0.50	10.56	0.08	0.47	0.06	1.60	0.20
8-21#2A	6.80	0.50	8.19	0.07	0.58	0.07	1.70	0.20
8-21#3A	6.20	0.50	11.63	0.09	0.51	0.07	1.50	0.20
8-21#5A	6.40	0.50	11.13	0.09	0.53	0.07	1.70	0.20
8-21#6A	5.90	0.50	10.99	0.09	0.55	0.07	1.70	0.20
8-21#7A	6.20	0.50	11.63	0.09	0.48	0.07	1.40	0.20
8-21#3B	6.20	0.50	11.26	0.09	0.47	0.07	1.60	0.20
8-21#4B	6.50	0.50	11.54	0.09	0.39	0.07	1.90	0.30
8-21#1CC	6.30	0.50	9.48	0.08	0.52	0.07	1.50	0.20
8-21#2C	6.30	0.50	11.65	0.09	0.49	0.07	1.70	0.20
8-21#3C	5.70	0.50	11.93	0.10	0.43	0.06	1.50	0.20
8-21#4C	6.10	0.50	12.08	0.09	0.51	0.07	1.40	0.20
8-21#5C	5.90	0.50	11.76	0.09	0.34	0.07	1.60	0.20
M	6.40	0.50	10.45	0.08	0.54	0.07	1.80	0.30
M1	6.60	0.50	11.82	0.10	0.55	0.07	1.50	0.20
M2	6.50	0.50	11.29	0.09	0.51	0.07	1.50	0.20
M3	6.00	0.50	11.16	0.09	0.36	0.07	1.70	0.20
M4	6.30	0.50	11.49	0.09	0.54	0.07	1.60	0.20
N	6.60	0.50	10.67	0.09	0.53	0.07	2.20	0.30
8-22#1C	6.50	0.50	11.56	0.09	0.50	0.07	1.80	0.30
8-22#3C	6.20	0.50	11.03	0.09	0.49	0.06	1.50	0.20
8-22#4C	6.20	0.50	11.30	0.09	0.49	0.07	1.60	0.20
MC4D	5.90	0.50	11.60	0.09	0.46	0.06	1.60	0.20
8PSU-CR-1	5.20	0.40	12.21	0.07	0.41	0.04	1.27	0.17
+W-2	2.60	0.20	9.03	0.05	0.52	0.04	0.66	0.10

* Portland State Standard used for counting.
+ U.S.G.S. Standard

TABLE LXVII CONTINUED

INNA DATA FROM 2ND COUNT FOR CERTAIN ELEMENTS FOLLOWED BY ITS ERROR

SAMPLE	YB		TH		RB		&BA	
8-20#1	5.90	1.30	7.10	0.50	41.00	14.00	570.00	150.00
8-20#2	5.70	1.30	7.00	0.50	47.00	15.00	610.00	140.00
8-20#3	4.80	1.10	7.20	0.50	49.00	14.00	610.00	140.00
8-20#4	6.10	1.30	6.20	0.50	46.00	13.00	490.00	140.00
8-20#5	5.10	1.20	6.90	0.50	64.00	17.00	570.00	140.00
8-22-SC#1	5.00	1.20	5.70	0.50	47.00	14.00	550.00	140.00
8-22-SC#2	6.10	1.40	5.20	0.40	47.00	14.00	480.00	120.00
8-22-SC#2B	4.70	1.10	5.30	0.40	32.00	11.00	660.00	170.00
8-22-SC#3	4.20	1.00	5.40	0.40	42.00	12.00	470.00	120.00
8-22-SC#4	4.90	1.10	5.60	0.40	60.00	18.00	610.00	140.00
8-22-T1A1	4.50	1.00	6.60	0.50	59.00	17.00	500.00	120.00
8-22-T1A2	5.20	1.20	7.10	0.50	66.00	17.00	630.00	150.00
8-22-T1A3	5.20	1.20	6.40	0.50	56.00	17.00	720.00	170.00
8-22-T1A1R	4.50	1.10	6.20	0.40	54.00	18.00	640.00	150.00
8-22-T1B	5.10	1.30	6.80	0.50	66.00	17.00	660.00	160.00
8-22-T1C	4.90	1.10	6.50	0.40	39.00	13.00	550.00	140.00
8-21#2A	5.70	1.30	6.90	0.50	73.00	20.00	720.00	170.00
8-21#3A	5.40	1.20	6.60	0.50	48.00	16.00	500.00	120.00
8-21#5A	5.10	1.20	6.60	0.50	61.00	18.00	620.00	150.00
8-21#6A	5.00	1.20	6.20	0.50	49.00	16.00	550.00	140.00
8-21#7A	4.80	1.10	7.20	0.50	63.00	17.00	520.00	130.00
8-21#3B	4.80	1.10	6.40	0.50	42.00	15.00	530.00	130.00
8-21#4B	4.50	1.10	6.80	0.50	64.00	17.00	560.00	140.00
8-21#1CC	4.20	1.00	6.30	0.50	90.00	20.00	600.00	140.00
8-21#2C	5.60	1.30	6.10	0.40	64.00	17.00	540.00	140.00
8-21#3C	4.10	1.00	6.70	0.50	54.00	15.00	600.00	150.00
8-21#4C	4.80	1.10	6.80	0.50	41.00	15.00	630.00	160.00
8-21#5C	5.40	1.20	6.90	0.50	48.00	16.00	590.00	150.00
M	5.50	1.30	6.40	0.50	54.00	17.00	570.00	140.00
M1	5.00	1.20	6.70	0.50	40.00	15.00	590.00	150.00
M2	5.90	1.30	6.80	0.50	52.00	16.00	680.00	170.00
M3	4.60	1.10	6.50	0.50	69.00	18.00	620.00	150.00
M4	5.80	1.30	6.20	0.50	58.00	18.00	630.00	150.00
N	5.60	1.30	6.70	0.50	68.00	19.00	750.00	180.00
8-22#1C	5.50	1.20	6.40	0.50	48.00	14.00	640.00	150.00
8-22#3C	5.10	1.20	6.30	0.50	53.00	15.00	550.00	140.00
8-22#4C	6.00	1.30	6.90	0.50	70.00	20.00	640.00	160.00
MC4D	4.00	1.20	6.60	0.50	42.00	13.00	540.00	140.00
*PSU-CR-1	4.30	0.90	6.60	0.40	58.00	14.00	490.00	110.00
+W-2	2.10	0.60	2.40	0.20	21.00	7.00	170.00	50.00

* Portland State Standard used for counting.
+ U.S.G.S. Standard
& U.S.G.S. Standard used for BA

TABLE LXVII CONTINUED

INNA DATA FROM 2ND COUNT FOR CERTAIN ELEMENTS FOLLOWED BY ITS ERROR

SAMPLE	$BA	
8-20#1	820.00	130.00
8-20#2	830.00	120.00
8-20#3	900.00	130.00
8-20#4	820.00	120.00
8-20#5	770.00	140.00
8-22-SC#1	690.00	110.00
8-22-SC#2	590.00	100.00
8-22-SC#2B	870.00	120.00
8-22-SC#3	670.00	110.00
8-22-SC#4	820.00	120.00
8-22-T1A1	770.00	110.00
8-22-T1A2	850.00	120.00
8-22-T1A3	900.00	120.00
8-22-T1A1R	840.00	130.00
8-22-T1B	820.00	110.00
8-22-T1C	720.00	110.00
8-21#2A	940.00	130.00
8-21#3A	730.00	120.00
8-21#5A	780.00	110.00
8-21#6A	720.00	110.00
8-21#7A	670.00	110.00
8-21#3B	750.00	110.00
8-21#4B	750.00	140.00
8-21#1CC	790.00	130.00
8-21#2C	770.00	120.00
8-21#3C	750.00	110.00
8-21#4C	750.00	130.00
8-21#5C	830.00	120.00
M	800.00	120.00
M1	780.00	120.00
M2	870.00	130.00
M3	820.00	120.00
M4	830.00	120.00
N	920.00	160.00
8-22#1C	800.00	120.00
8-22#3C	760.00	140.00
8-22#4C	780.00	150.00
MC4D	720.00	110.00
*PSU-CR-1	670.00	100.00
+W-2	240.00	60.00

* Portland State Standard used for counting.
+ U.S.G.S. Standard
$ Portlan State Standard used for BA

TABLE XII

XRF DATA FOR CERTAIN ELEMENTS

SAMPLE	SiO_2	Al_2O_3	TiO_2	Fe_2O_3	FeO	MnO	CaO
N	56.90	15.90	2.69	2.00	10.39	0.14	5.25
M4	56.22	15.29	2.55	2.00	10.98	0.18	5.37
M	57.02	15.76	2.63	2.00	9.49	0.19	5.55
8-21#7A	55.63	15.08	2.46	2.00	10.26	0.17	6.14
8-21#6A	55.67	15.25	2.57	2.00	9.84	0.18	6.40
8-21#5A	56.25	15.30	2.61	2.00	10.06	0.18	5.75
8-21#3A	55.78	15.08	2.52	2.00	10.25	0.21	6.10
8-21#2A	58.55	16.55	2.87	2.00	7.94	0.31	4.56
8-22#4C	56.34	15.15	2.48	2.00	9.96	0.23	6.01
8-22#3C	55.84	15.16	2.49	2.00	9.94	0.24	6.39

SAMPLE	MgO	K_2O	Na_2O	P_2O_5
N	1.93	2.07	2.22	0.51
M4	2.56	2.04	2.39	0.43
M	2.35	2.04	2.48	0.49
8-21#7A	3.48	1.79	2.54	0.44
8-21#6A	3.08	1.94	2.59	0.48
8-21#5A	2.84	2.10	2.41	0.48
8-21#3A	3.36	1.80	2.45	0.47
8-21#2A	1.29	2.90	2.49	0.57
8-22#4C	2.64	2.20	2.51	0.48
8-22#3C	3.19	1.85	2.48	0.42

Analyzed at Washington State University by P. R. Hooper, 1986.

APPENDIX E

DEFINITIONS

Basaltic arm is a single layer of basalt separated by joint traces and collectively with other layers form the confining walls of an explosion structure.

Brecciated flows are flows containing explosion structures at a stratigraphic section site and generally consist of two cooling units.

Breciated flow areas consist of the areas within the same flow where explosion structures are located and immediate adjacent of the same flow that were effective by the formation of explosion structures (both cooling units) (Figure 3).

Confining walls are the collection of jointed basalt layers that form an nested arch of an explosion structure. Individual layer are composed of different textured basalt and textures range from vitrophyric to intergranular.

Explosion structures consist of confining walls that form nested arches that surround a steeply dipping breccia spine and vesicular clasts/pockets intraflow zones. The confining walls are composed of banded textures of basalt that are separated by joint traces.

Nonbrecciated flow areas are areas in the same flow that are located between nearby explosion structures (Figure 3).

Unbrecciated flows are flows lacking explosion structures within the flow at a stratigraphic section sites and typically consist of a single cooling unit (Figure 3).

Unbrecciated flow areas are areas within the same flow that lack nearby explosion structures completely.

APPENDIX F

SUMMARY OF FIELD AND LABORATORY TECHNIQUES

TABLE LXIX

DETAILED SUMMARY OF FIELD TECHNIQUES AND EQUIPMENT

Operation or Measurement	Equipment Used	Comments on Process
plotting	7 1/2 minute topographic quadrangles	Portions of Troy, Eden Flora, Saddle Mountain, Mountain View, Diamond Peak, and Field Spring quadrangles.
sample numbering		Samples were prefixed either by date, location, or letters.
flow sampling	rock hammer	Samples were taken at key field locations and freshest possible rock was taken.
elevations	Model M-1 "Micro" surveying altimeter	Large altimeter used primarily for measured and collection of both rock samples and stratigraphic stratigraphic. Altimeter was calibrated at U.S.G.S. benchmarks before and after use.
strike, dips,	Brunton compass	Used primarily for structures breccia trends of the plane of bearing the steeply dipping breccia.
stratigraphic measured section	Model M-1 altimeter and hammer	Elevations of both the superjacent and subjacent contacts were investigated and measured by the M-1 altimeter. Jointing, vesicles, vesicular or scoriaceous zones, morphological profile and subjacent basal behavior were recorded in the field notes. If an explosion structure was being measured, the breccia and compact intervals were measured for each brecciated flow.
horizontal and vertical transverses	100 foot tape	The tape was stretched across an explosion structure exposure and the three different regions of rock were measured and significant remarks were recorded as field notes (Appendix C).
Counting of breccia clasts and clasts/pockets	100 foot tape or 4 bu 4 foot square grid	Distribution of clast types was found by using two different methods: 1) line method used a 100 foot tape which was stretch across an outcrop and 2) a square wooden grid was placed on the outcrop at particular points along the tape or a succession of horizontal intervals covering the width of an outcrop. Each outcrop was selected, because the outcrop face lacked extensive litchen coverage, was accessable, and safe since the best exposures were on steep slopes. The line method was used in conjunction with the measurement of the three regions of rock types of an explosion structure (Appendix C). A clasts was counted when the tape concided with its position on the rock face and its width was measured.

TABLE LXX

DETAILED SUMMARY OF LABORATORY TECHNIQUES AND EQUIPMENT

Operation or Measurement	Equipment Used	Comments
INAA	INAA equipment: balance, plastic vials, etc.	Preparation used has been learned from G 501 Advanced Geochemistry.
XRF	send to Hooper at Washington St. University	Same chips, but a different split.
Mossbauer	Don Howard PSU Physics Dept.	Powdered splits from remaining splits left over from INAA process.
Thin section	send out to Rockwell, Richland WA	Polished sections.
Modal Analysis	Zweiss microscope	1,000 counts per thin section.
Textures: grain sizes	Zweiss microscope with ocular micrometer	
Optical measurements	Zweiss microscope	Optical angles were done for proxenes by direct rotation
Plagioclase An content	Zweiss microscope	Michel-Levy method for phenocrysts, microphenos and for microltic plagioclase.

APPENDIX G

SUMMARY OF STATISTICAL ANALYSIS OF GEOCHEMICAL DATA

TABLE LXXI

INDIVIDUAL VARIANCES FOR EACH ELEMENT

Elements	Variances for Grouse Creek (GC)	Variances for Wenaha Ravine (WR)	F-test value
LA	2.43524	6.88557	2.83
CE	9.50000	7.20000	1.32
SM	0.12264	0.65628	5.35
EU	0.02193	0.02745	1.25
TB	0.01300	0.08700	6.69
YB	0.46200	0.09700	4.76
LU	0.00398	0.00763	1.92
BA	1370.00000	380.00000	3.61
CO	34.30000	18.30000	1.87
FE	1.15498	0.18389	6.28
K	0.09700	0.06200	1.56
HF	0.06799	0.02500	2.72
NA	0.00048	0.02088	43.50
RB	309.19995	43.00000	7.19
SC	0.25227	0.68120	2.70
TA	0.00557	0.00047	11.85
TH	0.11800	0.06699	1.76

Degrees of freedom for Grouse Creek is 4, while degrees of freedom for Wenaha Ravine is 9. The critical value for the F-test with a 0.05 significant is 3.63 for Grouse Creek values and 6.00 for Wehana Ravine values.